ABSTRACT

Title of Dissertation: A PROBABILISTIC MECHANISTIC APPROACH FOR ASSESSING THE RUPTURE FREQUENCY OF SMALL MODULAR REACTOR STEAM GENERATOR TUBES USING UNCERTAIN INPUTS FROM IN-SERVICE INSPECTIONS

Kaushik Chatterjee, Doctor of Philosophy, 2011

Dissertation directed by: Professor Mohammad Modarres
Department of Mechanical Engineering

One of the significant safety issues in nuclear power plants is the rupture of steam generator tubes leading to the loss of radioactive primary coolant inventory and establishment of a path that would bypass the plant's containment structure. Frequency of steam generator tube ruptures is required in probabilistic safety assessments of pressurized water reactors to determine the risks of radionuclide release. The estimation of this frequency has traditionally been based on non-homogeneous historical data that are not applicable to small modular reactors consisting of new steam generator designs.

In this research a probabilistic mechanistic-based approach has been developed for assessing the frequency of steam generator tube ruptures. Physics-of-failure concept has

been used to formulate mechanistic degradation models considering the underlying degradation conditions prevailing in steam generators. Uncertainties associated with unknown or partially known factors such as material properties, manufacturing methods, and model uncertainties have been characterized, and considered in the assessment of rupture frequency. An application of the tube rupture frequency assessment approach has been demonstrated for tubes of a typical helically-coiled steam generator proposed in most of the new small modular reactors. The tube rupture frequency estimated through the proposed approach is plant-specific and more representative for use in risk-informed safety assessment of small modular reactors.

Information regarding the health condition of steam generator tubes from in-service inspections may be used to update the pre-service estimates of tube rupture frequency. In-service inspection data are uncertain in nature due to detection uncertainties and measurement errors associated with nondestructive evaluation methods, which if not properly accounted for, can result in over- or under-estimation of tube rupture frequency. A Bayesian probabilistic approach has been developed in this research that combines prior knowledge on defects with uncertain in-service inspection data, considering all the associated uncertainties to give a probabilistic description of the real defect size and density in the tubes. An application of the proposed Bayesian approach has been provided. Defect size and density estimated through the proposed Bayesian approach can be used to update the pre-service estimates of tube rupture frequency, in order to support risk-informed maintenance and regulatory decision-making.

A PROBABILISTIC MECHANISTIC APPROACH FOR ASSESSING THE RUPTURE FREQUENCY OF SMALL MODULAR REACTOR STEAM GENERATOR TUBES USING UNCERTAIN INPUTS FROM IN-SERVICE INSPECTIONS

By

Kaushik Chatterjee

Dissertation submitted to the Faculty of Graduate School of the
University of Maryland College Park, in partial fulfillment
of the requirements for the degree of
Doctor of Philosophy
2011

Advisory Committee:
Professor Mohammad Modarres (Advisor/Chair)
Professor Ali Mosleh
Professor Hugh Bruck
Professor Emeritus George Dieter
Professor Norman M. Wereley (Dean's representative)

DEDICATION

To my parents for their understanding and support throughout

ACKNOWLEDGEMENTS

It is with immense gratitude that I acknowledge the support and help of my advisor, Professor Mohammad Modarres. I am honored and privileged to have the opportunity to work and learn with him. He provided deep insight and technical advice on all aspects of this research. His patience and support helped me overcome many crisis situations and finish this dissertation.

I am also deeply grateful to all the members of my PhD dissertation committee, Professor Ali Mosleh, Professor Hugh Bruck, Professor George Dieter, and Professor Norman Wereley for taking out their time and providing constructive feedback for my research.

Special thanks to Dr. Bill Shack and Dr. Bogdan Alexandreanu of Argonne National Laboratory for providing experimental data and material for Alloy 690. I am also grateful to all of my colleagues at the Center for Risk and Reliability and Department of Mechanical Engineering at University of Maryland College Park.

TABLE OF CONTENTS

DEDICATION ……..ii
ACKNOWLEDGEMENTS ……..iii
LIST OF TABLES ……..vii
LIST OF FIGURES ……..viii
1 INTRODUCTION 1
1.1 Motivation and Objectives 1
1.2 Scope and Assumptions 12
1.3 Principal Contributions 13
1.4 Organization of the Dissertation 13
2 PROBABILISTIC PHYSICS-OF-FAILURE BASED APPROACH FOR ASSESSING THE FREQUENCY OF STEAM GENERATOR TUBE RUPTURES 17
2.1 Historical Perspective on Steam Generator Tube Degradation Issues 17
2.2 Emergence of Small Modular Reactors 18
2.3 Issues with Traditional Steam Generator Tube Rupture Frequency Assessment Method 20
2.4 Historical Evolution of Physics-of-Failure 23
2.5 Probabilistic Physics-of-Failure Based Approach 31
2.5.1 Identification of Primary Degradation Mechanisms during Normal Operating Conditions 35
2.5.2 Probabilistic Physics-of-Failure Model Formulation 40
2.5.2.1 Fatigue 40
2.5.2.1.1 Literature Review 43

2.5.2.1.2 Proposed Probabilistic Physics-of-Failure Model 45
2.5.2.2 Fretting Wear 55
2.5.2.2.1 Literature Review.....56
2.5.2.2.2 Proposed Probabilistic Physics-of-Failure Model 58
2.5.3 Probabilistic Stress Agents Assessment Approach.....64
2.5.4 Probabilistic Approach for Uncertainty Propagation and Rupture Frequency Estimation 69
3 ASSESSMENT OF STEAM GENERATOR TUBE RUPTURE FREQUENCY FOR A TYPICAL HELICAL SMALL MODULAR REACTOR DESIGN.....74
3.1 Small Modular Reactor Steam Generator Tubes 74
3.1.1 Identification of Degradation Conditions and Mechanisms 76
3.1.2 Finite Element Analysis to Assess the Stress Agents 77
3.2 Assessment of Steam Generator Tube Rupture Frequency 80
3.3 Discussion of Results 83
4 BAYESIAN PROBABILISTIC APPROACH FOR ESTIMATING DEFECT SEVERITY IN STEAM GENERATOR TUBES USING UNCERTAIN INPUTS FROM NONDESTRUCTIVE EVALUATION 85
4.1 Historical Perspectives on Steam Generator Tube In-Service Inspection 85
4.2 Uncertainties Associated with Nondestructive Evaluation Methods.....86
4.2.1 Probability of Detection and Associated Uncertainties 87
4.2.2 Measurement Error and Associated Uncertainties.....94
4.3 Structuring a Bayesian Probabilistic Approach for Estimating True Defect Severity Accounting for all Uncertainties and Errors.....96
4.3.1 Approach to Model Nondestructive Evaluation Uncertainties 98

4.3.2 Bayesian Model for Estimating True Defect Size 101
4.3.2.1 Likelihood Function for Detections 101
4.3.2.2 Likelihood Function for Non-Detections 104
4.3.2.3 Combined Likelihood Function (Detections and Non-Detections) 105
4.3.3 Bayesian Model for Estimating True Defect Density 107
4.3.4 Summary of Proposed Bayesian Approach 109
4.4 An Integrated Approach Incorporating Bayesian Results for Assessing In-Service Steam Generator Tube Rupture Frequency 111
5 ESTIMATING TRUE FLAW SIZE AND DENSITY DISTRIBUTIONS BASED ON IN-SERVICE EDDY CURRENT EVALUATION DATA 113
5.1 Modeling Eddy Current Evaluation Uncertainties 114
5.2 Estimating True Flaw Size and Density Distributions Using Proposed Bayesian Approach 116
6 CONCLUSIONS AND SUGGESTED FUTURE WORK 123
REFERENCES 128

LIST OF TABLES

Table 1: Historical data used to estimate the SGTR frequency 5

Table 2: Vibration excitation mechanisms in tube array caused by cross-flow 38

Table 3: Identification of leading failure mechanisms in SG helical tubes during normal operating conditions 39

Table 4: Comparison of proposed, Argonne, and Walker models 52

Table 5: Ranking of proposed, Argonne, and Walker models 53

Table 6: Proposed fatigue model parameters 54

Table 7: Proposed fretting wear model parameter values 64

Table 8: Composition of Alloy 600 and Alloy 690 materials (wt %) 75

Table 9: Geometrical parameters of tube 78

Table 10: Alloy 690 material properties 78

Table 11: Natural frequencies from Modal analysis 78

Table 12: Measurement error parameter values from Bayesian regression 115

Table 13: POD parameters 116

Table 14: Flaw size measurements (prorated) from eddy current evaluation 118

Table 15: True size corresponding to Table 14 (corrected for measurement errors) 118

Table 16: Actual/True number of flaws 121

LIST OF FIGURES

Figure 1: Typical nuclear power plant with large scale PWR (Source: US NRC) 1

Figure 2: New designs of SMRs (Not to scale): NuScale (left) and IRIS (right) 6

Figure 3: New designs of SMRs from left to right (Not to scale): NuScale, mPower, and IRIS 19

Figure 4: Basic design features of SMRs when compared to large scale PWRs 23

Figure 5: PPoF approach for SGTR frequency distribution assessment 33

Figure 6: Typical da/dN versus ΔK curve 42

Figure 7: Three modes of fracture 42

Figure 8: Alloy 690 fatigue crack growth data (log-log) 47

Figure 9: Stress ratio effect on Alloy 690 fatigue CGR (log-log) 48

Figure 10: Estimating fatigue PPoF model parameter distributions 49

Figure 11: Distributions of model parameters 51

Figure 12: Distributions of model error and standard deviation 52

Figure 13: Alloy 690 fretting wear data at room and elevated temperatures 58

Figure 14: Schematic of SG tube-support plate interaction 60

Figure 15: Estimating fretting wear PPoF model parameter distribution 62

Figure 16: Alloy 690/Stainless Steel fretting wear data 63

Figure 17: Posterior distributions of PPoF model parameters k & σ 64

Figure 18: Turbulent fluid pressures acting on tube cross-section in all directions (Blevins, 1990) 65

Figure 19: Force acting on a tube in a turbulent flow (Blevins, 1990) 65

Figure 20: Random vibration analysis approach 67
Figure 21: Flaw (e.g., crack) growth simulation using PPoF models 70
Figure 22: Considering parameter uncertainties 71
Figure 23: Helical tubes (left) and top view of tubes with support points (right) 75
Figure 24: Finite element model of one span of helical tube 77
Figure 25: Random vibration stresses along helical span of SG tube 80
Figure 26: Uncertainty representation of SGTR frequency due to fatigue 82
Figure 27: Uncertainty representation of SGTR frequency due to fretting-wear 82
Figure 28: Uncertainty representation of total SGTR frequency 83
Figure 29: Nondestructive evaluation and associated uncertainties 87
Figure 30: Hit/miss data 88
Figure 31: POD curve for hit/miss data 90
Figure 32: Signal vs. Noise 91
Figure 33: Response amplitude vs. True size 92
Figure 34: POD estimation from signal response data 93
Figure 35: Equivalent hit/miss data 94
Figure 36: Factors affecting measurements 95
Figure 37: Measurement error components 96
Figure 38: Regression analysis of measurement error 99
Figure 39: Bayesian approach for estimating true defect size and density 110
Figure 40: Flaw growth simulation using PPoF models starting from health condition at in-service inspection 112
Figure 41: Estimating SGTR frequency using In-service inspection data 112

Figure 42: Measurement error regression analysis 114

Figure 43: Distribution of parameters 115

Figure 44: POD curve 116

Figure 45: Marginal POD 117

Figure 46: Posterior flaw size intensity distribution 119

Figure 47: Posterior flaw size distributions 120

Figure 48: Box and whisker plot of actual/true number of flaws (log scale) 120

CHAPTER 1: INTRODUCTION

1.1 Motivation and Objectives

In nuclear power plants, pressurized water reactors (PWR) produce the heat that is used to generate electricity. This heat is generated through nuclear fission in the reactor core, which is carried by the primary coolants to the steam generators (SGs) where the heat is transferred across thin tubes to the secondary loop, to produce the steam that eventually expands through the turbine. The safety of PWRs depends to a great extent on the safety and reliability of its components and structures, especially the SG tubes. Besides keeping the reactor core at a safe temperature, SG tubes also act as one of the primary barrier between the radioactive (inside containment) and non-radioactive sides (outside containment) of a nuclear power plant (Figure 1).

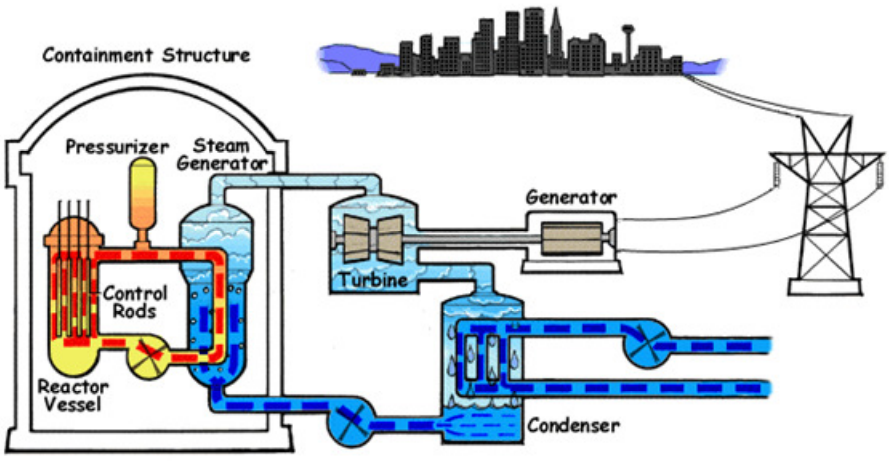

Figure 1: Typical nuclear power plant with large scale PWR (Source: US NRC)[1]

[1] US NRC, "The Pressurized water reactor (PWR)", Retrieved from http://www.nrc.gov/reading-rm/basic-ref/students/animated-pwr.html

Since SG tubes play such an important role, any degradation and rupture in the tubes can be catastrophic because it can lead to:

1. Loss of coolant, which can increase reactor core temperature and result in core meltdown.
2. Release of radioactivity into the atmosphere bypassing the plant's containment structure.
3. Damage and rupture of adjacent tubes because of the close proximity of the tubes in a tube bundle.
4. Rapid degradation and failure during other severe accident scenarios which create a harsh condition imposed against the tubes.

Unmitigated reactor core meltdown is the most severe of all adverse consequences listed above as it recently happened at some of the Fukushima-Daiichi reactors in Japan caused by earthquake-induced tsunami (primary cause was the reactor coolant pump failure due to loss of both offsite and emergency powers, i.e., the so-called station blackout event). The second adverse consequence listed above results when the radioactive primary coolant leaks into the secondary side where pipes provide the only outlet through the containment into the atmosphere by means of pressure relief valves. The third adverse consequence has rarely occurred but can be catastrophic in terms of amount of radioactivity that can release into the atmosphere in a short period of time. The fourth consequence has been identified, but not experienced.

There have been several occurrences of SG tube ruptures (SGTR) in the past. An SGTR event can be caused by any defect (e.g., crack, flaw, pit or other anomalies) that

propagates to 100% through-wall either under normal operating conditions or accident scenarios (e.g., station blackout or earthquake), leading to leakages, small or large scale ruptures having the potential to depressurize the primary side thus impairing its function (cooling the reactor core), and causing release of radioactivity into atmosphere. According to the Nuclear regulatory Commission (NRC), there have been 10 large-scale SGTR occurrences in the US between 1975 and 2000 (*US NRC, 2010*). These tube rupture occurrences caused loss of coolant accident (LOCA) that needed primary coolant replenishment using charging pumps.

There have been several other reported and unreported cases of SG tube leakages and low scale ruptures, e.g., more than 100,000 (*Diercks, Shack & Muscara, 1996*). One such incident occurred in McGuire Unit 1 power reactor near Charlotte, NC on March 7, 1989 (*US NRC, 1990*). The cause of the tube rupture was determined to be stress corrosion cracking (SCC) under normal operating conditions. In another incident, the North Anna power station in 1987 experienced an SGTR event when the plant reached its 100% capacity (*US NRC, 1988*). The cause of tube rupture was found to be fatigue, caused by combination of alternating stresses resulting from flow-induced tube vibration and flaws resulting from denting of tubes at support plates.

Probabilistic safety assessments (PSA) of PWRs as required by the NRC are conducted to ensure plant safety and support regulatory decisions by analyzing scenarios that cause severe adverse consequences (e.g., reactor meltdown) and their associated frequencies (i.e., probability of occurrence per year). PWRs are designed and licensed using the PSA as the safety assessment method. In PSA of PWRs, SGTR is one of the

initiating events that can lead to severe adverse consequences. Estimation of the frequency of SGTRs has traditionally been based on historical data, which are gathered over a long period from operating PWRs having different SG geometries, environmental and operating conditions. These non-homogeneous historical data are combined to estimate the SGTR frequency. As an example in NUREG 1829, *Tregoning, Abramson and Scott* (*2005*) queried SGTR data from a database for a 15-year time period between 1987 and 2002, shortlisted 4 SGTRs (Table 1) that had leak rates greater than 100 gallons per minute, and combined them to estimate the SGTR frequency based on calendar years of reactor operation.

Another report (NUREG-5750) conducted a similar assessment of SGTR frequency combining non-homogeneous historical data (*Poloski, Marksberry, Atwood, & Galyean, 1999*). Few things to note from Table 1 are that these four SGTR events were based on small break LOCA category 1 that were basically influenced by large diameter coolant pipes in large scale PWRs and injection pump capacity. About 75% of SGTR events resulted due to SCC, and the tube material was Alloy 600. Also, the non-homogeneous nature of the historical data makes the frequency estimates generic in nature and not plant-specific.

Applicability of the historical data-driven frequency of SGTR to new small modular reactor (SMR) helical SG designs[2] with different geometries, material properties, degradation mechanisms and thermal-hydraulic behaviors is certainly not valid. For example, in traditional SG designs SCC was the dominant degradation mechanism (*Diercks et al., 1996*) due to the use of Alloy 600 as tube material and the boundary

[2] Description of the basic design features of typical SMR SGs have been provided in Chapter 2 of this dissertation.

conditions (primary loop being internal to tubes). However, with the proposed use of Alloy 690[3] as tube material in new SMR SG designs (Figure 2) and different boundary conditions (high pressure primary loop applied to the outside of the SG tubes), risk of tube failure from SCC has been considerably reduced (*Berge & Donati, 1981; Lee, Kim, Kang, & Chung, 2001; Lim, Oh & Lee, 2003; Chatterjee & Modarres, 2012*). This makes the historical data totally irrelevant for the purpose of estimating SGTR frequency for new SG designs that are completely different from the operating fleet of PWRs. Further, SMR SGs have vastly different geometries, such as helical-shaped as opposed to U-shaped or straight-through tubes, which accommodates thermal stresses due to expansion of tubes during normal heating at start-up. Also, the SMRs do not have the large diameter coolant loop pipes as compared to large scale PWRs.

Table 1: Historical data used to estimate the SGTR frequency[4]

Power plant	Year	Degradation mechanism	Tube Material
North Anna, VA	1987	Fatigue	Alloy 600
McGuire, NC	1989	SCC	Alloy 600
Palo Verde, AZ	1993	SCC	Alloy 600
Indian Point, NY	2000	SCC	Alloy 600

There is a need for a new approach for assessment of the SGTR frequency that does not rely on historical failure data, but rather considers the underlying degradation

[3] More information on Alloy 690 material is provided in Chapter 3 of this dissertation.
[4] US NRC, 1988; US NRC, 1990; US NRC, 2000; Schallor et al., 1995;

conditions and the underlying mechanical, electrical, thermal, and chemical processes that lead to failure (*Chatterjee & Modarres, 2012*). Further, a deterministic approach that predicts a point estimate of the time-to-failure is not so useful. This is because of uncertainties associated with unknown or partially-known factors such as material properties, manufacturing methods, model uncertainties and measurement errors, which can affect the final SGTR frequency estimates. Hence, a mechanistically-based probabilistic approach is necessary to simulate applicable degradations, characterize all uncertainties associated with various factors and propagate the uncertainties to determine the probability distribution of the SGTR frequency and associated confidence levels.

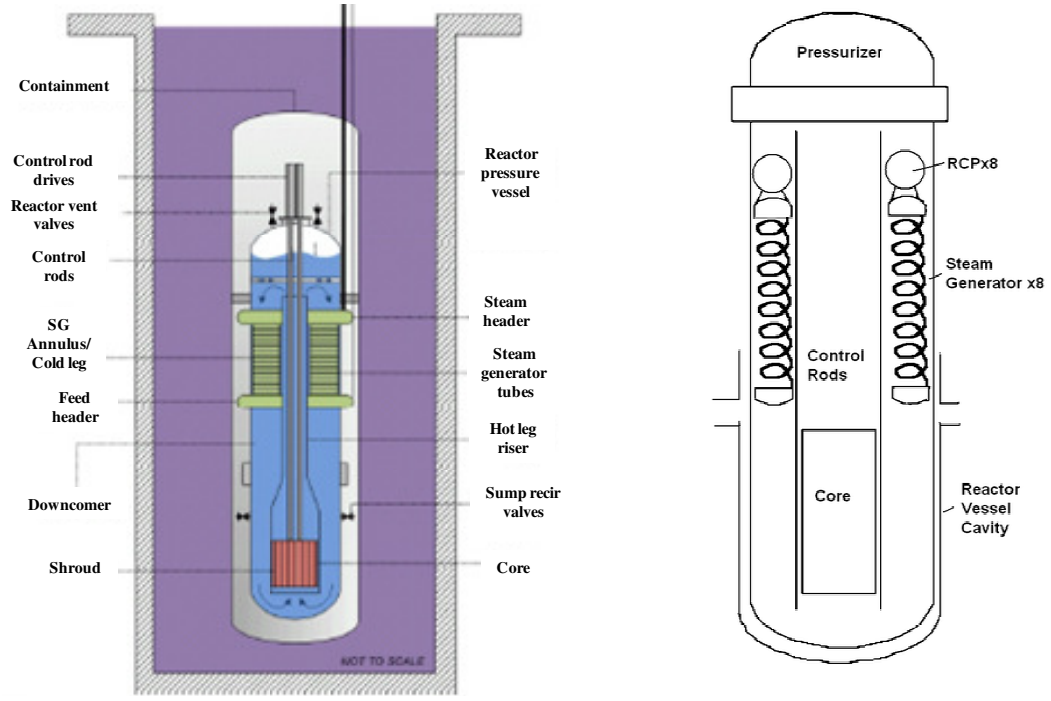

Figure 2: New designs of SMRs (Not to scale): NuScale[5] (left) and IRIS[6] (right)

[5]US NRC, "NuScale", Retrieved from http://www.nrc.gov/reactors/advanced/nuscale.html (Modified nomenclature from original)
[6]Wikipedia, "International Reactor Innovative and Secure", Retrieved from http://en.wikipedia.org/wiki/International_Reactor_Innovative_and_Secure

Most cases in literature have used statistical approaches for evaluating SGTRs rather than probabilistic mechanistic models (*Gosselin, Simonen, Pilli & Lydell*, 2007). Only few previous studies have considered underlying degradation mechanisms to estimate the SGTR frequency. However, they were all focused on tube failures from specific degradation mechanisms (e.g., creep, SCC) that are a result of severe accidents (e.g., feedwater line break). This may have to do with the traditional design of PWRs, where thicker and large diameter primary coolant loop pipes posed far greater risk to overall plant safety than relatively thinner (of the order of 1-2 mm) and small diameter SG tubes. Hence, only those accident scenarios were considered in the past that could lead to large rupture in tubes resulting in large loss of coolants.

Liao and Guentay (2009) used a creep rupture model to estimate SGTR probability in the reactor coolant pressure boundary, under severe accident conditions with countercurrent natural circulating high temperature gas in the hot leg and SG tubes. *Cizelj and Roussel* (2011) presented a SCC model for estimating tube rupture probability during severe accident conditions caused by feedwater line break. Although accident-induced SGTRs (e.g., earthquake, loss of off-site power) could provide a high potential of severe adverse consequences (e.g., the release of radioactivity into atmosphere), such accident-induced SGTRs are easily detectable. More important in such accident scenarios is the safety of the high temperature reactor core and other critical components (e.g., large diameter coolant loop pipes).

With changing designs, and emphasis on SMRs with integrated reactor and SGs and passive safety operations (that use natural forces such as gravity or natural circulation to

operate), nuclear power plants have become inherently safer. However, this has also brought new risk assessment challenges because the SGs are integrated into the reactor vessel directly above the core, and even small leakages from tubes can pose different type of risks to overall plant safety. Frequency of SGTRs during normal operating conditions needs careful attention as they can often go undetected (due to small leak rates) and lead to release of radioactivity into atmosphere and other adverse consequences (e.g., adjacent tube failure from increased turbulence level). Further, a comprehensive approach is needed to consider all the probable degradation mechanisms that can occur during normal operating conditions in PWR SGs, and estimate the total SGTR frequency.

In this research a probabilistic physics-of-failure (PPoF) based approach has been developed for assessing the frequency of SGTRs that can support risk-informed safety analyses of new and existing PWRs. This approach is based on the principle that failure of passive systems is governed by mechanistic degradations created through the underlying environmental and operating conditions. The PPoF-based approach identifies, probabilistically models, and simulates potential degradations in new and existing SG designs to assess degradation versus time, until such degradation exceeds a known endurance limit. Physics-of-failure[7] concept has been used to develop mechanistic degradation models for primary failure mechanisms considering the underlying degradation conditions prevailing in SGs. Uncertainties associated with unknown or partially known factors such as material properties, manufacturing methods, model uncertainties and measurement errors have been characterized. Procedures for assessment of stress agents during normal operating conditions have been provided considering

[7] Detailed description of physics-of-failure concepts have been provided in Chapter 2 of this dissertation.

uncertainties in tube geometry and material properties. A probabilistic approach has been provided for simulating the degradations in the SG tubes using the proposed PPoF models and under the applied stress agents, propagating all the associated uncertainties to estimate the distribution of SGTR frequency. An application of the SGTR frequency assessment approach has been demonstrated for a typical SMR that consists of helically coiled tubes fabricated with advanced alloys. The SGTR frequency estimated based on this probabilistic mechanistic approach is plant-specific and more representative for use in risk-informed safety assessment of new as well as existing PWRs.

Since the SG tubes are subjected to variety of operating conditions during their life-cycle, the degradations in tubes may not propagate as anticipated during the licensing or pre-service phase. Hence, it is critical to characterize the health condition of the SG tubes during in-service inspections, and update the pre-service estimates of the SGTR frequency. Tube degradations/defects are characterized through nondestructive evaluation methods during in-service inspections. Nondestructive evaluation methods are quite complex and it requires considerable skills from the operators to extract useful data from them. Also, the analysis and processing of the test data, to yield quantitative estimates of unknown existing defects, require careful consideration of various factors (e.g., physics-of-failure) on the part of the analyst, whose level of experience is a critical determinant of the quality of the evaluation. Hence, the nondestructive evaluation process induces considerable detection uncertainties and measurement errors into the defect severity estimates. These uncertainties and errors, if not properly accounted for, can result in defect severity estimates not representative of actual tube degradations, and over- or under-estimation of SGTR frequency.

A defect of a given size might be detected only a certain percentage of the time (out of total attempts during nondestructive testing) depending on factors such as, noise level, test probe sensitivity, test equipment repeatability and human error. Hence, a defect has an associated Probability of Detection (POD), which can be defined as the probability that the inspection will detect the defect having the true size, a, and is denoted by $POD(a)$ (*Kurtz, Heasler & Anderson, 1992*).

The precision and accuracy of nondestructive test equipment, and also the techniques used to analyze and process the test results can contribute to measurement errors. For example, large volume of sensor data (such as ultrasound or digital images) are filtered, smoothed, reduced, and censored into another form by subjectively accounting for only certain features of the data. Also, often measurement models are used to convert the form of a measured or observed data into the corresponding value of the reality of interest (i.e., defect size). Uncertainties associated with model selection and human errors can also contribute to measurement errors. These detection uncertainties and measurement errors need to be considered in order to estimate real defect severity in the tubes.

In the past, there have been some efforts to model defect severity in structural components using nondestructive evaluation data. However, they have not been successful in considering all the uncertainties and errors associated with nondestructive evaluation methods. *Rodriguez and Provan* (1989) present a method to model pitting corrosion based on data from in-service inspection, considering only the POD in a simplified manner and ignoring the effect of measurement error. *Cizelj and Dvorsek* (1998) consider the impact of measurement error in inspection data on SGTR frequency,

neglecting the effect of POD. *Lee, Park, Lee, Kim and Chung* (2005) only considered the effect of POD to estimate the actual number of defects without considering the measurement error in inspection data. *Hovey, Meeker and Li* (2008) present a method to provide a joint estimate of in-service POD and crack size distribution through nondestructive evaluation. However, they assume that definite crack size information can be obtained through destructive methods, and hence did not consider the effect of measurement errors.

Datla, Jyrkama and Pandey (2008) present an eddy current inspection-based pitting corrosion model considering only big size pits (> 50% through-wall depth), in order to overcome the nondestructive inspection uncertainties associated with small sizes. Though detection uncertainties are negligible, there is still considerable measurement error (especially systematic error) associated with big sizes. *Celeux, Persoz, Wandji and Perrot* (1999) describe a method to model defects in PWR reactor vessel welds considering the POD and random error in measurements. *Yuan, Mao and Pandey* (2009) followed the idea of *Celeux et al.* (1999), to propose a model for pitting corrosion in SG tubes considering the POD and random error of the eddy current measurements. However, both *Celeux et al.* (1999) and *Yuan et al.* (2009) did not consider the effect of systematic error or bias in measured defect sizes. Further, they did not consider uncertainties in the values of the POD, which can affect the defect severity estimates considerably.

This research addresses some of the limitations of current techniques, and develops a Bayesian probabilistic approach for modeling defect severity (size and density) in SG tubes considering the detection uncertainties (i.e., POD and associated uncertainties) and

measurement errors (systematic and random errors, and associated uncertainties) associated with nondestructive evaluation methods. The proposed Bayesian approach combines prior knowledge of defect size and density with uncertain data from nondestructive evaluations considering the POD, measurement errors (systematic and random), and associated uncertainties to infer the posterior distributions of defect size and density.

The combined effect of POD, measurement error, and associated uncertainties on measured defect sizes is captured by a likelihood function. An application of the proposed Bayesian approach has been provided to estimate real/true flaw size and density distributions in SG tubes based on in-service eddy current evaluation data. An approach for updating the pre-service estimates of the SGTR frequency based on in-service flaw size and density distributions has been provided. The updated SGTR frequency can be used for in-service PSA of SMRs, in order to support risk-informed maintenance (replacement/plugging) of SG tubes and regulatory decision-making.

1.2 Scope and Assumptions

The scope and assumptions of this research are as follows:

1. Only normal operating conditions-induced SGTRs have been considered.
2. The primary degradation mechanisms identified in this research are based on normal operating conditions in typical new designs of helical SMRs.
3. The PPoF approach for SGTR frequency assessment developed in this research can be applied both at pre-service stage as well as during in-service inspections.

4. Defects in SG tubes are assumed to be independently and identically distributed with a constant mean intensity (i.e., occurrences of defects may be represented by the homogenous Poisson process).
5. Small leakages are included into the definition of SGTRs in SMRs, unlike the LOCA-based definitions that are not relevant to SMRs due to the absence of large diameter coolant pipes.

1.3 Principal Contributions

The principal contributions of this research are:

1. Development of a PPoF-based SGTR frequency prediction approach for SMRs.
2. Development of two PPoF models for fatigue and fretting wear failure mechanisms in Alloy 690 SG tubes, addressing the limitations of existing deterministic models.
3. Development of a Bayesian approach to estimate real/true defect severity in SG tubes using uncertain nondestructive evaluation data, involving POD, measurement errors, and associated uncertainties.
4. Development of MATLAB-based tools to carry out the complex simulation and Bayesian inference numerical computations.

1.4 Organization of the Dissertation

There are four major parts to this dissertation. The first part contained in Chapter 2 presents the PPoF approach for assessment of SGTR frequency. Historical perspectives on SG tube degradation issues are first presented; discussing the evolution of tube degradation types over the years and measures taken to mitigate the risks from them.

Then the emergence of SMRs is presented discussing the need for such advanced designs and the economic benefits and safety features they provide. The issues with the current SGTR frequency assessment technique are then discussed, highlighting the need for new methods to assess the SGTR frequency for new SMR designs. Chapter 2 then presents historical evolution of physics-of-failure methodologies, and the emergence of PPoF approach for reliability prediction. The PPoF based SGTR assessment approach is then presented, detailing the various steps and considerations for its use. The degradation conditions existing in SMR designs during normal operating conditions are then discussed, including the applicable degradation mechanisms. Chapter 2 then presents proposed PPoF models for some of the applicable primary failure mechanisms occurring in SMR SG tubes during normal operating conditions. All epistemic and aleatory uncertainties associated with model and data are characterized using Bayesian regression approach in the form of probability distribution of model parameters. Procedures for assessment of stress agents are then provided considering uncertainties with tube geometry and material properties. Also, Chapter 2 presents a probabilistic approach for propagating all the uncertainties to estimate the probability distribution of SGTR frequency considering the proposed PPoF models and the acting stress agents.

Chapter 3 provides an application of the PPoF approach for predicting SGTR frequency of a typical SMR design. The SMR design is first discussed in detail, along with prevailing degradation conditions during normal operating conditions and applicable primary failure mechanisms. The stress agents acting on the tubes are then determined using the proposed procedure in Chapter 2, which uses finite element analysis to obtain the stresses applied on the SG tubes during normal operating conditions. Then the

distribution of SGTR frequency is estimated for the SMR design, followed by a comparison between PPoF estimation and the historical estimation of the SGTR frequency.

Chapter 4 presents the Bayesian approach for estimating in-service defect size and density distributions in SG tubes using uncertain information from nondestructive evaluations. Some historical perspectives on SG tube in-service inspections are first discussed. Then a detailed description of detection uncertainties and measurement errors associated with nondestructive evaluation methods is provided, along with various considerations for their modeling. Chapter 4 then presents a Bayesian probabilistic approach for estimating real defect severity in SG tubes accounting for nondestructive evaluation uncertainties and errors. Approaches for accounting epistemic and aleatory uncertainties associated with models and data used to characterize POD and measurement errors are presented. Then the Bayesian models for estimating posterior defect size and density are derived considering various types of nondestructive evaluation data, e.g., exact, interval, censored, and truncated. An integrated approach is then presented to incorporate the in-service defect size and density distributions estimated from the Bayesian approach to update the pre-service estimates of the SGTR frequency. The updated SGTR frequency can then be used for in-service PSA of SMRs to support risk-informed maintenance of SG tubes and regulatory decision-making.

Chapter 5 presents an application of the proposed Bayesian approach for estimating real flaw size and density distributions in SG tubes based on eddy current evaluation data. Eddy current evaluation uncertainties are first modeled using the techniques proposed in

Chapter 4. Then the flaw size and density distributions are inferred using the proposed Bayesian approach that uses in-service eddy current evaluation data for SG tubes.

Finally, Chapter 6 provides summary and conclusions regarding the methods and approaches developed in this research for the assessment of the SGTR frequency. The principal contributions of this research are discussed in terms of their significance in improving the safety and reliability of new designs of SMRs. Recommendations for future work are provided to supplement the current research with more investigations and analysis, e.g., 3D thermal hydraulic analysis.

CHAPTER 2: PROBABILISTIC PHYSICS-OF-FAILURE BASED APPROACH FOR ASSESSING THE FREQUENCY OF STEAM GENERATOR TUBE RUPTURES

2.1 Historical Perspectives on Steam Generator Tube Degradation Issues

Commercial PWRs were first introduced in the late 1950s in US. Since then it has become the second largest source for electricity generation in the United States (accounts for more than 20% of total electricity generated). Various safety issues have plagued PWRs over the years. Degradation of SG tubes is one such issue that is an important consideration in the overall safety of PWRs. SG tube degradations have resulted in the plugging of more than 100,000 tubes around the world (*Diercks et al., 1996*).

Early problems with SG tubes were caused due to wastage, which is caused by chemical attack from acid phosphate residues in areas of low water flow (*Wade, 1995*). This problem was associated with the use of specific water chemistry (low Na/P04 molar ratio phosphate). With the introduction of secondary water treatment for pH control, this problem was mitigated (*Diercks et al*, *1996*). Then in the later years, problems with tube denting of Alloy 600 tubes became prominent. Denting is caused when corrosive material accumulates in the space between the SG tube and the support plate, leading to deformation of the tube. This problem was primarily attributed to the use of Carbon Steel support plates. Due to redesign of support plates and use of Stainless steel as plate material, the problem with denting was mitigated.

Once the problems with denting of tubes were solved, Alloy 600 (heat treated and mill annealed), became the primary choice of all SG tubes in most PWRs, because Alloy 600 was considered to be resistant to corrosion. However, a new problem surfaced in the form of a degradation mechanism called SCC of Alloy 600 tubes, which became the most dominant cause of SG tube plugging across the world (*Diercks et al., 1996*). It was found that Alloy 600 was susceptible to SCC cracks due to chrome depletion and carbides formation in grain boundaries. Once the susceptibility of Alloy 600 tubes to SCC and other forms of corrosion was established, it was deemed fit to replace the tubes with a new material called Alloy 690, which had double the Chromium content (30%). Subsequent research established the high corrosion resistance of this new material. Majority of Alloy 600 tubes in operating PWRs were then replaced by Alloy 690, which helped solved to a great extent the problem with SCC failures. Currently, out of 69 PWRs with SGs in US, 61% have tubes made of Alloy 690, while the remaining is still made of Alloy 600 (*US NRC, 2011*).

2.2 Emergence of Small Modular Reactors

Usable electricity was first generated by nuclear power in 1951 in Idaho[8]. The first commercial PWR in US had a capacity of 60 MWe, run by Shippingport Atomic Power Station, Beaver County, Pennsylvania (1957)[9]. The trend in the subsequent years was more towards large reactors due to the economies of scale. This led to the development of large scale reactor designs with capacity of around 1600 MWe. However, in recent years there has been renewed interest in small scale designs, such as SMRs (Figure 3). SMRs

[8] Idaho National Laboratory, www.inl.gov

[9] Wikipedia, "Shippingport atomic power station", Retrieved from http://en.wikipedia.org/wiki/Shippingport_Atomic_Power_Station

have an equivalent electrical power output of less than 300 MWe. SMRs are under development in South Korea (SMART), USA (NuScale, mPower, IRIS), and also in Argentina and France. The objective of SMRs is to provide a flexible, cost-effective energy alternative, manufactured centrally and transportable by truck. As such, SMRs are more suitable for use in the developing countries (low electricity demand). Besides electrical applications, SMRs can also be used for applications such as, as desalination of seawater (*International Atomic Energy Agency, 2005*).

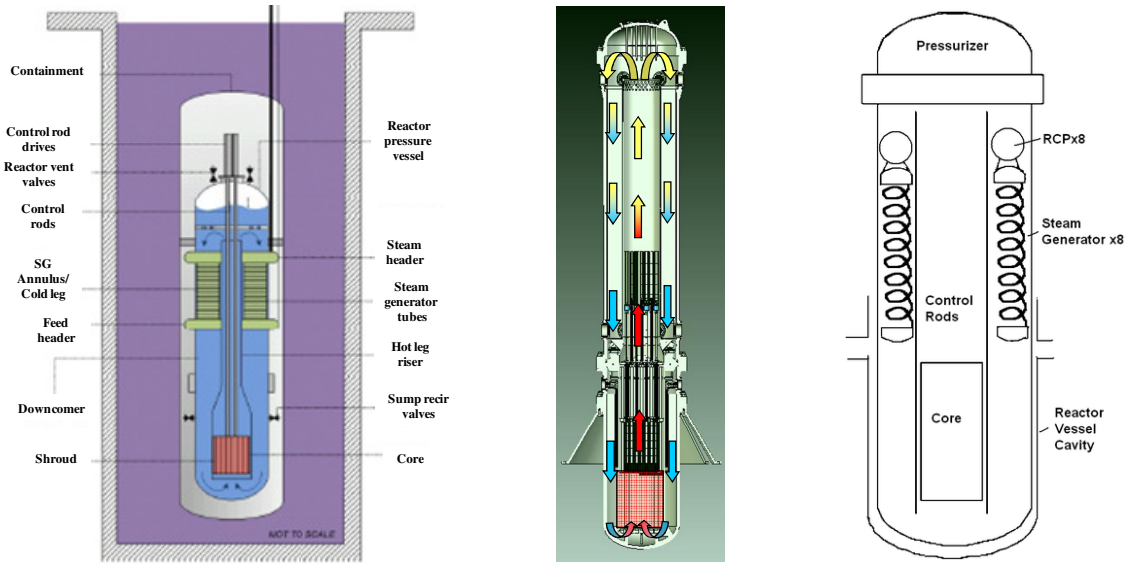

Figure 3: New designs of SMRs from left to right (Not to scale): NuScale[10], mPower[11], and IRIS[12]

Since SMR designs have small power output, the electricity would cost relatively more than for a large scale PWR. This necessitates simplification of the overall plant design and mass production, in order to beat the economy of scale (*International Atomic*

[10] US NRC, "NuScale", Retrieved from http://www.nrc.gov/reactors/advanced/nuscale.html (Modified nomenclature from original)

[11] Halfinger, J., "mPower: a Progressive Energy Solution", April 2009, available online at www.state.nj.us/dep/cleanair/hearings/powerpoint/09_mpower.ppt

[12] Wikipedia, "International Reactor Innovative and Secure", Retrieved from http://en.wikipedia.org/wiki/International_Reactor_Innovative_and_Secure

Energy Agency, 2005). Hence, the SMR designs are very different from traditional large scale PWRs that are in operation today. For example, the SGs and reactor core are integrated into one vessel and containment, doing away with the large diameter primary coolant loops. Further, use of passive safety features, such as natural circulation of primary coolant makes it more compact and safe as it does away with coolant circulation pumps. The compact design of the SMRs provides some economic benefits, in terms of the initial cost of building the plant, which is expected to be much less than those of constructing a large scale PWR. Also, the enhanced safety features make the SMRs a low-risk venture for power companies than other large scale PWRs (*International Atomic Energy Agency, 2005*).

2.3 Issues with Traditional Steam Generator Tube Rupture Frequency Assessment Method

While nuclear power plants provide affordable and clean electricity, there are severe adverse consequences, such as release of radioactivity into the atmosphere, associated with its failure. Risks from a nuclear power plant can be assessed by means of PSA[13] methods, which aim at answering three basic questions (*Modarres*, 2008):

- What are the initiating events that lead to adverse consequences?
- What is the probability or frequency of occurrence?
- What and how severe are the adverse consequences?

[13] For more information on PSA techniques please refer to IAEA-TECDOC-1200 (*IAEA, 2001*).

There are three levels of a PSA. PSA level 1 identifies the initiating events (e.g., SGTR) and assesses the frequency of reactor core meltdown starting from initiating events. PSA level 2 assesses the frequency of release of radioactivity to the atmosphere starting from the reactor core meltdown. PSA level 3 assesses the risk to public health and environment by the release of radioactivity from the power plant.

SGTR is one of the initiating events considered in level 1 PSAs that if not mitigated can potentially lead to core meltdown. SGTRs cause leakage of primary coolant to the secondary side leading to depletion of primary coolant inventory. This leads to insufficient cooling of reactor core, which can cause core meltdown. Further radioactive coolant that leaks to secondary side can release into the atmosphere through pressure relief valves in the secondary side. All scenarios involving SGTR are modeled in the PSA level 1.

In traditional PWR designs, significant initiating events were identified as the rupture or leakage in primary coolant loop pipes connecting the reactor with the SGs. These coolant loop pipes had large diameters (approximately 10 times that of SG tube). Severe loss of coolant accidents through this large diameter pipes had the potential to cause rapid meltdown of core, due to inability of emergency injection pumps to replace the lost coolants. Hence, more research efforts were directed into analysis and quantification of frequency of primary coolant pipe ruptures. With SMR designs doing away with the large diameter primary coolant pipes due to integration of SG with the reactor core, SGTR failures became prominent initiating events.

Estimation of the frequency of SGTRs has traditionally been based on historical data, which are gathered over a long period from operating PWRs having different SG geometries, environmental and operating conditions. These non-homogeneous historical data are combined to estimate the SGTR frequency. Several US NRC reports, e.g., NUREG-1829 (*Tregoning, Abramson & Scott, 2005*) and NUREG-5750 (*Poloski, Marksberry, Atwood, & Galyean, 1999*) have used historical data to estimate SGTR frequency. An essential drawback of this approach is that these historical data are non-homogeneous in nature, because they are collected from different operating PWRs. Hence the SGTR frequency would be generic and not-reactor specific. Another thing to note is that 75% of the cases of SGTR historically were caused by SCC mechanism due to the use of Alloy 600 material. Applicability of the historical data-driven frequency of SGTR to new SMR SG designs with different geometries, material properties, degradation mechanisms and thermal-hydraulic behaviors is certainly not valid (*Chatterjee & Modarres, 2012*).

A comparison of some important features of SMRs with that of large scale PWRs (Figure 4) would reveal that the SMR design is very different from existing designs of PWRs. SMRs have helically-coiled tube bundles that accommodate thermal stresses; have advanced tube material Alloy 690, which has been found to be resistant to corrosion-related mechanisms; the high pressure primary coolant loop is on the shell side, which causes low level compressive stresses. This reduces the potential of SCC in SMRs to negligible levels, because SCC occurs under constant tensile stresses in corrosion susceptible materials. Therefore these historical frequency estimates that are dominated by SCC related failures do not apply to new designs of SMRs.

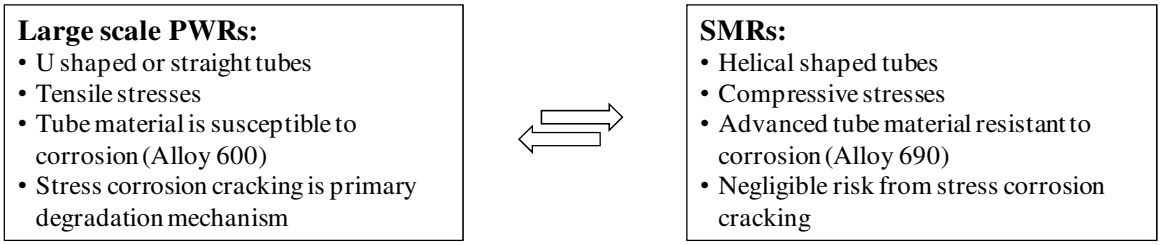

Figure 4: Basic design features of SMRs when compared to large scale PWRs

2.4 Historical Evolution of Physics-of-Failure

Reliability modeling and prediction of components has been considered historically by two different approaches: part stress modeling and physics-of-failure. Part stress modeling approach is an empirical method that is based on counting the number and type of components of the system, and the operating stresses[14]. Various standards (for electronics) have been published to specify how part stress modeling should be carried out, e.g., MIL-HDBK-217 (*Department of Defense, 1991*). These standards assume constant failure rate for components and require large amount of field data (*Bowles, 1992*). The constant failure rate assumption works when failures are due to random events. However, wear-out dominated failures (e.g., fatigue, wear) could not be described by this assumption (*White & Bernstein, 2008*). This approach relies on databases of historical failures obtained mainly from field data and sometimes from reliability test data. However, these databases would not represent new designs that are completely different from existing ones. Further, these databases include data from different sources and environments, which make them generic in nature and not component-specific. These factors led to decrease in use of these empirical standards.

[14] Adopted from Wikipedia, "Reliability Engineering", available online at http://en.wikipedia.org/wiki/Reliability_(engineering)#Reliability_prediction_and_improvement

Physics-of-failure approach, on the other hand, uses an understanding of physical failure mechanisms (e.g., corrosion, fatigue) to evaluate reliability of components. Physics-of-failure was first formally conceptualized in a symposium in 1962 organized by the Rome Air Development Center (RADC) [15]. The driving force that established this approach to reliability were concerns in the 1940s and 1950s in US military establishments regarding the reliability of electronic systems. However, mechanistic treatment of failures had its roots in the late nineteenth century when in 1870 A. Wohler summarized fatigue test results on rail-road axles, and concluded that cyclic loads are more important for determining fatigue life than peak loads. Thereafter, much of the reliability work in the first half of the twentieth century was related to fatigue and fracture of materials (fatigue failure was the main concern during World War I). For example, *Basquin* (1910) proposed a log-log relationship for stress-life (S-N) curves using Wohler's fatigue test data. *Griffith* (1921) introduced his theory of fracture while exploring the strength of elastic brittle materials.

At the start of World War II, it was discovered that over 50% of the airborne electronics equipment in storage was "unable to meet the requirements of the Air Core and Navy" (*McLinn,* 2011). In 1950 the US Department of Defense (DOD) initiated an ad hoc group on reliability of electronic equipment, which stated that to improve part reliability it was essential to develop better parts, establish quantitative reliability requirements for parts, and collect field failure data to determine the root cause of problems (*Ebel,* 1998). However, the formation of the Advisory Group on the Reliability of Electronic Equipment (AGREE) in August 1952 by DOD is often considered the

[15] Now known as the Rome Air Force Research Laboratory.

turning point in modern reliability engineering. Several reliability techniques were recommended by AGREE, which were accepted by the Department of Defense and later by NASA and many other organizations supplying high technology equipment (*Chatterjee, Modarres & Bernstein*, 2012). Thereafter, several conferences began in the 1950s to focus on various reliability topics. One conference that warrants special mention is the Holm Conference on Electrical Contacts, begun in 1955, which emphasized reliability physics. This conference established itself over the years as the primary source of reliability physics information on connectors (*Ebel,* 1998).

Against the backdrop of the developments in mechanistic-based life models (particularly to assess fatigue and fracture failures) and the AGREE recommendations, RADC introduced a physics-of-failure program in 1961 to address the growing complexity of military equipment and the consequent higher number of failures observed. In 1962, researchers from Bell Labs published a paper on "High Stress Aging to Failure of Semiconductor Devices" that justified using the kinetic theory's interpretation of the Arrhenius equation, a simple yet accurate formula for the temperature dependence of the reaction rate constant as a basis for assessment of temperature-induced aging of semiconductor devices (*Dodson & Howard,* 1961). Later, the RADC and Armour Research Foundation of the Illinois Institute of Technology (now IIT Research Institute) organized the first physics-of-failure symposium in electronics in September 1962 in Chicago. This symposium laid the groundwork for future research and development activities related to physics-of-failure by RADC and several other organizations. Numerous original papers and ideas introducing and explaining the physics-of-failure concepts and methods were presented in these symposia.

In one of the papers presented in the first physics-of-failure symposium, *Vaccaro* (1962) opined that physics-of-failure attempts to relate the fundamental physical and chemical behavior of materials to reliability parameters. This approach is based on the principle that to eliminate the occurrence of failures, it is essential to eliminate their root causes, and to do that one must understand the physics of the material and mechanisms of the failure involved. *Davis* (1962) described the need for identifying probable failure mechanisms by which components fail as a function of time, environmental and operating stresses, as well as developing mathematical models to represent these mechanisms in order to meet reliability requirements of components. Various companies and universities conducting research on failure mechanisms were identified during the symposium, e.g., Raytheon, Syracuse University, and Motorola. Although physics-of-failure was key to improving design and reliability of components, higher costs in terms of facilities and manpower was identified as the key reason for not using physics-of-failure at that time (*Ryerson, 1962*). The various key elements of physics-of-failure approach such as, failure mode, mechanism, and cause were defined for the first time in this symposium (*Zierdt, 1962; Earles & Eddins, 1962*).

Due to the success of the first symposium in 1962, four physics-of-failure symposia were held in consecutive years (until 1966) with many more papers describing concepts related to physics-of-failure. For example, *Tamburrino* (1963) provided key points about the requirements of a reliability physics program, e.g., materials, measurement techniques, and failure mechanisms. The need for part vendors to be kept abreast of available knowledge and understanding in failure physics was identified. It was stated that any changes in pre-established part processing or fabrication can potentially be a key

factor in inducing new failure mechanisms, and should be closely coordinated with reliability engineers. *Bretts, Kozol and Lampert* (1963) provided accelerated tests results for resistors, which they correlated with physical degradation models to estimate time to failure. Physics-of-failure was identified as an essential step in planning accelerated tests as well as evaluating them.

Ingram (1964) for the first time described performance characteristics and failure mechanisms of a device in probabilistic terms. He suggested that "Environmental and stress conditions applicable to the device, and its performance and strength characteristics, are expressed in the form of multidimensional probability distributions. By joint evaluation of these probability distributions, a quantitative estimate of the reliability of the device can be obtained." *Beau* (1964) described methods for managing the human elements in physics-of-failure. He described three classical causes of failure as: reliability limitation inherent in the design; reliability degradation caused by the factory process; and reliability degradation caused by the user. The human element according to him is introduced in the factor process by the factory operator, e.g., poor workmanship or operator error. *Workman* (1964) described the failure analysis practices followed in Texas Instruments at that time, and the need for incorporating information gained from failure analysis in new reliability test design, process control, and new device design.

Shiomi (1965) introduced a generalized cumulative degradation model for estimation and prediction of component life under successive different stress levels. *Partridge, Hall, and Hanley* (1965) described the need for qualification and engineering evaluations to

select vendors who are capable of supplying reliable semiconductor parts. They further stated that qualification tests alone are insufficient to determine the ability of vendors, but production procurement data from screen and burn-in can provide sufficient vendor history. *Church and Roberts* (1965) presented different causes of failure of a component, such as due to accidental damage during manufacture, assembly, testing, storage, or failure in service due to operating conditions or failure of another component.

Thomas (1966) used basic concepts of dimensional analysis to make general examination of mathematical models, e.g., Eyring's equation. He opined that the concepts of signal, noise and dimensionless variable can be used to formulate mathematical models, physical laws, and probability distributions. *Schenck* (1966) presented two forms of progressive failure mechanisms of a commercial silicon diode, and studied them as a function of various stress and measurement variables. *Gill and Workman* (1966) presented reliability screening procedures for integrated circuits, consisting of destructive tests as well as nondestructive inspections and screening.

From 1967 on, IEEE sponsored the Reliability Physics Symposium (IRPS) that continues today to present a wide range of physics-of-failure related research. For example, *Ryerson* (1967) presented mathematical models for semiconductor diodes illustrating how failure mechanisms, part strengths, and application stresses interact and affect the failure rate of component parts. *Keen, Loewenstern, and Schnable* (1967) presented mechanisms of failure in ohmic and expanded contacts, including metal-semiconductor contacts and bonds to metallization in semiconductor devices. *Payne* (1967) presented a failure mechanism for barium titanate capacitors studying the physics-

of-failure. *Frankel and Kinsolving* (1970) discussed the need of reliability testing of components for hostile environments, by first simulating field conditions and then developing accelerating laboratory conditions. *Hollingshead* (1970) introduced a technique for optimizing the selection of parts for system application by reliability and quality levels through systematizing the compilation and processing of necessary data. The comparative influence of performance parameters such as repair cost, storage time, and cost of failure were discussed. *Schwuttke* (1970) showed that peripheral yield loss in silicon wafers can be minimized whenever temperature gradients arising during cooling of a row of wafers are eliminated.

The IEEE symposium on reliability physics continued to be organized through the 1970s and 1980s disseminating a plethora of knowledge on physics-of-failure. Several failure mechanisms and mathematical models were reported for a wide range of electronic components such as capacitors, semiconductors, resistors, and interconnects. *Agarwala* (1975) presented experimental results for electromigration failures in thin-film conductors. *Brodeur* (1975) described high temperature operating life test as a measure of processes used in fabrication of semiconductor wafers. *Crook* (1979) presented a model for time dependent dielectric breakdown of semiconductors as a function of operational and environmental conditions, as well as the device physical parameters. *Hieber and Pape* (1984) presented a creep-rupture equation that calculates time to rupture as a function of applied mechanical load and temperature. *Conrad, Mielnik, and Musolino* (1988) presented a methodology to monitor and predict early life reliability failure mechanisms.

The IEEE Reliability Physics Symposium continued to be held in 1990s until today presenting physics-of-failure research. By the late 1980s and early 1990s, several publications on physics-of-failure related research separate from the IEEE *Reliability Physics Symposium* also appeared. For example, *Pecht, Dasgupta, Barker, and Leonard* (1990) advocated use of physics-of-failure approach for reliability assessment as opposed to the part count technique. *Dasgupta and Pecht* (1991) presented material failure mechanism and damage models. *Engel* (1993) presented failure models for mechanical wear modes and mechanisms. *Pecht and Dasgupta* (1995) discussed physics-of-failure as an approach to reliable product development.

Although several studies related to physics-of-failure continued to be published through the 1990s and 2000s, a trend towards probabilistic consideration of physics-of-failure also emerged from the early 1990s. For example, *Hu, Pecht, and Dasgupta* (1991) presented a probabilistic approach for predicting thermal fatigue life of wire bonding in microelectronics. *Mendel* (1996) formally described probabilistic physics-of-failure (PPoF) as a technique in which the statistical lifetime model is derived considering the physics-of-failure, and presented a case for applying PPoF in design for reliability. Later *Modarres, Kaminskiy, and Krivtsov* (1999) also recognized that prediction of failure is inherently a probabilistic problem due to uncertainties associated with physics-of-failure models and their parameters and with failure-inducing agents that can result from changes in environmental, operating, and use conditions. Several publications related to the PPoF then appeared from the early 2000s. For example, *Haggag, McMahon, Hess, Cheng, Lee and Lyding* (2000) presented a PPoF approach to reliability assurance of high-performance chips that considered common defect activation energy distribution.

Hall and Strutt (2003) presented PPoF models for component reliabilities by considering parameter and model uncertainties. *Azarkhail and Modarres* (2007) presented a Bayesian framework for physics-based reliability models. *Matik and Sruk* (2008) highlighted the need for physics-of-failure to be probabilistic in order to consider variations of variables involved in processes contributing to the occurrence of failures. *Chamberlain, Chookah, and Modarres* (2009) presented a PPoF model for reliability assessment of gas cylinders incorporating various uncertainties.

Although quite a bit of research has been done on PPoF modeling for reliability assessment, this approach is still in its infancy stage with lot of scope for future research in terms of addressing the physics-of-failure of new materials and designs; more expansive characterization of uncertainties in failure-inducing agents, manufacturing methods, environmental conditions, model uncertainties and measurement errors; and propagating all the uncertainties (including parameter and model) to predict the failure frequency.

2.5 Probabilistic Physics-of-Failure Based Approach

In this research, a PPoF-based SGTR frequency assessment approach has been developed that considers physics-of-failure to formulate mechanistic degradation models affecting SG tubes; characterizes various uncertainties associated with factors such as, manufacturing methods, environmental conditions, operating conditions, material properties, model uncertainties, and measurement errors; and then simulates the degradations using PPoF models propagating the uncertainties to predict the SGTR frequency.

In this section, the PPoF-based framework for SGTR frequency assessment is first presented with detailed discussions of key steps in the PPoF approach. This is followed by sub-sections on the identification of primary applicable failure mechanisms in SMRs considering the underlying degradation conditions; proposed PPoF models for primary applicable failure mechanisms considering all the epistemic and aleatory uncertainties; approach for assessment of stress agents acting on SG tubes considering uncertainties in tube geometrical and material properties; and a probabilistic approach for propagating the uncertainties to estimate the distribution of the SGTR frequency.

The PPoF-based SGTR frequency assessment approach is as shown by Figure 5. The approach starts with identification of the degradation conditions prevailing in the SG during normal operating conditions, which are created by a combination of factors, including the SG design and the operating conditions (*Chatterjee & Modarres, 2012*). The design can be captured in terms of tube material, tube coil shape and geometry, tube geometry, number of support points, horizontal and vertical pitch, and primary and secondary coolant composition. The operating condition can be captured in terms of the primary and secondary coolant pressure and temperature, the mode of primary coolant circulation (forced or natural), presence of flow-induced turbulence or other vibration excitation mechanisms in the tube bundle, and presence of any corrosive particles in the primary coolant. The factors above create the degradation conditions that activate the failure (degradation) mechanisms in the SG tubes.

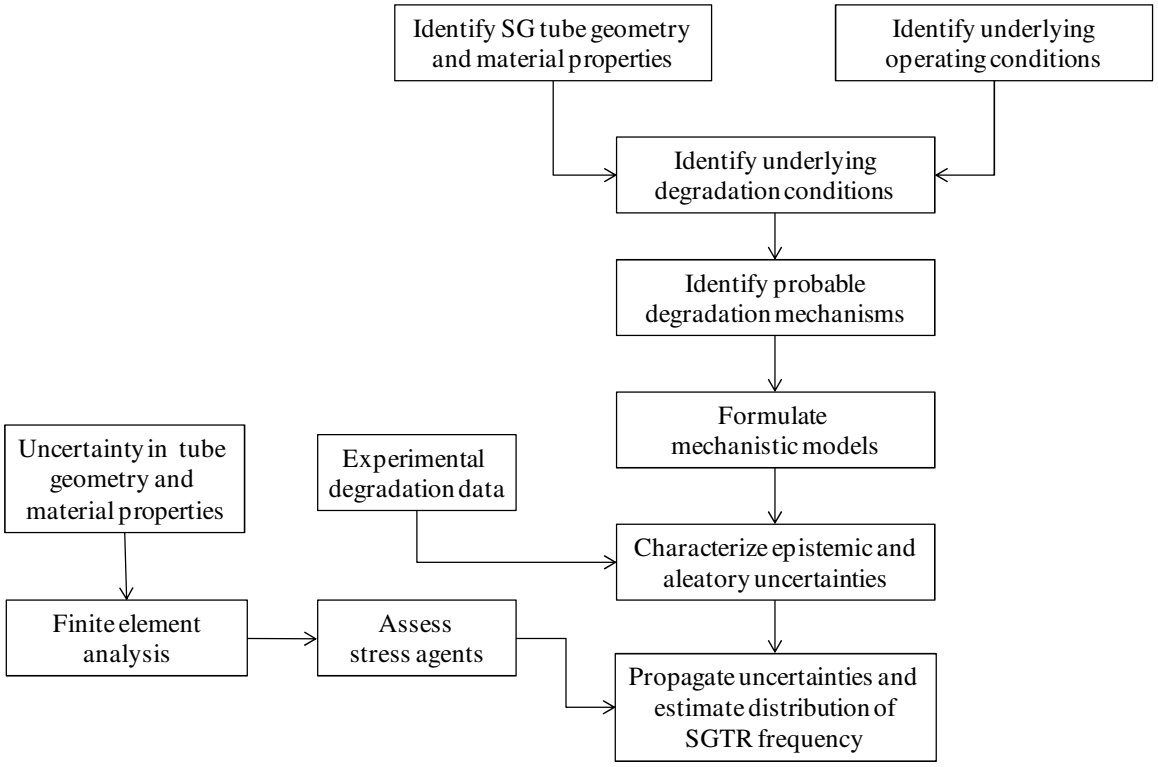

Figure 5: PPoF approach for SGTR frequency distribution assessment

Based on the prevailing degradation conditions in the SG, the dominant failure mechanisms are then identified. For example, the use of Alloy 600 tube material makes the tube more susceptible to corrosion related mechanisms, such as SCC. Fluidelastic instability or turbulence excitation leads to alternating stresses in the tubes that can cause fatigue if there is any localized degradation in the tubes. It is important to note that certain degradation conditions can lead to initiation of more than one degradation mechanisms. For example, corrosive conditions can cause corrosion fatigue and also SCC of tubes. However fatigue corrosion is caused by alternating tensile stresses (e.g., caused by tube vibrations), whereas SCC is caused by constant tensile stresses (e.g., caused by pressure differentials or residual stresses). Therefore it is important to understand each degradation mechanisms properly.

Having identified the primary applicable failure mechanisms, the next step is to formulate their PPoF models. The PPoF models (damage-endurance) are formulated considering the critical variables (e.g., among material properties, environmental conditions, stress agents, and geometry) that contribute to the creation of degradation conditions leading to onset of physical failure mechanisms. For example, critical variables responsible for tube degradation by fretting wear mechanism are normal loads, oscillation amplitudes, oscillation frequency, operating temperature and material hardness of the contacting surfaces. Quantitative models are then formulated to correlate these critical variables with the damage growth parameter (e.g., wear volume loss rate) for the concerned mechanism (e.g., fretting wear). Material degradation data obtained experimentally at PWR environments are used to formulate the correlations. In some cases, well established correlations from literature for the concerned degradation mechanism are also used for this purpose, provided they apply to the experimental data. It is critical to ensure that the developed PPoF models properly represent the underlying degradation conditions and the underlying mechanical, chemical, or thermal processes that lead to failure of SG tubes. The epistemic and aleatory uncertainties associated with model and data are then characterized. For this a Bayesian regression framework needs to be developed that can combine prior information on model parameters with experimental data to infer the posterior probability distributions of parameters, including model error.

Each failure mechanism has specific stress agents that propagate the degradations. For example, fatigue stress agents are alternating stresses whereas SCC stress agents are constant tensile stresses. A detailed finite element analysis (or other alternative approach) is required to determine the stress agents resulting from the prevailing operating

conditions, e.g., flow-induced vibration. Uncertainties in the input parameters for the finite element analysis, e.g., tube geometry, material properties, and environmental conditions need to be considered in the evaluation of stress agents.

An approach needs to be then developed to propagate all the associated uncertainties (e.g., model, parameters, and initial flaws) to estimate the distribution of SGTR frequency using the PPoF models under the prevailing stress agents. Appropriate failure criteria need to be defined for each failure mechanism considering the operability or safety requirements of a particular PWR. For example, a failure criterion for normal operating condition-induced fatigue mechanism can be defined as the through-wall cracks reaching the wall thickness of tubes (*Chatterjee & Modarres, 2012*). However, in some cases such as accident induced failures, the failure criterion need to consider burst pressure and go beyond the wall thickness criterion.

2.5.1 Identification of Primary Degradation Mechanisms during Normal Operating Conditions

Degradation mechanisms are the physical, thermal, chemical, or electrical processes by which degradations (e.g., cracks, pits) initiate or propagate in a structural component. Degradation mechanisms occur due to operating conditions combined with geometrical and material properties. Operating conditions consist of environmental conditions and physical loads. Normal operating conditions[16] in SMRs may include constant pressure differential (primary side: 15 MPa and secondary side: 6 MPa) across the tube thickness, inlet and outlet temperature conditions in the shell side (primary: superheated water) of

[16] Values for pressure differential and temperature conditions are not the actual ones used in any SMR SGs. The intent is to provide an idea of normal boundary conditions in typical SMR SGs.

315C and 275C respectively, inlet and outlet temperature conditions in the tube side (secondary: liquid water) of 220C and 275C respectively.

The primary coolant flows by natural circulation through the tube bundle in the shell side of the SMR SG. This means that the flow velocity would not exceed small values in the SMR SG during normal operating conditions. Low-level of tube vibrations is generally observed in SG tube bundles during normal operating conditions. Due to cross-flow through the helically-shaped tube bundles (as opposed to U-tubes or straight-through tubes used in currently operating PWRs) in the SMR SGs, tube vibrations would be the primary cause of operational stresses.

Performance demands were modest in the earlier days and also the power plant equipments were made robustly. Therefore, flow induced vibration problem was not considered a serious issue then. However, with increasing demand for higher performance and availability of better quality materials (e.g., high strength), SG tubes became more flexible and were subjected to higher flow rates (*Weaver, Ziada, Au-Yang & Chen*, 2000). Flow-induced vibration phenomena thus became an issue of significance. In PWR SGs, vibration of tubes can be excited by flow-induced mechanisms such as, fluid-elastic instability, turbulence excitation, and vortex shedding.

Fluid-elastic instability is a self-excited mechanism and depends on the mutual interaction of fluid dynamic forces and the elastic structural displacements (*Weaver, Ziada, Au-Yang & Chen*, 2000). Fluid-elastic instability occurs only if effective gap flow velocity exceeds a certain critical velocity, and will lead to very high amplitude tube vibration (*Axisa, Antunes, & Villard, 1990; Taylor & Pettigrew, 2000*). Fluid-elastic

instability can be avoided through proper design of SGs. Vortex shedding is a form of periodic excitation and also leads to high amplitude vibration but is inhibited by turbulence. Fluid-elastic instability and vortex shedding lead to resonant vibration in the tubes, causing failure in quick time or overstress failures. These high amplitude vibration excitation mechanisms should not occur for normal operating conditions in SGs (*Connors, 1981*).

Unlike vortex-induced vibration and fluid-elastic instability, turbulence-induced vibration cannot be avoided completely. Turbulence-induced vibration of tubes occurs even at low primary coolant velocities in SG tube bundles. Low levels of turbulence are desirable because it increases the efficiency of heat transfer. Turbulence-induced excitation forces the tubes to vibrate and induces enough response to cause long-term damage, e.g., fatigue and fretting-wear (*Taylor & Pettigrew, 2000*). Table 2 summarizes the vibration excitation mechanisms in SG, their occurrence conditions, and effect on tube reliability.

Any severe transient condition that can lead to change in normal pressure differential or temperature conditions, or cause high-amplitude tube vibrations such as due to feedwater or steam header line break are not considered as normal conditions. Also, other accident scenarios such as loss of off-site power and earthquakes that can cause severe transients are not part of normal operating conditions.

Table 2: Vibration excitation mechanisms in tube array caused by cross-flow

Vibration excitation mechanisms	Occurrence conditions	Effects
Fluid-elastic instability	High gap flow velocities	High amplitude vibration and failure in quick time
Vortex shedding	Medium gap flow velocities	High amplitude vibration and failure in quick time
Turbulence excitation √	Low gap flow velocities	Low amplitude vibration causing long-term damage, e.g., fatigue, fretting wear

Several probable degradation mechanisms may be prevalent in SGs during normal operating conditions, such as wastage, denting, pitting, SCC, fatigue, fretting wear. As discussed earlier, with the use of Alloy 690 risks from most of the corrosion related degradation mechanisms have been mitigated to a great extent (Table 3). Risks from creep failure were not considered because it is not likely to occur during normal operating conditions, due to high melting point of Alloy 690 material (approximately 1350C) and absence of any serious long term constant stress conditions during normal operation in the SMR SGs. However, Alloy 690 tubes with pre-existing flaws in the SMR SGs would be more susceptible to mechanical fatigue damage due to fluctuating stresses resulting from flow-induced tube vibration, thermal fatigue damage from thermal stresses, and fretting-wear damage from the relative motion between the tube and supports (*Chatterjee & Modarres, 2012*).

Thermal stresses can result due to factors such as thermal coefficient mismatch between two dissimilar materials, and/or restraint on thermal growth. Temperature transients, e.g., during normal heating-up of tubes, can lead to thermal expansion of the tubes. In the helical-coil tube design, the tubes are free to expand radially and hence the helical coils in the SMR SGs accommodate thermo-mechanical stresses from thermal

expansion of tubes during normal heating-up (*Cinotti, Bruzzone, Meda, Corsini, Lombardi, Ricotti & Conway, 2002*). Also, thermal stresses by itself cannot cause a crack to grow, unless there is frequent shut downs and start-ups, chances of which are negligible unless there is abnormal conditions (severe temperature transients such as during meltdown). Table 3 summarizes the leading failure mechanisms that have been responsible for SGTRs in the past. Since the SMR SG tubes are made of Alloy 690 material, which is resistant to SCC and other general corrosion mechanisms, mechanical fatigue and fretting wear have been considered in this research as the primary failure mechanisms with the potential to cause SGTR events under the normal operating conditions.

Table 3: Identification of leading failure mechanisms in SG helical tubes during normal operating conditions

Failure mechanisms	Degradation conditions	Conditions in helical SG design
Stress corrosion cracking	Constant tensile stresses, corrosion susceptible material, corrosive environment	Compressive stresses, Alloy 690 tube material (high corrosion resistance)
Pitting corrosion	Corrosive environment, corrosion susceptible material	Alloy 690 tube material (high corrosion resistance)
Fatigue √	Alternating stresses, localized degradation	Alternating stresses due to flow-induced tube vibration, manufacturing flaws
Fretting wear √	Oscillatory small amplitude sliding motion between contacting components	Relative fretting motion between tube and support plates due to flow-induced tube vibration

2.5.2 Probabilistic Physics-of-Failure Model Formulation

In this section, PPoF models are proposed for mechanical fatigue and fretting wear degradation mechanisms in Alloy 690 SMR SG tubes. The PPoF models are developed considering the underlying degradation conditions that are a result of operating conditions and tube geometrical and material properties. All important variables that contribute to the creation of degradation conditions leading to onset of physical failure mechanisms (mechanical fatigue and fretting wear) have been considered systematically to formulate the PPoF models. Uncertainty analysis has been performed to characterize the epistemic and aleatory uncertainties associated with the models and the data, and estimate probability distributions of the PPoF model parameters. In the following sub-sections, basic understanding of the failure mechanisms is first presented, followed by a literature survey of quantitative modeling efforts and experimental investigations. Then the proposed PPoF models are presented discussing the approach used to formulate the model considering the physics-of-failure, and characterize the uncertainties in the model and data.

2.5.2.1 Fatigue

Fatigue-induced fracture and rupture is one of the significant failure mechanisms in SG tubes that initiates from localized degradation and damage. For example, it may originate from corrosion pits or pre-existing manufacturing flaws. This research focuses on the cracks originated during the manufacturing process since the potential for pitting is negligible for Alloy 690.

ASTM Standard E-1150 (2010) defines fatigue as "the process of progressive localized permanent structural damage occurring in a material subjected to conditions that produce fluctuating stresses and strains at some point or points and that may culminate in cracks or complete fracture after a sufficient number of fluctuations". Two types of fatigue failure can result depending on the load applied. If applied load is higher than the yield strength but lower than tensile strength of the material (enough to cause plastic deformation) then this results in low-cycle fatigue. However, if the applied load is lower than the yield strength (by two or three times) and causes elastic deformation then this results in high-cycle fatigue.

Fatigue occurs due to alternating or cyclic stresses, e.g., bending and torsion. Also, the stresses need to be always tensile for fatigue crack propagation. Generally, stress concentrations in a structural component, e.g., pits, holes, corners, welds, and inclusions, are the hot spots that act as initiation point for fatigue failures. A typical fatigue rate curve is represented by crack growth per cycle of loading (da/dN) versus the fluctuation of the stress-intensity factor at the tip of the crack (ΔK) as shown in Figure 6, where N is the number of fatigue cycles. The curve is defined by three regions, i.e., I, II and III (*Beden, Abdullah, & Ariffin,* 2009). Region I represents the nucleation and initiation point for fatigue cracks; Region II represents the crack propagation zone where the crack growth rate (CGR) varies approximately linearly with the change in stress intensity factor; and Region III represents the unstable fatigue crack growth leading to sudden fracture. This research focuses on region II of fatigue rate curve, i.e., linear elastic region, since manufacturing flaws are considered to be the cause of initial cracks. Also, since the through-wall depth of SG tubes are of the order of few millimeters, the cracks are

assumed to grow linearly through the thickness of tubes. Accordingly in this research, fatigue failure is assumed to occur when through-wall cracks propagate to 100% through-wall thickness of the tubes.

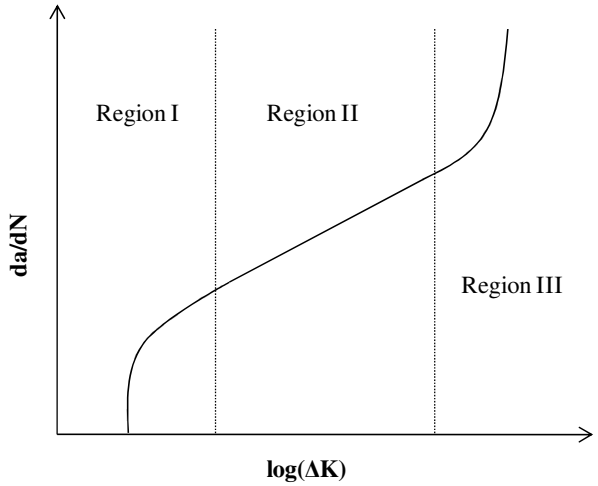

Figure 6: Typical da/dN versus ΔK curve

In order to understand fatigue mechanism it is also necessary to describe the three different modes of fracture, which represents ways of applying a load for crack propagation, as shown in Figure 7. Mode I crack is the opening mode, mode II crack is the sliding mode, and mode III crack is the tearing mode[17]. In this research we analyze the Mode I crack opening mode, because it is typically more critical from the design standpoint (lower fracture toughness with respect to Mode II and Mode III).

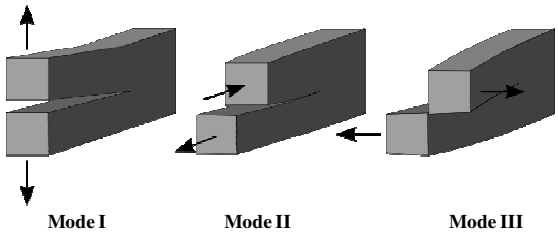

Figure 7: Three modes of fracture[17]

[17] Wikipedia, "Fracture", Retrieved from http://en.wikipedia.org/wiki/Fracture

2.5.2.1.1 Literature Review

The fatigue crack growth prediction models are developed to support the damage endurance concepts in structures, and are based on fracture mechanics (*Beden, Abdullah, & Ariffin,* 2009). In the past, several models have been developed to predict fatigue crack growth under constant and variable amplitude loading. *Paris and Erdogan* (1963) proposed a power-law relationship between fatigue CGR and stress intensity factor range, which is more popularly known as the Paris Law. It is given by the following relationship, where c is the intercept and p is the slope on the log-log plot of da/dN versus ΔK.

$$\frac{da}{dN} = c(\Delta K)^p \tag{1}$$

The limitation of the Paris law is that it does not consider the effect of stress ratio, R. *Walker* (1970) improved the Paris model by including the effect of stress ratio, as shown in Eq. (2):

$$\frac{da}{dN} = c\left[\frac{\Delta K}{(1-R)^{1-b}}\right]^p \tag{2}$$

Although stress ratio effect was introduced in the Walker model, it did not account for the region III (unstable) of fatigue curve. *Forman* (1972) proposed a model that can represent region III of the fatigue CGR curve, which is given by:

$$\frac{da}{dN} = \frac{c(\Delta K)^p}{(1-R)(K_c - K_{max})} \tag{3}$$

where K_c is the fracture toughness. All the models discussed so far are for the case of constant amplitude loading, which do not represent the fatigue CGR process during variable amplitude loading. During variable amplitude loading, stresses of differing magnitudes affect the CGR depending upon their sequences, as well as there are load interactions that can alter the CGR behavior (*Beden, Abdullah, & Ariffin,* 2009). *Barsom* (1976) proposed the following relationship for fatigue CGR under variable amplitude loading conditions:

$$\frac{da}{dN} = c(\Delta K_{rms})^p \tag{4}$$

where,

$$\Delta K_{rms} = \sqrt{\frac{1}{n}\left(\sum_{i=1}^{n} \Delta K_i^2\right)} \tag{5}$$

In Eq. (5), ΔK_i is the stress intensity factor range in the i_{th} cycle. *Hudson* (1981) used the RMS approach for predicting the fatigue CGR under variable amplitude loading that is based on *Forman* (1972) model:

$$\frac{da}{dN} = \frac{c(\Delta K_{rms})^p}{(1 - R_{rms})K_c - \Delta K_{rms}} \tag{6}$$

Several investigations on fatigue crack growth in Alloy 690 material have also been conducted in the past. NUREG-6721 (*Chopra, Soppet, & Shack,* 2001) presents a model (Eq. 7) for fatigue failure of Alloy 690 SG tubes in PWR environments, based on some

investigations performed at the Argonne National Laboratory[18]. We term this model as the "Argonne model" in this research.

$$\frac{da}{dN} = C_{A690}(1 - 0.82R)^{-2.2}(\Delta K)^{4.1} \quad (7)$$

where, C_{A690} expresses the dependence on temperature. *Park, Kim, Lee, and Rheem* (1996) conducted fatigue crack growth tests to study the effects of heat treatment on fatigue behavior of Alloy 600 and Alloy 690 materials. Previous fatigue test results have shown no enhancement to the CGR of Alloy 690 in a PWR environment as opposed to CGRs in air. It has been demonstrated that SG Alloy 690 tube fatigue crack growth response under PWR environments can be characterized using standard specimen geometries (e.g., plates) in air (*Young & King, 2005; Young, Gaoa, Srivatsan, & King, 2006; Young, Van Der Sluys, & King, 2006*).

2.5.2.1.2 Proposed Probabilistic Physics-of-Failure Model

For austenitic stainless steels, temperature, stress ratio, and cyclic frequency have a significant effect on CGRs (*Chopra, Soppet, & Shack,* 2001). In the Argonne model (Eq. 7), the value of the exponent of stress intensity factor range was assumed to be the same as that for Alloy 600. This assumption can lead to fatigue CGR not representative of Alloy 690 since it has different material composition as compared to Alloy 600. Also, the functional form as well as the corresponding parameter values for stress ratio dependence was assumed to be same as that of Alloy 600, which again can lead to inaccurate prediction of fatigue life for Alloy 690 SG tubes. Further, all the parameter values were

[18] www.anl.gov

determined deterministically and hence the uncertainties in models and data were not characterized. These uncertainties can affect the fatigue life of Alloy 690 substantially.

As has been discussed in earlier sections, fatigue CGR in a material can be affected by several variables prominent among them being loading ratio, loading frequency, applied cyclic loading, crack geometry, and component geometry. In this research we represent fatigue CGR in Alloy 690 SG tubes as a function of the critical variables that can affect the CGR in PWR environments, as shown in Eq. (8):

$$\frac{da}{dN} = f(fr, R, \Delta\sigma, a, Y) \tag{8}$$

where, fr is the loading frequency, R is the loading ratio given by $\frac{\sigma_{min}}{\sigma_{max}}$, where σ_{max} is the maximum stress in a loading cycle, and σ_{min} is the minimum stress in a loading cycle, $\Delta\sigma$ is the applied load variation given by $\sigma_{max} - \sigma_{min}$, a is the crack through-wall depth, and Y is the geometric factor that accounts for the crack length and component geometry. The effect of the applied load variation, crack through-wall depth, and geometry factor is represented by the stress intensity factor range, as shown in Eq. (9):

$$\Delta K = \Delta\sigma\sqrt{\pi a}Y \tag{9}$$

Paris and Erdogan (1963) established the power law relationship between the CGR and stress intensity factor range, which is widely accepted and used until today. This relationship also applies to the experimental data for fatigue crack growth in Alloy 690 material in PWR environments, as shown in Figure 8. In this research, the power law

relationship is used between the CGR and stress intensity factor range, as shown in Eq. (13):

$$\frac{da}{dN} \propto (\Delta K)^p \tag{10}$$

The frequency dependence of the CGR was analyzed using available data for Alloy 690 and was found to have no considerable effect on CGRs for the temperature range of interest (normal conditions). This was also substantiated by NUREG-6721 (*Chopra et al., 2001*). The loading ratio significantly affects the fatigue CGR (Figure 9). NUREG-6721 (*Chopra et al., 2001*) proposed the following functional form for stress ratio dependence of CGRs for the Argonne model, as shown in Eq. (11). However, it has not been described as to how this relationship has been formulated. Also, the deterministic values of function parameters estimated for Alloy 600 has been applied to Alloy 690.

$$f(R) = (1 - 0.82R)^{-2.2} \tag{11}$$

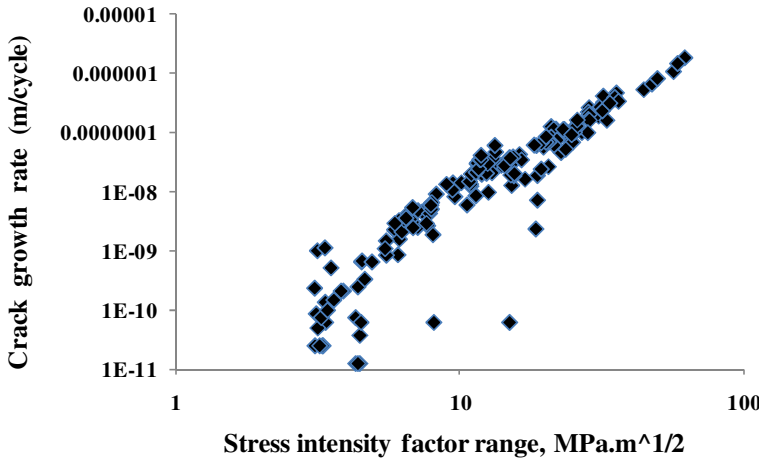

Figure 8: Alloy 690 fatigue crack growth data (log-log)[19]

[19] Argonne National Laboratory, www.anl.gov

Several other forms for stress ratio have been proposed, e.g., $(z - R)^p$ (*Bamford, Liaw, & Eason, 1990*); $(z + bR)$ (*James & Jones, 1985*); and $(\frac{1}{[1-0.05R]})^4$ (*Bernard & Salama, 1982*) where $z, p,$ and b are constants. As can be seen from the Figure 9, decrease in stress ratio leads to increase in the CGR as a function of maximum stress intensity factor. Based on literature review and also some preliminary analysis using the experimental Alloy 690 fatigue crack growth data, we propose a functional form for stress ratio dependence as shown in Eq. (12), where $z, t,$ and b are parameters.

$$f(R) = (1 - zR^t)^{-b} \tag{12}$$

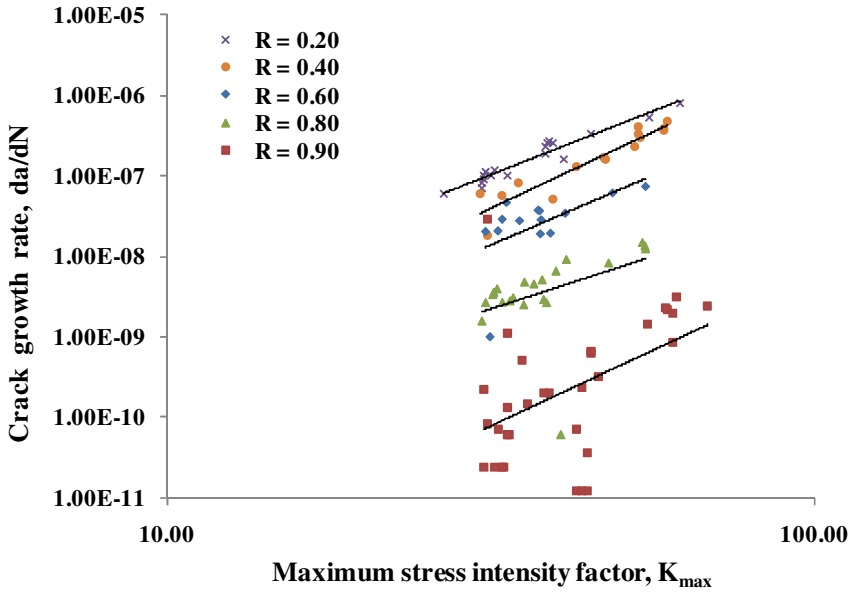

Figure 9: Stress ratio effect on Alloy 690 fatigue CGR (log-log)[20]

Using this functional form for stress ratio, the basic model structure for fatigue crack growth in Alloy 690 material can be represented as shown in Eq. (13):

[20] Argonne National Laboratory, www.anl.gov

$$\frac{da}{dN} = c(1 - zR^t)^{-b}(\Delta K)^p \quad (13)$$

where, c, p, z, t, b are the model parameters expressing dependence[21] on environmental conditions (e.g., temperature) and material properties (e.g., yield and tensile strengths). In order to verify the model structure and estimate the parameters characterizing all the uncertainties, a Bayesian regression approach (Figure 10) was developed. There are two basic forms of uncertainties: epistemic and aleatory. *Moss and Kiureghian* (2006) defined aleatory uncertainty as "inherent randomness that is a function of the phenomena that the model strives to predict". This type of uncertainty cannot be reduced, whereas the other type of uncertainty (i.e., epistemic) can be reduced by using more and accurate data (without measurement errors), and also incorporating uncertainty in the input parameters.

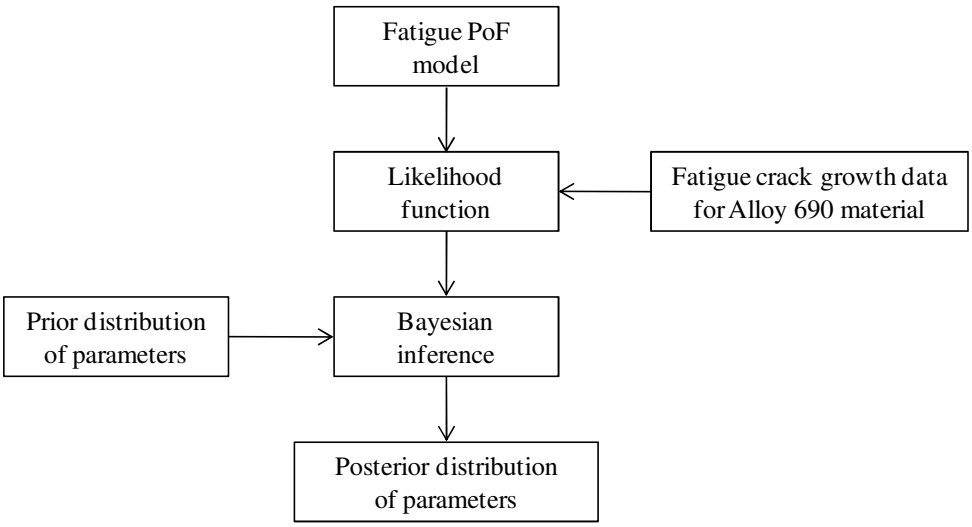

Figure 10: Estimating fatigue PPoF model parameter distributions

[21] Values of these parameters are obtained through regression analysis that uses Alloy 690 material degradation data obtained experimentally at PWR environments. Hence, values of these parameters represent dependence of CGR on environmental conditions and Alloy 690 material properties.

Bayesian approach was chosen for this analysis because it provides for the updating concepts, which provide a powerful means for knowledge management (*Azarkhail & Modarres, 2007*). In the Bayesian approach to regression, a large value of the likelihood function represents a better model fit to the data. The likelihood function is defined based on the distribution of model error, which for the best fitted model is assumed to be normally distributed with mean zero and standard deviation, σ.

The epistemic uncertainties are expressed partly in terms of posterior distributions of model parameters, e.g., c and p, and partly by the model error distribution. Aleatory uncertainties are expressed partly in terms of the model error distribution, and partly by the scatter in the measured data (e.g., CGR). The method used in this research to assess the proposed model is based on the value of the likelihood function. The likelihood function value was calculated using the posterior model parameters obtained from Bayesian regression. A model that results in a larger value of the likelihood function is the best-fit model. The proposed fatigue model equation is further re-written as following in order to make the variables on right side independent of each other.

$$\frac{da}{dN} = c(1 - zR^t)^{-b}[K_{max}(1 - R)]^p \tag{14}$$

In order to define the likelihood function, we assume that the model error follows a normal distribution with mean zero and standard deviation σ.

$$\frac{da}{dN} = c(1 - zR^t)^{-b}[K_{max}(1 - R)]^p + \varepsilon(0, \sigma) \tag{15}$$

The likelihood function of n CGR data points for Alloy 690 material is defined using Eq. (20) assuming a normal distribution for the dependent variable, i.e., CGR, with same standard deviation as that of the model error, as shown in Eq. (16).

$$L(CGR\ data|c,p,z,b,t,\sigma^2) = \frac{1}{\sqrt{(2\pi)^n \sigma^{2n}}} exp\left[-\frac{1}{2\sigma^2}\sum_{i=1}^{n}\left(CGR_i - c\left(1 - zR_i{}^t\right)^{-b}\left[K_{max,i}(1-R_i)\right]^p\right)^2\right] \quad (16)$$

Since we started with no past experience (i.e., prior information about the distribution of parameters) in this research, non-informative or uniform prior distributions were assumed for parameters c, p, z, b, t and σ. Experimental data for fatigue crack growth in Alloy 690 tubes from Argonne National Laboratory (Figure 8) were used to determine the marginal posterior probability density distributions for the parameters. WinBUGS v.14 (*Cowles, 2004*) software was used to perform the Bayesian regression analysis and obtain the posterior distributions. The resulting distributions of some of the parameters and model error are shown in Figures 11 & 12 below:

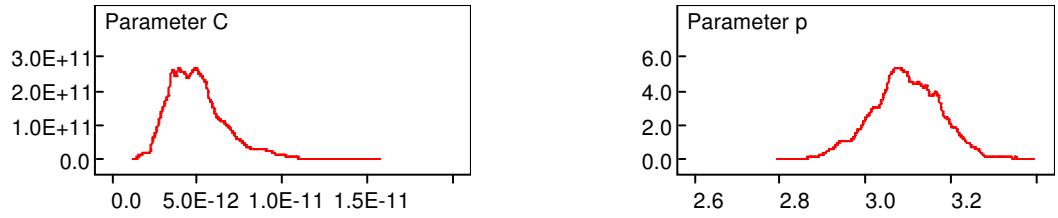

Figure 11: Distributions of model parameters

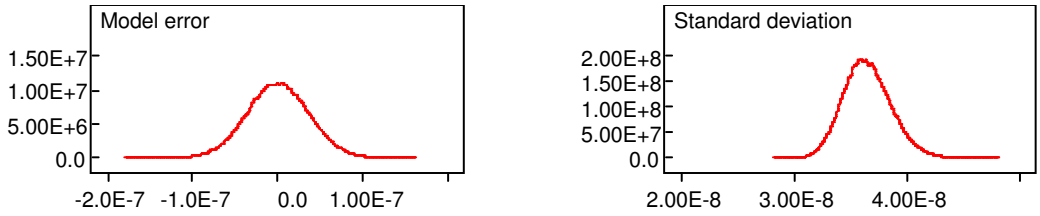

Figure 12: Distributions of model error and standard deviation

In order to compare the extent of fit of the proposed model with that of other models to Alloy 690 fatigue crack growth data, Bayesian regression analysis was also performed with the Argonne and Walker (*Walker*, 1970) models. These two models were chosen for comparative analysis based on the facts that Argonne model was developed specifically for Alloy 600 and 690 SG tubes, and the Walker model is the earliest and most popular generic model for stress ratio dependence of CGRs in the linear region (Region II). It was found that model error was lower in case of the proposed model when compared to Argonne and Walker models. The likelihood function value was higher for the proposed model than the Argonne and Walker models (Table 4).

Table 4: Comparison of proposed, Argonne, and Walker models

Model	Model error standard deviation	Log-Likelihood function values
Proposed	3.64e-8	1123.52
Argonne	3.74e-8	1090.68
Walker	3.71e-8	1061.38

In order to rank the three models according to goodness of fit, two information criteria were used: Akaike information criterion (AIC) (*Akaike, 1974*) and Bayesian information criterion (BIC) (*Schwarz, 1978*), as shown by Eqs. (17) and (18).

$$AIC = 2k - 2log(L) \tag{17}$$

$$BIC = -2\,log(L) + klog(n) \tag{18}$$

where, k is number of independent model parameters, n is number of data points, and L is maximized value of likelihood function. According to these criteria, the preferred model is the one with minimum AIC or BIC values. The proposed model was the best-fit model for the Alloy 690 fatigue CGR data according to both the criteria (Table 5).

Table 5: Ranking of proposed, Argonne, and Walker models

Model	Akaike information criterion		Bayesian information criterion	
	Value	**Rank**	**Value**	**Rank**
Proposed	-2237.04	1	-2236.02	1
Argonne	-2173.36	2	-2172.54	2
Walker	-2116.76	3	-2116.15	3

This proposed model can better predict the fatigue crack growth in Alloy 690 materials in air as well as PWR environments. The mean and standard deviation values of the proposed PPoF model parameters are as shown in the Table 6.

Table 6: Proposed fatigue model parameters

Parameters	Values estimated through Bayesian regression
μ_c, σ_c	5.02e-12, 2e-13
μ_p, σ_p	3.1, 0.088
μ_t, σ_t	2.3, 0.48
μ_b, σ_b	3.03, 1.12
μ_z, σ_z	0.542, 0.187
μ_σ, σ_σ	3.64e-8, 2.04e-9

To account for operational stresses (i.e., resulting from flow-induced random vibrations) it is necessary to modify the proposed PPoF model accordingly. *Barsom* (1976), *Hudson* (1981), and *Kim, Tadjiev, and Yang* (2006), have modeled fatigue crack growth under random amplitude loading by using ΔK_{rms} and R_{rms} in Paris and modified Paris equations. During random vibration, the RMS value of the maximum stress intensity factor can be described as shown:

$$K_{max,rms} = \sigma_{max,rms}\sqrt{\pi a}Y \tag{19}$$

$$\sigma_{max,rms} = \sqrt{\frac{\sum_{i=1}^{n} {\sigma_{max,i}}^2}{n}} \tag{20}$$

where, $\sigma_{max,rms}$ is the RMS value of maximum applied stress for the variable amplitude loading, and $\sigma_{max,i}$ is the maximum value of stress in i_{th} loading cycle. As discussed earlier, R_{rms} can be calculated as:

$$R_{rms} = \frac{\sigma_{min,rms}}{\sigma_{max,rms}} \tag{21}$$

We substitute $K_{max,rms}$ and R_{rms} in the proposed PPoF model (Eq. 14) to represent fatigue crack growth in Alloy 690 SG tubes in PWR environments subject to random vibration stresses, as shown in Eq. (22):

$$\frac{da}{dN} = c\left(1 - z{R_{rms}}^{t}\right)^{-b}\left[K_{max,rms}(1 - R_{rms})\right]^{p} \tag{22}$$

2.5.2.2 Fretting Wear

Fretting wear is a surface degradation process that results due to small amplitude oscillatory motion between two surfaces in contact. During heat exchange in SG tube bundles, there is fine flow-induced vibrations of the tubes causing fretting-wear between the tubes and support plates. Fretting-wear is a very serious problem in the safety of nuclear power plants (*Kim, 1997; Lim et al., 2003; Jo et al., 2008*) because relative motion between tube and support plates leads to loss of tube wall thickness at the support locations, and may go to the point when the tube thickness is unable to withstand the stresses due to primary to secondary side pressure differential causing catastrophic rupture and loss of coolant (*Chatterjee & Modarres, 2012*).

Fretting wear occurs as a result of combination of mechanisms such as adhesion, delamination, and abrasion (*Fitch, 1992*). At the initial stages, the asperities on the contacting surfaces adhere under the applied load. The softer asperities then shear off due to oscillatory motion of the surfaces, resulting in wear particles that accumulate in between the contacting surfaces. The harder asperities then cause plastic deformation in

the softer material, and removes sheets of particles, which further accumulate in between the contacting surfaces. The accumulated wear particles then cause abrasion resulting in expansion of the wear zone (*Fitch, 1992*).

Both fluid flow as well as design of SG can impact the fretting wear of tubes. Vibration frequency and impact force at the supports are some of the parameters governed by fluid-flow. Tube-support clearance and material combinations are some of the parameters governed by the design.

2.5.2.2.1 Literature Review

The Archard's wear equation (*Archard & Hirst, 1956*) is the most popular wear model used even today in wide range of applications. The Archard's wear law is found to be applicable to most fretting wear experimental data. The most common form of the equation is shown in Eq. (23). Here V is the wear volume lost, k *i*s the wear coefficient, F is the normal force, and L is the sliding distance.

$$V = kFL \tag{23}$$

Frick, Sobek, & Reavis (1984) developed a model based on Archard wear relationship to correlate non-linear wear parameters (tube/support plate contact forces and tube motions) to wear volume in rate form, as shown in Eq. (24):

$$\dot{V} = k\dot{W} \tag{24}$$

where, $\dot{V}$ is the wear volume rate and $\dot{W}$ is the work rate (work per unit time) implied by tube/support relative motion and contact forces. Various other studies have also been

carried out to study the fretting-wear phenomena of heat exchange tubes. *Blevins* (1979) studied the fretting-wear of heat exchanger tubes in nitrogen/air moisture at room temperature. The effects of tube/tube support clearance eccentricity, vibration frequency and mid span displacement were investigated. It was established that tube wear decreases substantially with decreasing tube/tube support plate gap. Fretting wear studies have also been carried out for SG tubes at Chalk River National Laboratories (CRNL) to investigate the effect of various parameters (*Ko, 1985*). It has been determined that for certain tube material (e.g., Alloy 600) the wear rate increases with increase in temperature and tube/tube support plate gap.

The vibration mechanisms responsible for fretting wear of SG tubes are fluid-elastic instability, vortex shedding, and turbulence. These mechanisms have been discussed in detail in Section 2.5.1. Various other studies have been conducted to investigate wear behavior of SG tubes in PWR operating conditions (*Lee et al., 2001; Lee & Kim, 2002; Hong & Kim, 2005*). Different materials have been investigated, e.g., Alloy 600, Alloy 800, and Alloy 690, both at room temperatures and high PWR operating temperatures. It has been observed that for Alloy 690 material, fretting wear rate is less at higher operating temperatures than that at room temperatures (Figure 13). At room temperatures the material loss is due to abrasion and plastic deformation, while at higher operating temperatures the material loss is due to adhesion and plastic deformation. Also, it has been reported that wear rate of Alloy 690 is lower than that of Alloy 600 possibly because of stacking fault energy difference in between the two materials (*Hong & Kim, 2005*). To reduce fretting wear failures of SG tubes, tube/tube support materials should be

chosen with care because wear rate of some material combinations may be higher than others under similar vibration conditions (*Ko, 1985; Hong & Kim, 2005*).

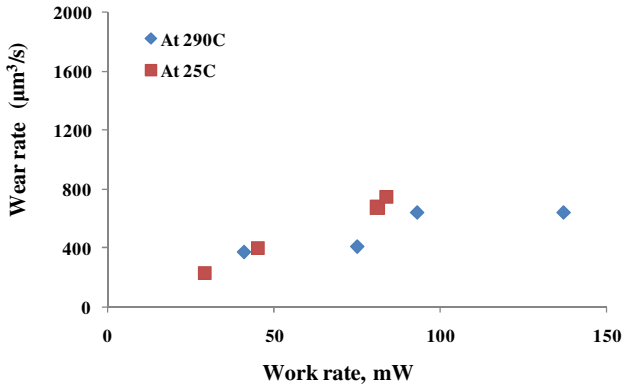

Figure 13: Alloy 690 fretting wear data at room and elevated temperatures[22]

2.5.2.2.2 Proposed Probabilistic Physics-of-Failure Model

Fretting wear mechanism is greatly affected by the oscillation amplitude, normal loads, material hardness, oscillation frequency and number of wear cycles. Fretting wear volume loss in Alloy 690 SG tubes can be expressed as a function of the following critical variables:

$$V = f(F, L, fr, H) \tag{25}$$

where, V is the volume of material lost, F is the normal load causing wear, L is the oscillation amplitude (sliding distance), fr is the frequency of oscillation, and H is hardness of contacting components. The Archard's equation (*Archard & Hirst, 1956*) for sliding wear correlates volume loss with some of the above variables. This equation has been shown to be adequate for evaluating fretting-wear in SG tubes (*Connors, 1981; Jo et*

[22] Hong and Kim, 2005

al., 2008). Archard's equation is a linear relation between wear volume, local loads and sliding distances, as shown in Eq. (26):

$$V = \frac{k'FL}{H} \tag{26}$$

where, k' is the wear coefficient. The wear volume loss is inversely proportional to the hardness of the softer material. The limitations with Eq. (26) are that it does not account for contacting surface geometry or interactions, and the effect of oscillation frequency.

The PPoF model for fretting wear of Alloy 690 SG tubes is developed in this research accounting for tube-support plate interactions and geometry, and also the frequency of oscillations. Eq. (26) can be expressed in rate form as:

$$\frac{dV}{dt} = kF\frac{dL}{dt} \tag{27}$$

where, $k = k'/H$ is the wear coefficient that includes the hardness property of the contacting materials. In this research we assume that failure by fretting wear occurs when the wear depth propagates to 100% through-wall thickness of the tube. Failure can also occur much earlier due to development of fatigue cracks in the wear area. However that possibility is neglected in this research and failure due to wall-thinning by pure fretting wear is considered. An equation that correlates the tube wear volume loss with the wear depth is needed in order to estimate the failure probability. In order to formulate such an equation we would need to consider the geometry and interaction between the tube and support plates. Progressive fretting-wear between the tube and support plate (as shown by horizontal lines in Figure 14) leads to reduction in tube through-wall thickness (due to

loss of black shaded wear area) as represented by wear depth, h and wear angle, α. Wear angle increases with the wear depth and reaches a maximum value when wear depth reaches 100% through-wall thickness of tube.

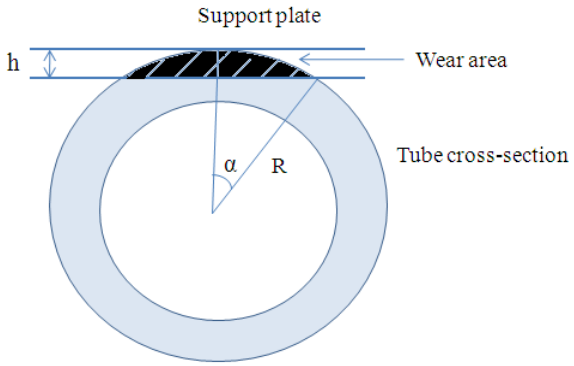

Figure 14: Schematic of SG tube-support plate interaction

This modeling effort assumes that volume loss during fretting-wear occurs only in the SG tube with negligible wear in support plates. Alternatively the wear volume, measured by the loss of material during fretting-wear, can be represented in terms of the wear angle as,

$$V = \frac{R^2 l}{2}[2\alpha - sin2\alpha] \tag{28}$$

where, R is outer radius of tubes, and l is effective support length. The Eq. (28) can be expressed in rate form as shown in Eq. (29):

$$\frac{dV}{dt} = R^2 l[1 - cos2\alpha]\frac{d\alpha}{dt} \tag{29}$$

From Eqs. (27) and (29), the rate of change of wear angle with time (wear rate) can be derived as shown in Eq. (30). Wear contact angle (α) is given by $cos^{-1}(1-h/R)$, which varies from $cos^{-1}(1-h_i/R)$ to $cos^{-1}(1-h_f/R)$, where h_i is initial wear depth and h_f is final or critical wear depth.

$$\frac{d\alpha}{dt} = kF\frac{1}{R^2 l[1-cos2\alpha]}\frac{dL}{dt} \tag{30}$$

The rate of change of sliding distance with time during fretting-wear between helical SG tubes and support plates under turbulence-induced vibration is expressed by Eq. (31), where RMS is root mean square displacement of helical tubes under turbulence-induced random vibrations, and ψ is fretting-wear period (*Jo et al., 2008*).

$$\frac{dL}{dt} = \frac{4RMS}{\psi} \tag{31}$$

Substituting Eq. (31) to the proposed fretting-wear PPoF model (Eq. 30) results in Eq. (32) for simulating fretting-wear in helical Alloy 690 SG tubes under turbulence-induced random vibrations, where N represents the number of wear cycles.

$$\frac{d\alpha}{dN} = kF\frac{4RMS}{R^2 l[1-cos2\alpha]} \tag{32}$$

In Eq. (32), wear coefficient k is considered as random and estimated probabilistically using a Bayesian regression approach, as shown in Figure 15. Experimental fretting wear volume loss data for Alloy 690/stainless steel plate combination (Figure 16) were used for the regression analysis. This accounts for

uncertainties in fretting-wear phenomena as well as the material properties of contacting components. The fretting wear data used for regression were obtained from experiments at room temperatures. As discussed earlier, fretting wear rate is lower at elevated PWR temperatures when compared to room temperatures. Therefore, the proposed PPoF model for fretting wear would give a conservative estimate of the SGTR frequency.

Wear data is obtained in the form of wear volume loss rate ($\dot{V}$) versus the work rate ($\dot{W}$), which involve the non-linear parameters (tube/support motion and dynamic contact forces). Wear volume rate is correlated with the work rate using the wear coefficient. This correlation is widely used to evaluate and estimate fretting wear damage in SG tubes (*Kim, 1997; Lee, 2001*). In order to define the likelihood function using the work rate equation, it was assumed that the model error follows a normal distribution with mean zero and standard deviation σ, as shown in Eq. (33).

$$\dot{V} = k\dot{W} + \varepsilon(0, \sigma) \tag{33}$$

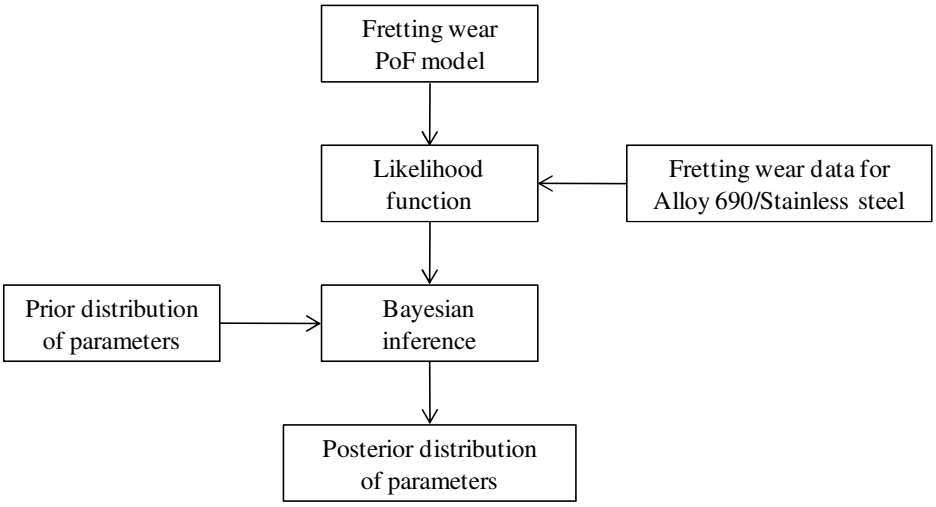

Figure 15: Estimating fretting wear PPoF model parameter distribution

A normal distribution for the dependent variable, i.e., $\dot{V}$ was assumed to define the likelihood function (Eq. 34) of n data points ($\dot{V}\ vs.\dot{W}$) with the standard deviation same as that of the model error.

$$L(Wear\ data|k,\sigma^2) = \frac{1}{\sqrt{(2\pi)^n\sigma^{2n}}} exp\left[-\frac{1}{2\sigma^2}\sum_{i=1}^{n}\left(\dot{V}_i - k\dot{W}_i\right)^2\right] \tag{34}$$

Non-informative or uniform prior distributions were assumed for the parameters k and σ. Experimental data (Figure 16) for fretting-wear rate in Alloy 690 tubes/stainless steel support plates was available to determine the marginal posterior distributions for the parameters.

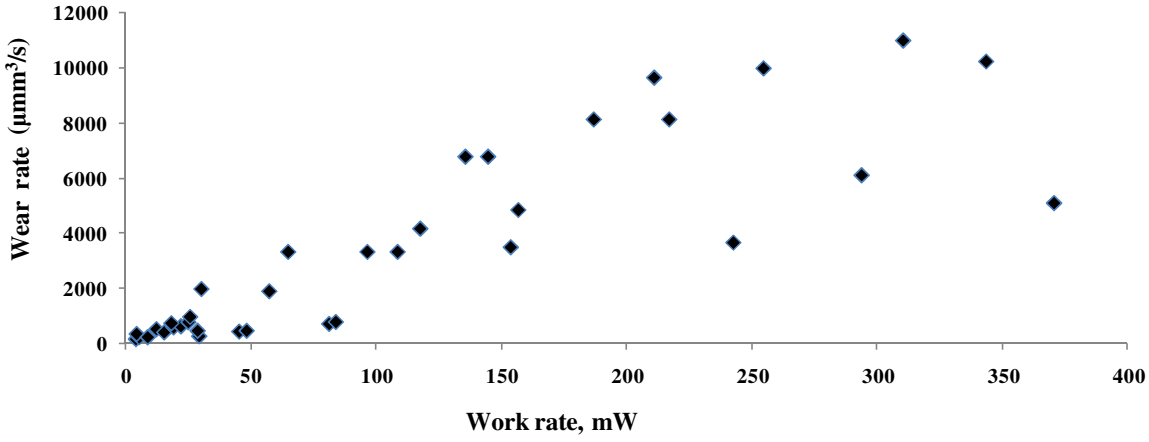

Figure 16: Alloy 690/Stainless Steel fretting wear data[23]

WinBUGS v.14 software (*Cowles, 2004*) was used to perform the Bayesian regression analysis and obtain the posterior distributions. Figure 17 illustrates the posterior marginal distributions of k and σ. The mean and standard deviation of model parameters are illustrated in Table 7.

[23] Lee et al., 2001; Lee and Kim, 2002; Hong and Kim, 2005

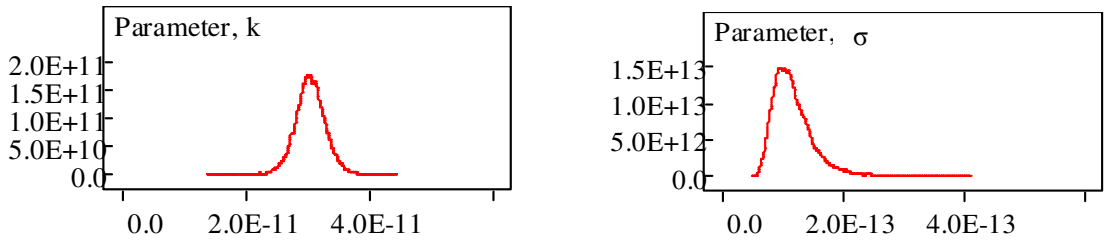

Figure 17: Posterior distributions of PPoF model parameters k & σ

Table 7: Proposed fretting wear model parameter values

Parameters	Values estimated through Bayesian regression
μ_k, σ_k	3.04e-11, 4.1e-12
μ_σ, σ_σ	1.172e-13, 2e-14

2.5.3 Probabilistic Stress Agents Assessment Approach

Fluid flow-induced turbulence on SG tube bundles is a classic case of random vibration, the analysis of which can be carried out in either the time or frequency domains. When using time domain the input is in the form of time history of turbulent forces. The structural response is derived using finite element analysis, and the output is also expressed as a time history, e.g., stress at some particular location in the tubes. In the frequency domain, the input is expressed as power spectral density (PSD) of turbulent forces. The output from the model is then expressed as PSD of stress (*Bishop, N. and Caserio, A.,* 1998).

Turbulence-induced tube vibration analysis is performed using the theory of random vibration in this research. Turbulent primary fluid pressures, $p(x, \theta, t)$, acting on the tube

surface in all directions is shown in Figure 18, where R is outer radius of the tube and t is time.

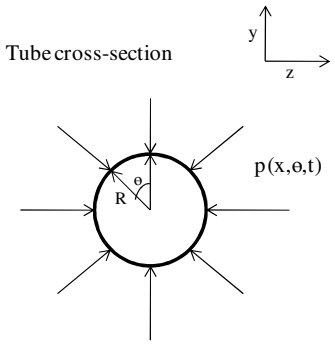

Figure 18: Turbulent fluid pressures acting on tube cross-section in all directions (*Blevins, 1990*)

At any instant in time, these surface pressures will exert a net lateral turbulence force per unit length, F_y, on the tube (Figure 19), as shown in Eq. (35) (*Blevins, 1990*).

$$F_y = -\int_0^{2\pi} p(x,\theta,t)cos\theta R d\theta dx \tag{35}$$

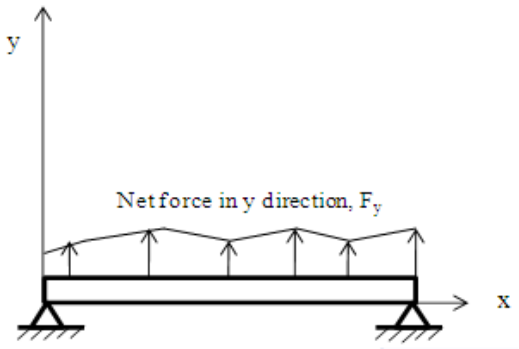

Figure 19: Force acting on a tube in a turbulent flow (*Blevins, 1990*)

The partial differential equation of motion of a uniform rod responding to this force is shown in Eq. (36) (*Blevins, 1990*), where $Y(z,t)$ is the displacement of the rod in the

vertical direction, E is the modulus of elasticity, m is the mass per unit length, and I is the moment of inertia of the cross-section about the neutral axis.

$$EI\frac{\partial^4 Y(z,t)}{\partial z^4} + m\frac{\partial^2 Y(z,t)}{\partial t^2} = F_y(z,t) \tag{36}$$

The approach developed in this research for determining the response of SG tubes to the turbulence forces is shown in Figure 20 (*Chatterjee & Modarres, 2012*). The approach uses finite element methods to determine the turbulence-induced random vibration amplitudes and stresses. The approach starts with the development of a finite element model of the SG tube based on tube geometrical parameters and material properties: e.g., tube diameter and thickness, young's modulus, and material density. Uncertainties in the geometrical parameters and material properties are considered in the analysis. Modal analysis is then required to determine the tube modal parameters such as natural frequencies and modal stresses.

The most critical step in this approach is to determine an appropriate PSD forcing function that characterizes the flow-induced turbulence conditions for the SG tube bundle. The PSD function can be developed experimentally for particular applications and operating conditions, e.g., single-phase cross flow. Once the PSD forces are determined based on flow parameters, the next and final step is to conduct random vibration analysis to determine the response of the SG tubes, i.e., random vibration amplitudes and stresses.

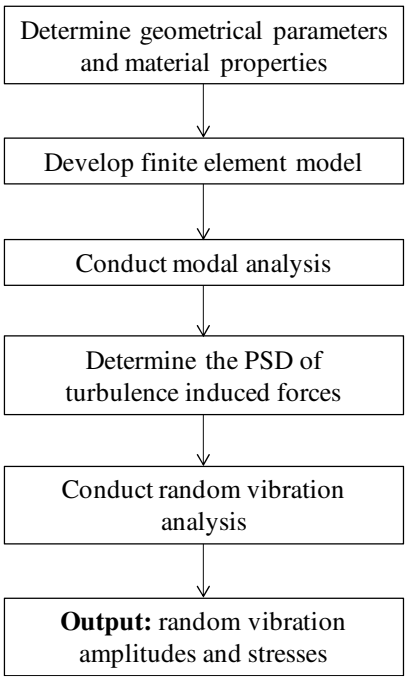

Figure 20: Random vibration analysis approach

The auto spectral density of turbulence-induced force normal to the axis of a cylinder in single-phase cross flow in SGs can be represented by Eqs. (37) and (38) (*Axisa et al., 1990*), where S_{Fy} is the auto spectral density of turbulence-induced force, ρ is fluid density, U is average cross-flow velocity through the minimum gap between tubes, D is tube outside diameter, and $\phi(f_i D/U)$ is dimensionless spectral shape function.

$$S_{F_y} = \left(\frac{1}{2}\rho U^2 D\right)^2 \frac{D}{U}\phi\left(f\frac{D}{U}\right) \tag{37}$$

$$\phi\left(f_i\frac{D}{U}\right) = \begin{cases} 4\times 10^{-4}\left(f_i\dfrac{D}{U}\right)^{-0.5}, & 0.01 \le f_i\dfrac{D}{U} \le 0.2 \\ 3\times 10^{-6}\left(f_i\dfrac{D}{U}\right)^{-3.5}, & 0.2 \le f_i\dfrac{D}{U} \le 3 \end{cases} \tag{38}$$

Force PSD calculations can be then performed using a range of fluid gap velocities in the tube bundle using Eqs. (37) and (38). These fluid gap velocities can be obtained using thermal hydraulic analysis of the primary coolant flow through the helical tube bundles. In order to ensure that there is no fluid-elastic instability in the tubes, critical velocity of the tubes need to be computed using Eq. (39) (*Connors, 1981*). The gap velocities in the tube bundle should not exceed this critical velocity.

$$\frac{V_{c,n}}{f_n D} = C\left(\frac{2\pi\zeta_t m_t}{\rho D^2}\right)^{0.5} \tag{39}$$

In Eq. (39), $V_{c,n}$ is the critical velocity for the n_{th} free vibration mode, C is fluid-elastic instability coefficient, ζ_t is damping ratio, m_t is total mass per unit length of tube, ρ is density of external fluid, and D is external tube diameter. Maximum PSD bending stresses and displacement amplitudes can be determined from finite element analysis for various gap flow velocities. The normal force initiating wear is determined assuming a clearance between the tube and its supports. Normal force initiating fretting-wear, F_n, can be expressed in terms of the normal component of rms response obtained from random vibration analysis as shown in Eq. (40):

$$F_n = k_c(|y_{rms}| - g), \quad if \ \ |y_{rms}| > g$$

$$F_n = 0, \quad if \ \ |y_{rms}| < g \tag{40}$$

where, k_c is equivalent stiffness of tube support interaction, g is diametric clearance between a tube and its support, and y_{rms} is a normal component of rms tube displacement (*Au-Yang, 2001*). The value of stiffness, k_c, can be obtained from the

standard tube localization model as shown in Eq. (41) (*Axisa, Desseaus, & Gilbert, 1984; Au-Yang, 2001*), where h is tube thickness and E is Young's modulus of tube material. The model assumes that an equivalent linear spring acts in the direction of motion as soon as tube-support impact occurs, and the tube is much less rigid than the support structure.

$$k_c = 1.9\frac{Eh^2}{D}\sqrt{\frac{h}{D}} \tag{41}$$

Since the stress agents result from turbulence-induced vibrations, different locations along the tube in SMRs would have different values of stress agents. For example, a helical span (length of tube between two support plates) would have different distributions of stress agents at different locations along the span. For each location along the span, distribution of stress values can be used in the fatigue reliability simulation, whereas vibration amplitudes at the tube/support locations can be used to calculate the normal force initiating wear and rate of change of sliding distance with time, which can then be used in the fretting-wear reliability simulation.

2.5.4 Probabilistic Approach for Uncertainty Propagation and Rupture Frequency Estimation

A probabilistic approach was formulated to propagate the PPoF model parameter uncertainties, and estimate SGTR frequency under the acting stress agents. The probabilistic approach is shown in Figure 21. Starting from initial flaw size distribution[24],

[24] To estimate remaining life of SG tubes during in-service inspections, initial flaw size and density distributions would be obtained from the nondestructive evaluations and PPoF approach would be applied from that point onwards. A Bayesian approach for true flaw size and density estimation using nondestructive evaluation data is presented in Chapter 4 of this dissertation.

degradation growth analysis is carried out for each mechanism of interest using their respective PPoF models and for random samples of model parameters, to obtain the final flaw size distribution[25] at the mean life of SG (t_m).

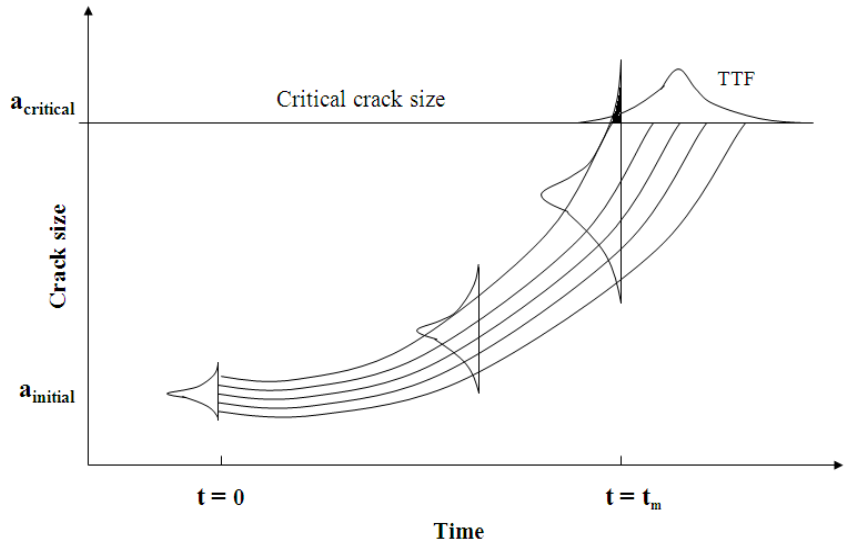

Figure 21: Flaw (e.g., crack) growth simulation using PPoF models

For each random sampling of PPoF model parameters for the mechanism of interest, final flaw (e.g., crack) size distribution is obtained at the mean life of SG, as shown in Figure 22. In Figure 22, the parameters p and c are for representation purpose only. As we have discussed earlier, fatigue PPoF model has five model parameters, whereas fretting wear PPoF model has one model parameter (wear coefficient). Each realization of final flaw size distribution is for one location of a tube span under the acting stress agent at that location. Generally the tube/support locations are the most critical in terms of flaw severity. However, it is probable that flaws can occur at all locations along a tube span.

[25] The time-to-failure (TTF) distribution shown in Figure 21 denotes the failure time for all cracks, whereas the final crack size distribution denotes the status of cracks (i.e., crack sizes) at the mean life of SG. The area of the TTF distribution corresponding to time less than mean life of SG is equivalent to the area of final crack size distribution shaded in black.

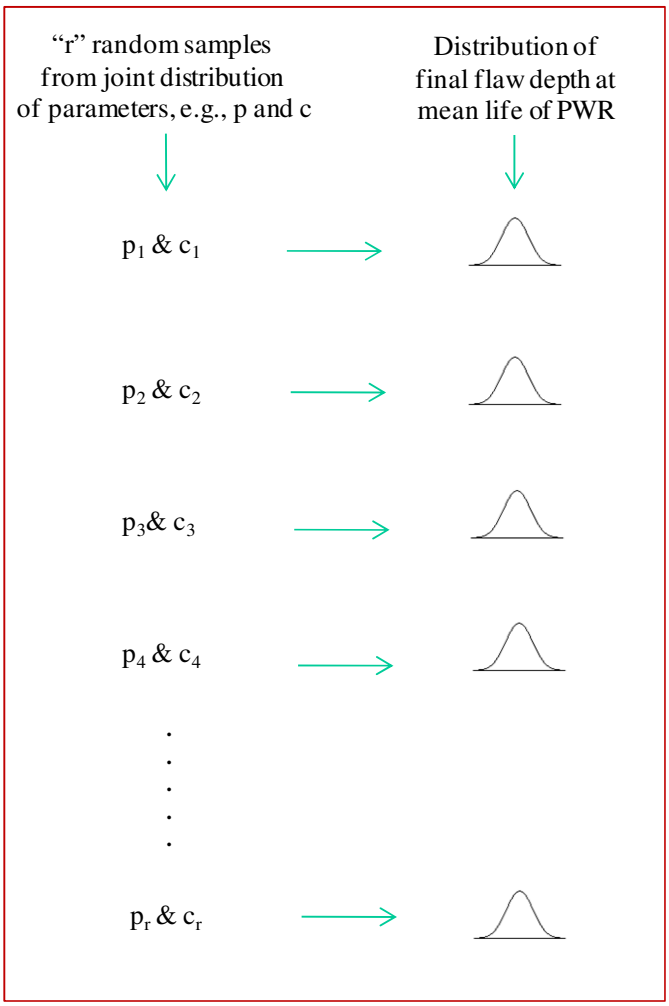

Figure 22: Considering parameter uncertainties

For SGTR frequency estimation using fretting wear PPoF model, we only consider the tube/support locations of a tube span, since fretting wear is not possible at other locations along a span. But for SGTR frequency estimation using fatigue PPoF model, we consider several different locations along a span. For example, one helical span can be divided into n equal size divisions. Each tube location/division would have several nodes and each node would have different values of stress agents (e.g., stress or amplitude). For each location, starting from initial flaw size distribution, final flaw size distributions

would be obtained at mean life of SG for all acting stress agents at all nodes, and a weighted distribution of final flaw size would be obtained for that location or division. The probability of SGTR at one location or division is then estimated by determining probability of flaws exceeding the critical flaw limit (from the cumulative density function of final flaw size), where critical flaw limit (a_{cr}) is assumed in this research as the through-wall thickness of tubes, as shown in Eq. (42).

$$Pr_r\left(SGTR_{Loc_i} \middle| SA_{Loc_i}\right) = Pr\left(a_f > a_{cr}\right) \tag{42}$$

In Eq. (42), SA_{Loc_i} are the prevailing stress agents at i_{th} location or division. Since, at one location there can be multiple flaws, a flaw density distribution is used assuming Poisson distribution to consider the probability of SGTR for all flaws at one location or division, $Pr_r\left(SGTR_{All\ flaws\ at\ Loc_i} \middle| SA_{Loc_i}\right)$. Similarly, the SGTR probability at all n locations or divisions in a span are estimated and summed (assuming independency) to obtain the SGTR probability for one helical span of the SG tube, as shown in Eq. (43).

$$Pr_r(SGTR_{Span_j}) = \sum_{i=1}^{n} Pr_r\left(SGTR_{All\ flaws\ at\ Loc_i} \middle| SA_{Loc_i}\right) \tag{43}$$

Since the number of spans in one helical turn of a tube bundle is equal to the number of support points in that turn, the total number of spans in a tube can be estimated by considering the total numbers of turns in that tube. Then the total number of spans in entire SG can be estimated by considering the total number of tubes in the SG. For example, if there are four spans in a helical turn and five helical turns in a tube, the total number of spans in a tube would be 20. If there are 1000 tubes in the SG then total

number of spans in the SG is 20,000. The SGTR probability for entire SG due to fatigue mechanism is then estimated by summing over all spans (assuming symmetry along all spans and independency), as shown by Eq. (44).

$$Pr_r(SGTR_{Entire\ SG}) = \sum_{All\ spans} Pr_r(SGTR_{Span_j}) \tag{44}$$

For estimating the SGTR frequency due to fretting wear, the SGTR probability at only the tube/support locations along a span are estimated. Then, considering the total number of support points for all tubes, SGTR probability for entire SG is obtained by summing (assuming independency) over all support points. The SGTR probability estimated by this approach is for one random sampling of PPoF model parameters. For r random sampling, there would be r SGTR probabilities, which can then be fitted into a probability distribution to represent the uncertainties. The SGTR frequencies are then estimated by dividing the SGTR probability values by the mean (or remaining) life of SG to provide yearly estimates of frequency. A MATLAB routine was developed to implement this approach. An application of the PPoF approach is presented in Chapter 3 to estimate distributions of SGTR frequency for a typical helical SMR design.

CHAPTER 3: ASSESSMENT OF STEAM GENERATOR TUBE RUPTURE FREQUENCY FOR A TYPICAL HELICAL SMALL MODULAR REACTOR DESIGN

3.1 Small Modular Reactor Steam Generator Tubes

The PPoF based SGTR frequency assessment approach has been applied to a new design of SMR SGs consisting of helically-coiled tubes, to determine the SGTR frequency. One important distinction from large scale PWRs is that these SMR designs do not have the large diameter coolant loop pipes. Hence, the injection pump capacity in these designs is much lower than large scale PWRs. Therefore, even small leakage rates would be critical for these SMR designs. In this research, we do not follow the LOCA category definitions that were basically influenced by the large diameter coolant loop pipes, and include small leakage rates in the definition of SGTR.

The helical SG design used in SMRs is very different thermal-hydraulically and geometrically from U-tube SGs used in conventional PWR plants (*Jo et al., 2008*). Each SG coil is a once-through heat exchanger with many helically coiled tubes (Figure 23). Preliminary probabilistic risk analysis developed in support of the typical helical design has shown that SGTR is one of the leading contributors to the overall risk of a reactor module.

Figure 23: Helical tubes (left) and top view of tubes with support points (right)

In the helical SG design, primary coolant (superheated light water) flows downward externally to the tube through the tube bundle by natural circulation at higher pressure and temperature, whereas secondary coolant (water) flows upward internally through the helical tubes at lower pressure and temperature. Thus, the helical tubes are subjected to liquid cross-flow externally and multi-phase flow internally. The helical tubes are made of Alloy 690, which has almost twice the chromium content of Alloy 600 (*Berge & Donati, 1981*) (tube material in traditional designs), as shown in Table 8. The higher chromium content in Alloy 690 material makes them resistant to corrosion related mechanisms. The problem with Alloy 600 was that most of the chromium was precipitated as carbides at the grain boundaries leading to chromium depletion. However, in the case of Alloy 690 material, there is enough chromium left over after the formation of carbides at the grain boundaries to form a passivation layer and prevent corrosion.

Table 8: Composition of Alloy 600 and Alloy 690 materials (wt %)

	Cr	Fe	C	Si	Mn	S	Co	Ni
Alloy 600	14-17	6-10	<0.15	<0.5	<1	<0.015	<0.1	Balance (>72)
Alloy 690	27-31	7-11	<0.05	<0.5	<0.5	<0.015	<0.1	Balance (>58)

3.1.1 Identification of Degradation Conditions and Mechanisms

In SMR SGs, fluid flow in the tube bundle generates a flow-induced vibration phenomenon, which is composed of fluid-elastic instability, turbulence excitation, and vortex shedding. Among the mechanisms of flow induced vibration in PWR SGs, turbulence-induced excitation generates random pressure fluctuations around the tube surfaces, forcing them to vibrate and inducing enough vibration response to cause long-term damage (*Pettigrew et al.,* 1991). As has been discussed in the Section 2.5.1, vortex shedding and fluid-elastic instability lead to resonant vibration in the tubes, causing failure in quick time or overstress failures. These high amplitude vibration excitation mechanisms should not occur for normal operating conditions in SGs (*Connors, 1981*).

In this research we consider operating stresses resulting from turbulence induced vibrations of tubes. We also analyzed other sources of operating stresses, e.g., thermal stresses, which can lead to thermal fatigue. However, the helical shape of tube bundle accommodates the thermal stresses due to expansion of tubes (e.g., during normal heating at start-up) and hence would not contribute significantly to the operating stresses.

As discussed earlier, with the use of Alloy 690 risks from most of the corrosion related degradation mechanisms have been mitigated to a great extent. However, Alloy 690 tubes with pre-existing flaws are more susceptible to fatigue damage due to fluctuating stresses resulting from flow-induced tube vibration, and fretting-wear damage from the relative motion between the tube and supports.

3.1.2 Finite Element Analysis to Assess the Stress Agents

The finite element model of one span of the helical Alloy 690 tube (Figure 24) was developed using commercial software ANSYS[26] v.12.1. The finite element model was developed using the pipe element (PIPE16), which is a uniaxial element with tension-compression, torsion, and bending capabilities. The element has six degrees of freedom at two nodes: translations in the nodal x, y, and z directions, and rotations about the nodal x, y, and z axes. Simply supported boundary conditions (as well as symmetry) were used at each end of the helical span to simulate the support points. Tables 9 and 10 provide the mean values of geometrical parameters of tubes, and material properties respectively (actual values are not shown due to confidentiality issues). All these parameters were considered probabilistically to estimate the response stresses and vibration amplitudes and associated uncertainties.

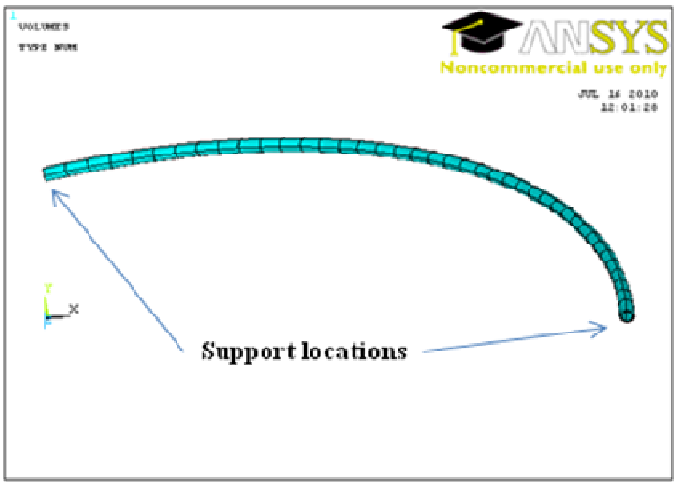

Figure 24: Finite element model of one span of helical tube

[26] ANSYS, "Structural Analysis Guide," ANSYS Inc., Canonsburg, PA, 2009.

Table 9: Geometrical parameters of tube

Geometrical parameters of tube	Mean value
Tube diameter (mm)	15.75
Tube wall thickness (mm)	1.55
Coil diameter (mm)	500
# of support points per helical turn	4

Table 10: Alloy 690 material properties

Alloy 690 material properties	Mean value
Young's modulus	211000 MPa
Poisson's ratio	0.289
Density	8.19E-9 Mg/mm^3

Modal analysis was first performed on one span of the helical tube using ANSYS v.12.1 to obtain the natural frequencies and the modal stresses. The reduced method was used for the eigenvalue and eigenvector extractions to calculate first five natural frequencies. All degrees of freedom in the y-direction were selected as master degrees of freedom (MDOF). Table 11 lists the natural frequencies for first five modes of vibration.

Table 11: Natural frequencies from Modal analysis

Modes	Natural Frequencies (Hz)
1	21
2	121.9
3	261.86
4	465.40
5	720.38

Random vibration analysis was then carried out assuming a constant damping factor and a random uniform force PSD (nodal excitation). A frequency range of 0.1 to 70 Hz was used as an approximation to the PSD forcing function frequency. Force PSD calculations were carried out using Equations (37) and (38). Standard assumptions were used to carry out random vibration analysis: there is negligible fluid-elastic force; PSD force is relatively constant over the frequency range close to the tube natural frequency; a single mode dominates the tube displacement and coupling between modes is negligible; and gap velocity caused by turbulence in a tube bundle is homogeneous along a tube span (*Blevins, 1994; Taylor & Pettigrew, 2000*).

The critical velocity in the tube bundle for first natural frequency was determined in order to ensure that there is no fluid-elastic instability in the tube bundles for the velocity range of interest. A 2-D thermal hydraulic analysis provided the gap flow velocities across various regions of the tube bundle. These gap flow velocities were used to determine the PSD forces. Due to confidential nature of the data, the PSD force values, stress results, and other parameters (e.g., damping factor, gap flow velocities) are not provided in this dissertation. Maximum PSD stresses were determined for gap flow velocity range (obtained from thermal hydraulic analysis) for various locations along a helical span (Figure 25). For each location or node along a helical span, RMS values of maximum stresses for all possible gap flow velocities were then calculated. Stress values were used in the fatigue PPoF model, whereas vibration amplitudes at the tube/support locations were used to calculate the normal force initiating wear and rate of change of sliding distance with time, which were used in the fretting-wear PPoF model for estimating the SGTR frequency.

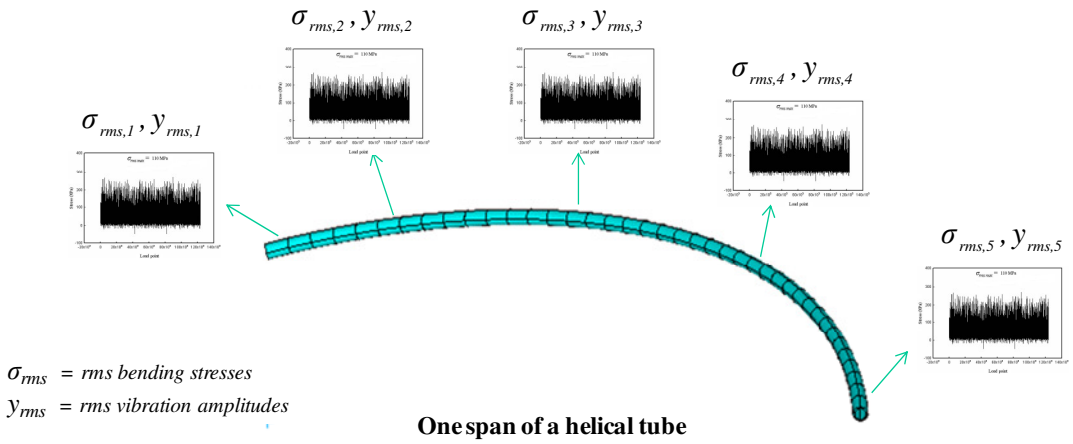

Figure 25: Random vibration stresses along helical span of SG tube

3.2 Assessment of Steam Generator Tube Rupture Frequency

Pre-service inspection is performed to detect any pre-existing defects in tubes that may have resulted during manufacturing or transportation. It is important to detect such defects since degradation mechanisms often initiate from such defects to failure. There have been cases in the past when tube rupture occurred from flaws that originated during fabrication and packaging. For example, a US NRC report (*US NRC, 2004*) stated that a tube had a leak in a replacement SG (tubes made of Alloy 690) at the Palo Verde nuclear generating station, which was attributed to a flaw (dent) that originated during packaging and handling.

The SMR designs in consideration are still in pre-licensing stage, and hence no pre-service inspection data was available. Since the primary purpose of estimating SGTR frequency in this research is to demonstrate the utility and applicability of the PPoF approach, initial crack size and density distribution used in this paper were hypothetically derived from in-service inspection data for PWR SG Alloy 690 tubes (through-wall

cracks) (*Liao & Guentay, 2009*). The data were scaled to represent potential fabrication flaws to a reasonable extent. The scaled data was further prorated for total number of tubes in the SMR. The initial flaw size was assumed to follow the gamma PDF, with higher size flaws having lower probability densities. The flaw density (number of flaws in a segment) was generated for each segment assuming Poisson distribution (*Chatterjee & Modarres, 2012*).

Fatigue and fretting-wear mechanisms in helical Alloy 690 SG tubes were simulated using their PPoF models under turbulence-induced random vibration stresses and forces (calculated in the previous section). The simulation of failures were performed using developed MATLAB routines (Chapter 2), and resulting uncertainties in SGTR frequency is presented in terms of probability densities, confidence limits, and box and whisker plots (Fatigue – Figure 26; Fretting wear – Figure 27; Total – Figure 28). Finally, we compare the results of the calculated total SGTR frequency for SMRs with that of historical SGTR frequency estimates currently used for PRA of existing PWR designs.

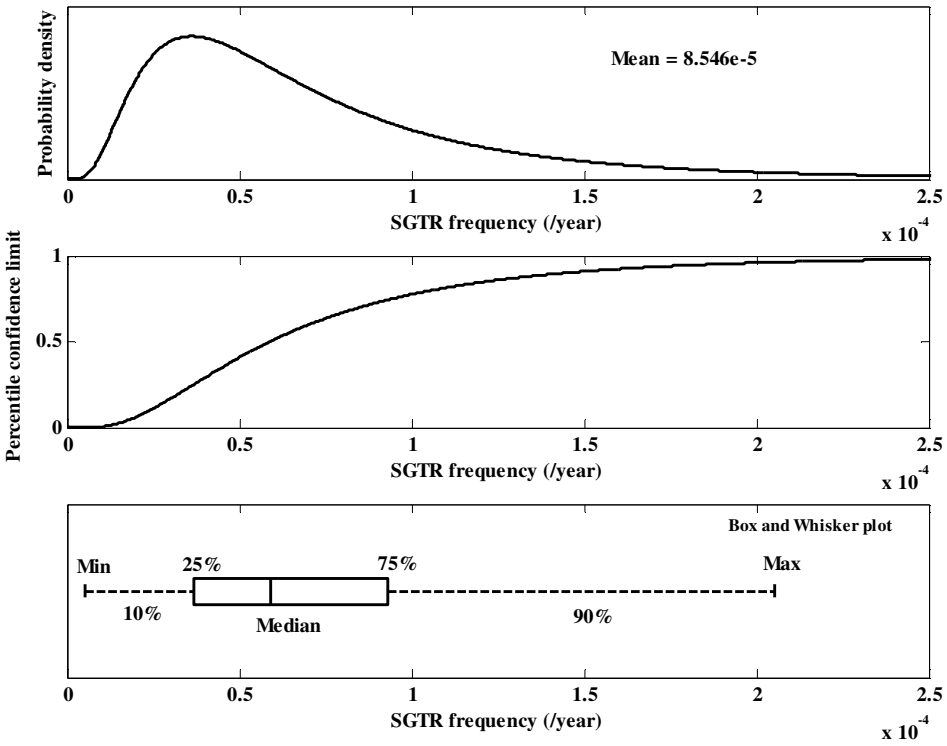

Figure 26: Uncertainty representation of SGTR frequency due to fatigue

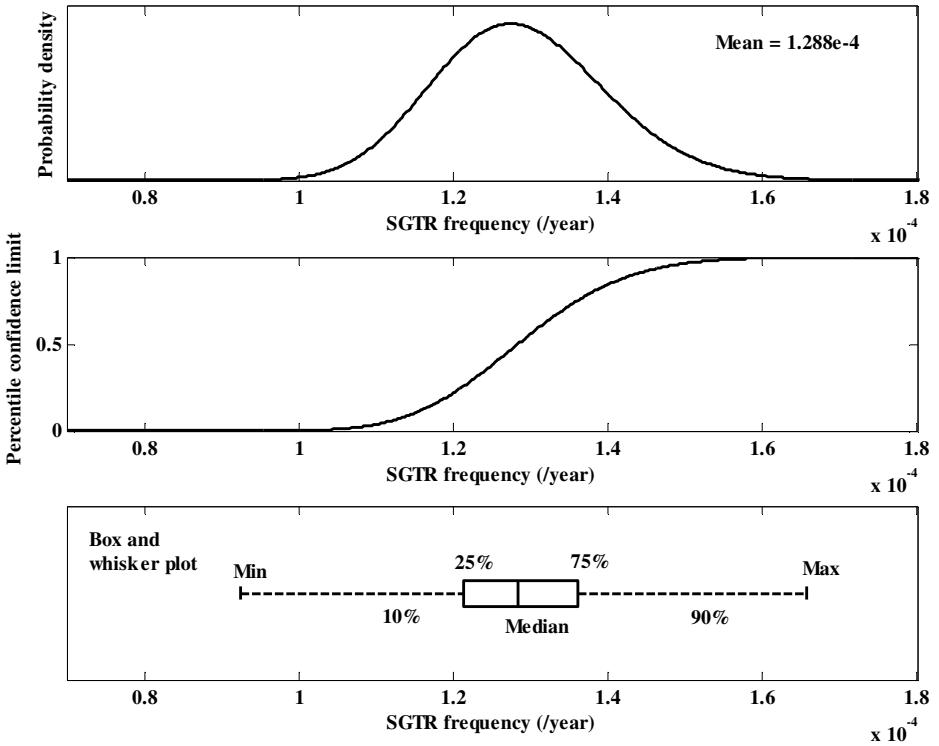

Figure 27: Uncertainty representation of SGTR frequency due to fretting-wear

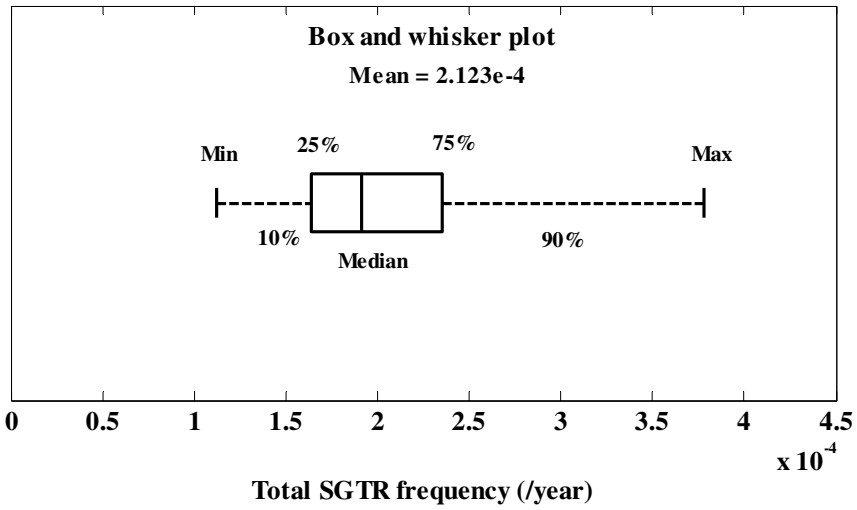

Figure 28: Uncertainty representation of total SGTR frequency

3.3 Discussion of Results

The PPoF estimation of total SGTR frequency for SMRs was compared with that of historical SGTR frequency currently used for PRA of PWRs. The historical SGTR frequency (which is of the order of 10^{-3}) is based on past ruptures in operating PWR designs that have different tube lengths, primary to secondary side pressure differential and dominated by the SCC mechanism. Hence, for proper comparison with the calculated PPoF-based frequency for SMR designs, the historical data-based SGTR frequency was prorated based on total tube length, pressure differential and failure mechanisms (*Chatterjee & Modarres, 2012*).

For example, approximately 70% of past failures of SG tubes were caused by the SCC mechanism (*Diercks et al., 1996*), which has a very negligible chance of occurrence in new SMR designs because of advanced tube materials (Alloy 690) with higher chromium contents, and different boundary conditions (high pressure primary loop on the

shell side). Hence, the operating PWR SGTR historical frequency estimate was scaled accordingly to consider only failures caused by failure mechanisms other than SCC and related corrosion mechanisms (e.g., fatigue, fretting wear), the tube length and pressure differential of a typical helical SMR design. The scaling assessment resulted in an estimated SGTR frequency for SMR of around $8x10^{-5}$. Hence, the PPoF-based SGTR frequency estimate calculated in this paper, while being a bit on the conservative side (due to higher flow-induced vibrations in helical tube bundles), is more relevant and reliable given that actual degradation conditions prevailing in SMR designs and the corresponding mechanical, electrical, thermal, and chemical processes leading to failure have been formally considered while estimating the SGTR frequency.

The SGTR frequencies estimated through the PPoF approach can support PSA of SMRs to determine potential and frequency of severe adverse consequences. It is also necessary to update the pre-service prediction of SGTR frequency using the health condition information obtained from in-service inspections. Often during service stage, many degradation conditions affect the tubes, e.g., accidents, emergency shut-down for maintenance. Hence, the degradations in tubes may not propagate as anticipated during the licensing phase. However, in-service inspection data are highly uncertain in nature due to detection uncertainties and measurement errors associated with the nondestructive evaluation methods. Chapter 4 presents a Bayesian probabilistic approach for estimating real defect severity in SG tubes considering the nondestructive evaluation uncertainties.

CHAPTER 4: BAYESIAN PROBABILISTIC APPROACH FOR ESTIMATING DEFECT SEVERITY IN STEAM GENERATOR TUBES USING UNCERTAIN INPUTS FROM NONDESTRUCTIVE EVALUATION

4.1 Historical Perspectives on Steam Generator Tube In-Service Inspections

SGs are critical components of a PWR, and have a number of important safety functions, e.g., keep the reactor core at a safe temperature, and act as a barrier between the primary and secondary sides of a nuclear plant. Failure of SG tubes can contribute significantly to nuclear power plant station unavailability. It is critical to ensure that SG tubes perform reliably consistent with their licensing basis and satisfactorily meeting the applicable regulatory requirements. This can be achieved through in-service inspection of the SG tubes in order to detect the presence of unknown existing defects, and then characterize them. If these unknown defects are not detected and characterized effectively, they can impair tube integrity.

At the beginning in-service inspection of SG tubes of water-water energetic reactors (WWER), a series of PWRs developed by Russia, was based on the leakage tests (*International Atomic Energy Agency, 2007*). Based on the results of the leakage tests, defective or damaged tubes were identified and were subsequently plugged with various types of plugs (e.g., welded and mechanical).

Since the early seventies, nondestructive evaluation methods such as eddy current inspection techniques were developed and used on PWR SGs and also later on WWER SGs (*International Atomic Energy Agency, 2007*). Eddy current inspection technique detects the existence of tube damage by measuring distortions in eddy current signals that are induced in the tubes using probes. Only 100% through-wall cracks can be detected through leakage tests, while defects of various sizes can be detected using eddy current inspection, so that tubes with the potential to leak before next inspection can be plugged. A plugging criterion of 40% through-wall thickness was adopted in general by most countries (*Clark & Kurtz, 1988*). This plugging criterion was calculated for PWR SGs with Alloy 600 tubes, with specific tube diameters and thickness, and specific degradation mechanism (wastage) (*International Atomic Energy Agency, 2007*).

4.2 Uncertainties Associated with Nondestructive Evaluation Methods

Nondestructive evaluation equipments (e.g., eddy current) are often used to detect and characterize unknown existing defects[27] or degradations in structural components. Reliable detection and measurement of such hidden defects (rogue defects) is crucial for structural health diagnosis purposes. Nondestructive evaluation equipments are quite complex and it requires considerable skills from the operators to extract useful data from them. For example, ultrasonic-based nondestructive test equipment induces ultrasonic pulses into structural components, detects reflected ultrasonic pulses from defects or discontinuities, and then displays them in the form of electric signals (e.g., voltage). These electric signals are then analyzed and processed to provide quantitative estimates

[27] In this research defect may indicate a crack, flaw, pit, or any other degradation in a structural component. Size may refer to either through-wall depth or surface length of a defect, unless specified. Density refers to number of defects in a given volume.

of unknown existing defects that require careful consideration of various factors (e.g., physics-of-failure) on the part of the analyst, whose level of experience is a critical determinant of the quality of the evaluation. Hence, nondestructive evaluation process induces considerable detection uncertainties and measurement errors into the defect size and density estimates (Figure 29) (*Chatterjee & Modarres, 2011*).

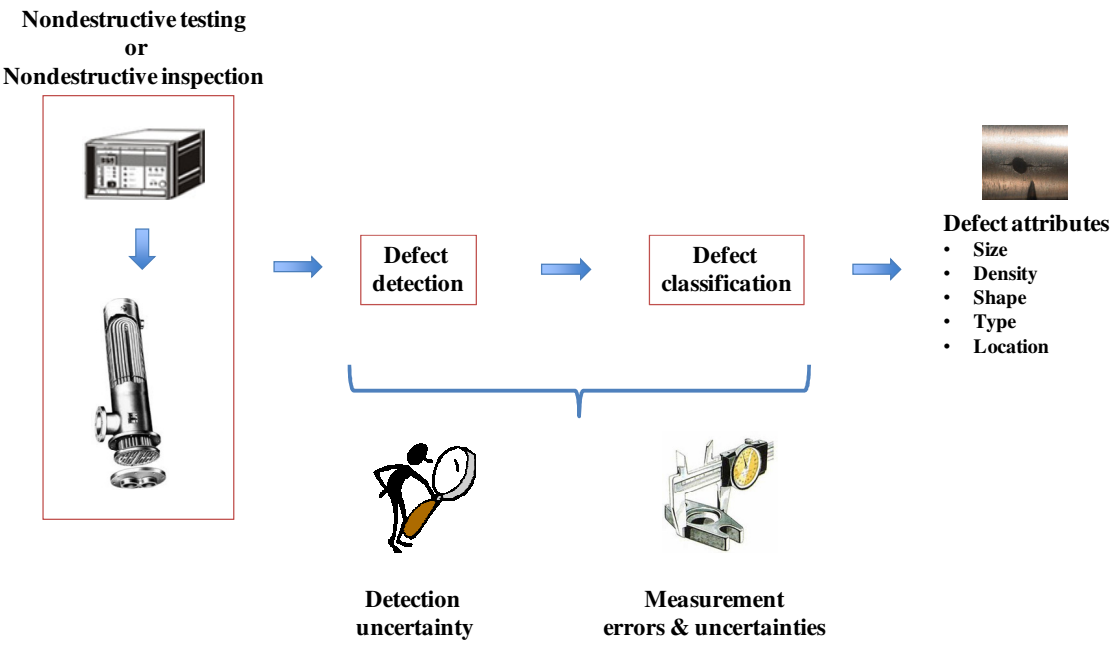

Figure 29: Nondestructive evaluation and associated uncertainties[28]

4.2.1 Probability of Detection and Associated Uncertainties

A defect of a given size might be detected only a certain percentage of the time (out of total attempts during nondestructive testing) depending on factors such as, noise level, test probe sensitivity, test equipment repeatability and human error. Hence, a defect has

[28] Some of the images in the Figure 29 are obtained through random Google search. The defect image is from IAEA-TECDOC-1577 (IAEA, 2007).

an associated POD, which can be defined as the probability the inspection will detect the defect of true size, a, and is denoted by $POD(a)$ (*Kurtz, Heasler & Anderson, 1992*). The data from which POD curves are generated can be categorized into two types: qualitative data, i.e., hit/miss; and quantitative data, i.e., signal response amplitude ($\hat{a}\ vs.\ a$), where $\hat{a}$ is signal response. The hit/miss data type is based on a binary process, i.e., whether a defect is detected or not detected (Figure 30). In Figure 30, D is the random variable that assumes a value of 1 representing detections, and a value of 0 representing non-detections.

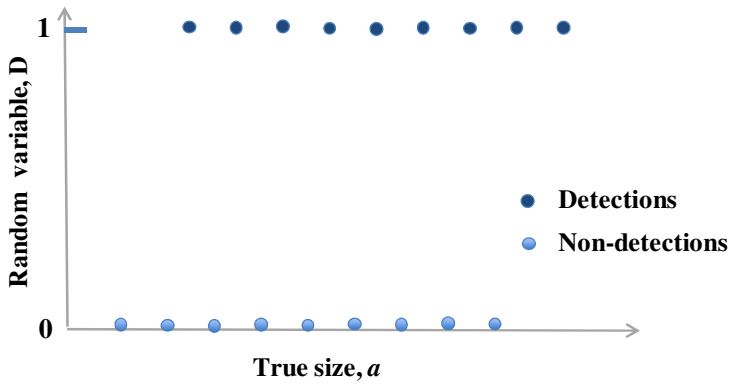

Figure 30: Hit/miss data

Hit/miss data are obtained from test equipments such as Sonic IR, and are very subjective in nature depending on operator experience (*Li & Meeker, 2008*). This induces uncertainty in the values of the POD generated for the hit/miss data. This kind of data provides less information than signal data, since it lacks repeatability. Also, in this data only the inspection outcome is known, but no information is available about the defect size. The POD for this data type is calculated as the ratio of the number of successful

detection over the total number of inspections performed for a particular defect size, and is called the averaged POD (Eq. 45).

$$POD(a) = \frac{Number\ of\ successful\ detections}{Total\ number\ of\ inspections} \tag{45}$$

These POD values are for discrete defect sizes. In order to obtain continuous POD curve (Figure 31), the logarithm of the odds is assumed to be correlated to the true size of defect (Eq. 46). This correlation is often assumed to be linear or log-linear. Based on this, the POD is modeled using a logistic function for this data type (*Georgiou, 2006; Jenson, Mahaut, Calmon, & Poidevin, 2010*), as shown by Eq. (47), where, θ is the set of parameters of the POD logistic model, and ε is the model error. A regression analysis is then performed to fit a continuous curve to the averaged POD values, as shown in Figure 31. Uncertainties associated with the logistic model and data are characterized through the regression analysis in terms of probability distributions of parameters θ and model error.

$$log\left(\frac{POD(a)}{1 - POD(a)}\right) \propto a \tag{46}$$

$$POD(a) = logistic(a, \theta) + \varepsilon \tag{47}$$

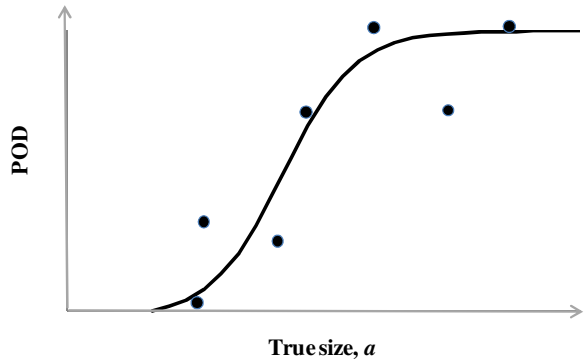

Figure 31: POD curve for hit/miss data

The other type of POD data is more continuous in nature and is a measure of the amplitude of signal response recorded by the nondestructive test equipment, e.g., ultrasonic or eddy current. Signal is the measured response of the nondestructive evaluation system to a defect. The unit of measured signal depends on the inspection equipment, and can be number of counts, volts, scale divisions, or pixels. For signal response data, much more information is supplied in the signal for analysis than is in the hit/miss data. The defect signal detection capability of inspection equipment depends on various factors, such as noise, repeatability, human error, material properties of component evaluated, and defect attributes. The noise factor is very important for detecting small defect sizes, because noise and signal distribution overlap. Hence, it is very critical to determine the noise distribution appropriately. In the signal response data-based POD estimation method, the most important parameters are the inspection threshold and the decision threshold (Figure 32).

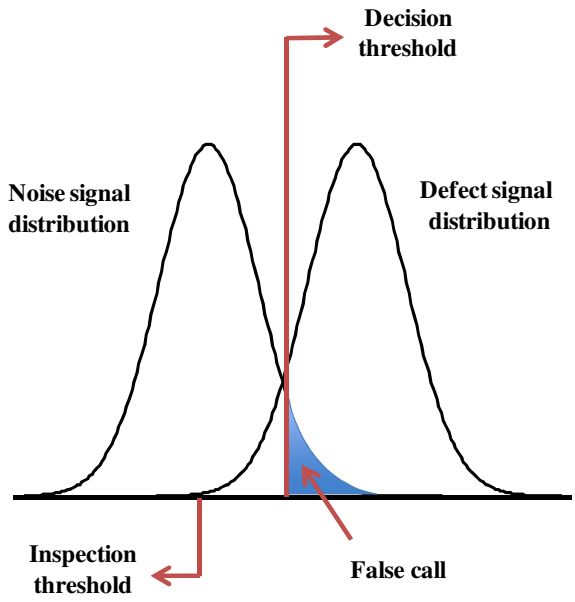

Figure 32: Signal vs. Noise

Inspection threshold is the smallest value of defect signal that the nondestructive evaluation system records, whereas decision threshold is used to make detection/non-detection decisions. A signal above a decision threshold is considered as "detected" while a noise that is above this threshold is considered as false call[29]. Decisions threshold is selected based on noise distribution, operator experience, and field inspection experience. Decision threshold is always equal to or higher than the inspection threshold. If decision threshold is chosen to be above the upper bound of noise distribution then there will be no possibility of false call. However, there is always a trade-off between detecting small flaws and probability of false call ($POFC$). If decision threshold is chosen to be below the noise upper bound (Figure 32) then there is an associated false call probability which needs to be adjusted in the POD. Then probability of indication (POI) can be written as shown by Eq. (48) (*Department of Defense,* 1999).

[29] A nondestructive test equipment response interpreted as having detected a crack but associated with no known crack at the inspection location (*Department of Defense, 1999*).

$$POI\ (a) = POFC(a) + \big(1 - POFC(a)\big).POD(a) \tag{48}$$

For POD estimation from signal data (Figure 33), it is generally assumed that the logarithm of the signal response amplitude is linearly correlated to the logarithm of the defect size as shown in Eq. (49), where β' and β'' are the correlation parameters, and ε is the model error. The model error is assumed to follow a normal distribution with mean zero and standard deviation σ.

$$log(\hat{a}) = \beta' + \beta'' log(a) + \varepsilon(0, \sigma) \tag{49}$$

Figure 33: Response amplitude vs. True size

Using the correlation of Eq. (49), a regression analysis is performed (Figure 34) to estimate the correlation parameters and the random error. The shaded region in Figure 34 represents signal amplitudes higher than the decision threshold signal. The POD for a defect size is then estimated (Eq. 50) by determining the probability of defect signal ($\hat{a}$) to be higher than the threshold signal ($\hat{a}_{th}$), which is given by a cumulative lognormal distribution as shown in Eq. (51) (*Georgiou,* 2006). Uncertainties in the parameters β' and β'' can be represented by probability distributions. Random values of these

parameters can be sampled from their respective distributions, which when used in Eq. (51) can result in all possible values of POD for a given defect size.

$$POD(a) = P(\hat{a} > \hat{a}_{th}) = P(\log(\hat{a}) > \log(\hat{a}_{th})) \tag{50}$$

$$POD(a) = 1 - \Phi\left(\frac{\log(\hat{a}_{th}) - \{\beta' + \beta'' log(a)\}}{\sigma}\right) \tag{51}$$

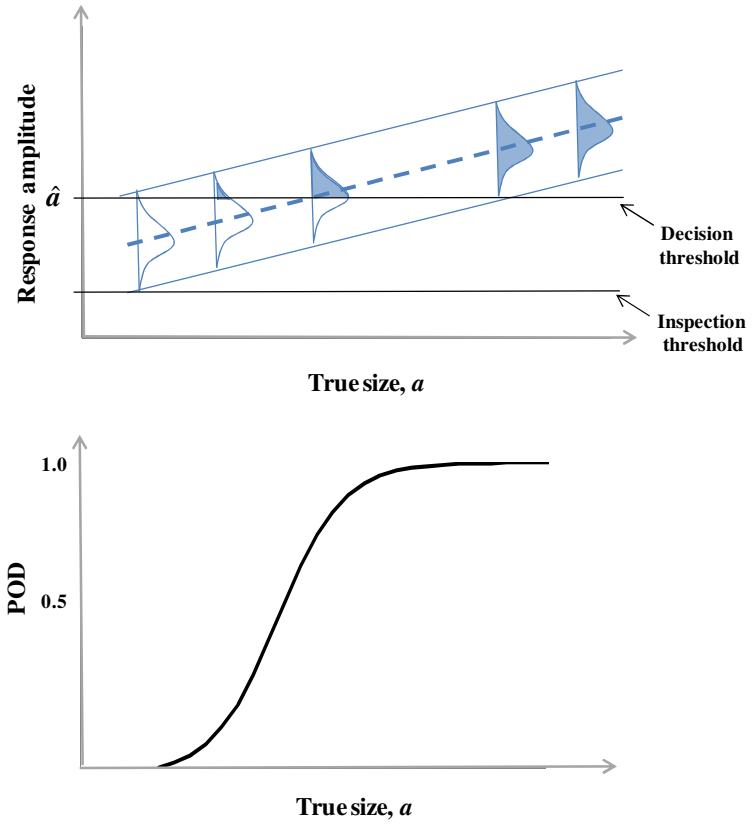

Figure 34: POD estimation from signal response data

In some cases, the signal response data is also converted into equivalent hit/miss data (*Jenson et al., 2010*) by using the decision threshold. Signal responses above the decision threshold are considered as detected while those below are considered not detected, as shown in Figure 35. Averaged POD values are then estimated for each defect size using

Eq. (45), which is then fitted into a logistic function by using the same procedure as that for hit/miss data discussed earlier in this section.

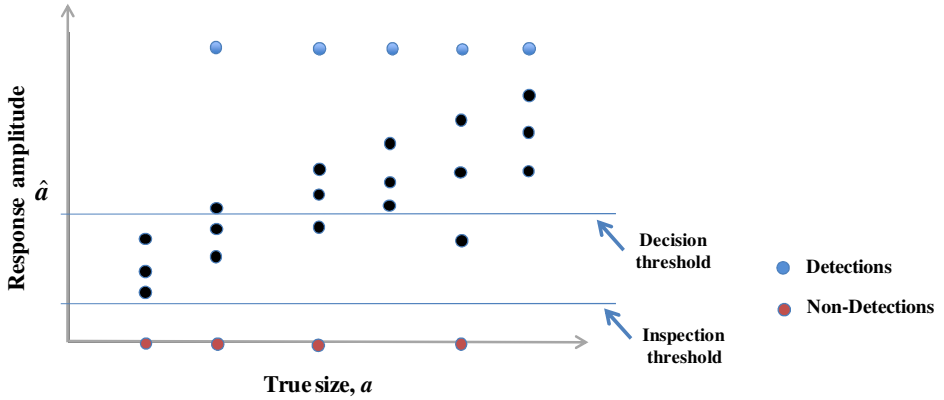

Figure 35: Equivalent hit/miss data

4.2.2 Measurement Error and Associated Uncertainties

The nondestructive evaluation measurement process must be monitored to ensure that the process is operating correctly (*Olin & Meeker, 1996*). This requires cross-validating the measurement results with known defect sizes to estimate the measurement errors and associated uncertainties. The precision and accuracy of nondestructive test equipment as well as the techniques used to analyze and process the test results contribute to measurement errors. For example, large volume of sensor data (such as ultrasound or digital images) are filtered, smoothed, reduced, and censored into another form by subjectively accounting for only certain features of the data. Also, often measurement models are used to convert the form of a measured or observed data into the corresponding value of the reality of interest (i.e., defect size). Uncertainties associated with model selection and human errors can also contribute to measurement errors.

After a defect is detected, the signal amplitudes are processed and analyzed to estimate corresponding sizes (Figure 36). Measurement error is then assessed as the deviation of measured size from the true value. The true value is obtained from destructive evaluations. In classical measurement error, it is assumed that the error is independent of, or uncorrelated with, the true value of the underlying variable (*Hyslop & Imbens, 2001*). However, in general there is a correlation between measurement error and true value.

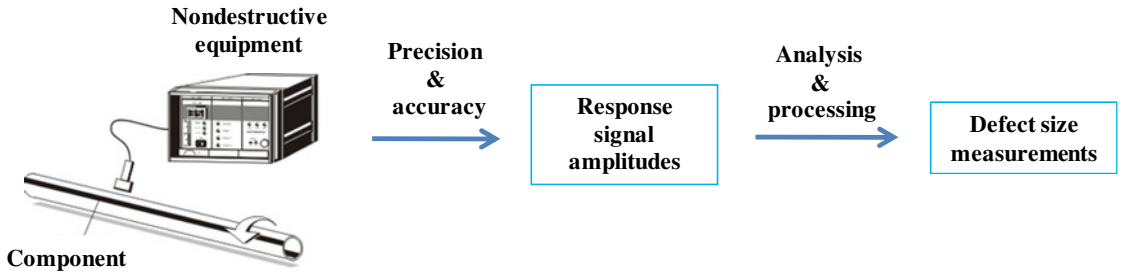

Figure 36: Factors affecting measurements[30]

In order to describe the components of measurement error and associated uncertainties, let us consider the measured size distribution, which is obtained through repeated measurements of a single defect size (Figure 37). There are two components of measurement error: systematic (bias) error and random (stochastic) error (*Jaech, 1964; Hofmann, 2005*). The deviation of the mean of the measured size distribution (Figure 37) from the true value gives the bias or the systematic error. Bias or systematic error is defined as a continuous deviation in the same direction from the true value (*Hofmann, 2005*). Bias can be overestimated or underestimated. Often in the case of nondestructive evaluation, bias represents overestimation for small sizes and underestimation for large

[30] The NDE equipment image has been obtained from random Google search and modified.

sizes (*Kurtz et al., 1992; Wang & Meeker, 2005*). Other than the bias, there is also a random error, which arises due to the scattering or random variation in measured values (measurement uncertainty). For nondestructive measurement process to be "in control", it is essential that the measurement precision (randomness) remains constant, and there is no appreciable drifting or shifting from the true value (bias) (*Olin & Meeker, 1996*). A method for modeling measurement error is discussed in detail in the next section.

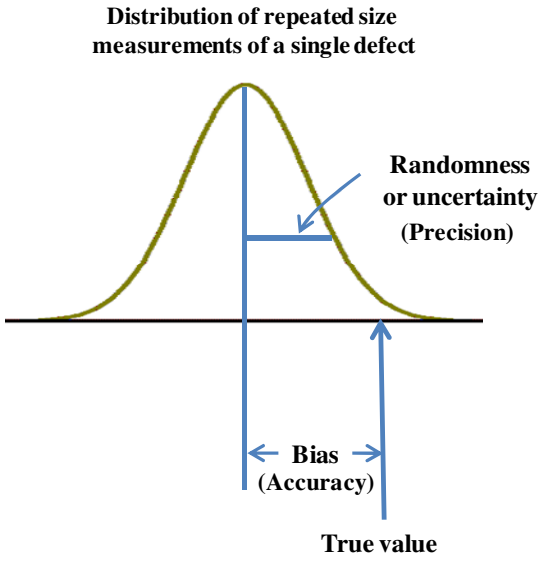

Figure 37: Measurement error components

4.3 Structuring a Bayesian Probabilistic Approach for Estimating True Defect Severity accounting for all Uncertainties and Errors

Past efforts in modeling defect severity in structural components have not been successful in considering all the uncertainties and errors associated with nondestructive evaluation methods[31]. Most of the authors have neglected the effect of some uncertainties or errors. For example, *Rodriguez and Provan* (1989) present a method to model pitting

[31] A detailed literature survey has been presented in the introduction section of this dissertation.

corrosion based on data from in-service inspection, considering only the POD in a simplified manner and ignoring the effect of measurement error. *Cizelj and Dvorsek* (1998) consider the impact of measurement error in inspection data on SGTR probability, neglecting the effect of POD. Some authors have considered only big size defects in order to overcome the uncertainties associated with detecting and measuring small sizes. For example, *Datla, Jyrkama and Pandey* (2008) present an eddy current inspection-based pitting corrosion model considering only big size pits (>50% through-wall depth), in order to overcome the nondestructive inspection uncertainties associated with small sizes. Though detection uncertainties are negligible, there is still considerable measurement error (especially systematic error) associated with big sizes.

Celeux, Persoz, Wandji and Perrot (1999), describe a method to model defects in PWR vessels considering the POD and random error in measurements. *Yuan, Mao and Pandey* (2009), followed the idea of *Celeux et al.* (1999), to propose a model for pitting corrosion in SG tubes considering the POD and random error of the eddy current measurements. However, both *Celeux et al.* (1999) and *Yuan et al.* (2009) did not consider the effect of systematic error or bias in measured defect sizes. Further, they did not consider uncertainties in the values of the POD, which can affect the defect severity estimates considerably.

In order to address some of the limitations of existing techniques, a Bayesian probabilistic approach has been proposed in this research that combines prior knowledge of defect size and density with uncertain nondestructive evaluation data, considering the POD, measurement errors (systematic and random), and associated uncertainties, to infer

the posterior distributions of defect size and density. The combined effect of POD, measurement errors, and associated uncertainties on measured defect sizes is captured by a likelihood function. In this section, approach to model nondestructive evaluation uncertainties, e.g., measurement errors, POD, and associated uncertainties, will be first presented; followed by the Bayesian models for defect size and density.

4.3.1 Approach to Model Nondestructive Evaluation Uncertainties

Nondestructive evaluation uncertainties consist of POD, measurement errors, and associated epistemic and aleatory uncertainties. As discussed in the previous section, the analysis of measurement errors is based on assessing the deviation of the measured defect size from the actual or true defect size, as shown by Eq. (52):

$$E_{me} = a^* - a \tag{52}$$

where, E_{me} is the measurement error, a^* is measured and a is the true defect size. Generally a linear regression relationship of the form shown in Eq. (53) is used to model measurement error (*Jaech, 1964; Kurtz et al., 1992*):

$$a^* = ma + c + \varepsilon(0, \sigma) \tag{53}$$

where, m and c are regression coefficients obtained through a regression analysis (Figure 38) of $a^* \; vs. \; a$, and ε is the random error in measurement (scattering of the data), which is assumed to follow a normal distribution with mean zero and standard deviation σ. This standard deviation can also often be a function of defect size, which needs to be verified. For example, a form of $\gamma * exp(\delta * a)$ can be assumed for standard deviation in the regression analysis to estimate the parameters γ and δ, along with m and c. Based on the

values of parameter, δ, the dependency of standard deviation σ on defect size can be established. For example, if $\delta \approx 0$, then σ can be assumed to be independent of defect size.

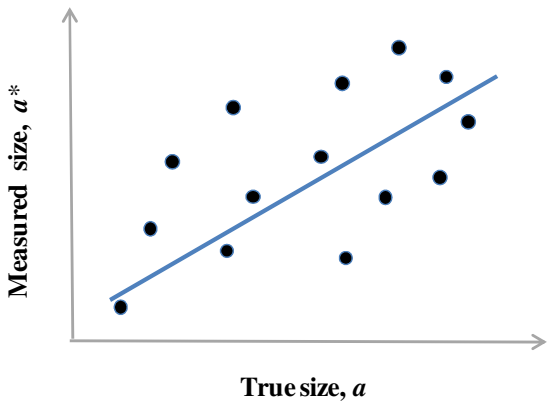

Figure 38: Regression analysis of measurement error

The regression coefficients (m & c) are jointly measure of systematic error or bias in measurements. For different values of bias parameters, systematic error can be zero, constant, or variable. For example, if $m = 1 \; and \; c = 0$, then systematic error is zero. If $m = 1 \; and \; c \neq 0$, then systematic error is constant. If $m \neq 1$, then systematic error is variable. The distribution of bias parameters represents epistemic uncertainty in the chosen measurement error model. From Eqs. (52) and (53), the measurement error can be expressed as:

$$E_{me} = \overbrace{(m-1)a + c}^{Bias} + \overbrace{\varepsilon(0,\sigma)}^{Random\ error} \tag{54}$$

Since nondestructive evaluation data are in the form of measured defect sizes, measurement error is further expressed as a function of measured defect size using Eqs. (52) and (54), as shown in Eq. (55):

$$E_{me} = \overbrace{\left(\frac{m-1}{m}\right)a^* + \frac{c}{m}}^{Bias} + \frac{\overbrace{\varepsilon(0,\sigma)}^{Random\ error}}{m} \tag{55}$$

The PDF of the measurement error as a function of measured defect size can then be defined using a normal distribution with mean as the bias, B_{a^*}, standard deviation as that of random error, $\frac{\sigma}{m}$, and measurement error as random variable, as shown in Eqs. (56) and (57).

$$g_{a^*}(E_{me}) = N\left(B_{a^*}, \frac{\sigma}{m}\right) \tag{56}$$

$$g_{a^*}(E_{me}) = \frac{1}{\sqrt{2\pi\left(\frac{\sigma}{m}\right)^2}} e^{-\frac{1}{2\left(\frac{\sigma}{m}\right)^2}\left\{E_{me}-\left(\frac{m-1}{m}\right)a^*-\frac{c}{m}\right\}^2} \tag{57}$$

All the defects in a structure are not detected during nondestructive testing. The probability of detection of a defect depends on its true size and is represented by the POD curve. The POD of a defect of true size, a, can be represented by a function $POD(a|\theta, a_{th})$, where, θ is vector of parameters of the POD function, and a_{th} is detection threshold size below which the POD assumes a value of zero. The POD function is selected based on the type of data, e.g., hit/miss (logistics) or signal response (lognormal) as discussed in Section 4.2.1. The expected POD independent of uncertain parameters, θ can then be expressed as shown in Eq. (58), where, $k(\theta)$ represents the joint PDF of the parameters of the POD function. The joint PDF, $k(\theta)$, represents the epistemic uncertainty in the chosen POD model or function.

$$POD(a) = \int_{\theta} POD(a|\theta)k(\theta)d\theta \tag{58}$$

4.3.2 Bayesian Model for Estimating True Defect Size

Due to associated POD, all defects of a given size may not be detected during nondestructive testing. Further, it may also be possible that no defects are detected for very small-sized defects (above detection threshold). Small-sizes defects have low PODs associated with them and hence reliable characterization of such defects is often not possible. Therefore it may be possible that "no-detection" category is assigned to those small defect sizes. In this section, the likelihood functions are derived for both detections as well as non-detections cases.

4.3.2.1 Likelihood Function for Detections:

The conditional probability of a true defect size, a, given that the defect is detected can be expressed as (*Celeux et al., 1999*):

$$Pr(a < A < a + da|D = 1) = \frac{Pr\,[a < A < a + da \cap D = 1]}{Pr\,(D = 1)}$$

$$= \frac{Pr(a < A < a + da)\,.\,Pr\,(D = 1|a < A < a + da)}{Pr\,(D = 1)} \tag{59}$$

where, A is true defect size random variable, and D is a binary random variable indicating whether or not a defect is detected, i.e., D=1 if defect is detected and 0 otherwise. Limit $da \to 0$ was applied to both sides of Eq. (59) to obtain the conditional probability of detecting a defect of true size, a, as shown in Eq. (60):

$$\lim_{da\to 0}\frac{Pr(a<A<a+da|D=1)}{da}=\frac{f(a|\psi)\times POD(a)}{M_{POD}(\psi)} \tag{60}$$

where, $f(a|\psi)$ is the PDF of true defect size given the vector of the PDF parameters, ψ, and $M_{POD}(\psi)$ is the marginal POD that is a function of ψ only (independent of defect size), and can be expressed as:

$$M_{POD}(\psi)=\Pr(D=1)=\int_0^{\infty} POD(a)f(a|\psi)da \tag{61}$$

Nondestructive evaluation data consists of measured defect sizes (exact or interval) and number of detections. In this research, the purpose is to first update prior knowledge of true defect size PDF parameters with uncertain nondestructive evaluation data considering measurement errors and POD; and then update the defect density (number of defects per unit volume) distributions based on posterior true defect size PDF parameters. The likelihood function of true defect size PDF parameters, ψ, given nondestructive evaluation data consisting of n_e^* defects detected with exact size measurements, can be represented (using Eq. 60) considering measurement errors, as shown in Eq. (62), where, $Data_{exactdet}$ represents exact defect size detections data:

$$L(\psi|Data_{exactdet})=P(Data_{exactdet}|\psi)$$
$$=\frac{1}{[M_{POD}(\psi)]^{n_e^*}}\prod_{i=1}^{n_e^*}\int_{E_{me}} POD(a_i^*-E_{me})f\big((a_i^*-E_{me})|\psi\big)g_{a^*}(E_{me})dE_{me} \tag{62}$$

An alternative way of expressing Eq. (62) is to correct measured defect sizes for measurement errors first by using Eq. (63), and then express the likelihood function in

terms of true defect size, as shown in Eq. (64). This helps in reducing the complexity of the likelihood function and makes Bayesian inference computation easier.

$$a = \int_{E_{me}} (a^* - E_{me}) g_{a^*}(E_{me})\, dE_{me} \tag{63}$$

From Eq. (57), corresponding to each random sampling of bias and random error parameters, there is a probability distribution of measurement error. Hence, for each realization of measurement errors, an expected value of true defect size[32] corresponding to a measured size is estimated using Eq. (63). The Eq. (62) can then be also expressed as:

$$L(\psi|Data_{exactdet}) = P(Data_{exactdet}|\psi)$$
$$= \frac{1}{[M_{POD}(\psi)]^{n_e^*}} \prod_{i=1}^{n_e^*} POD(a_i) f(a_i|\psi) \tag{64}$$

Nondestructive measurements are in most cases interval or left censored, in which case the likelihood function of ψ given nondestructive evaluation data consisting of $n^*_{interval,j}$ defects detected with interval size measurement, i.e., lying in the j_{th} size interval (a_{j-1}, a_j), can be expressed considering measurement errors, as shown in Eq. (65). Eq. (65) can also be expressed in terms of true defect size by correcting for measurement errors first as shown in Eq. (66).

[32] In some cases depending on measurement error distribution, it is possible that the expected value of true defect sizes obtained using Eq. (63) corresponding to very small measured sizes is negative. In those cases, the true defect size is assumed to be zero, i.e., no detection.

$$L(\psi|Data_{intdet}) = P_j(Data_{intdet}|\psi) =$$

$$\left[\frac{1}{M_{POD}(\psi)}\int_{a_{j-1}^*}^{a_j^*}\int_{E_{me}} POD(a^* - E_{me}) f\big((a^* - E_{me})|\psi\big) g_{a^*}(E_{me}) dE_{me}\, da^*\right]^{n^*_{interval,j}} \quad (65)$$

$$L(\psi|Data_{intdet}) = P_j(Data_{intdet}|\psi)$$

$$= \left[\frac{1}{M_{POD}(\psi)}\int_{a_{j-1}}^{a_j} POD(a) f(a|\psi)\, da\right]^{n^*_{interval,j}} \quad (66)$$

In Eqs. (65) and (66), $Data_{intdet}$ represents interval (or a left[33] censored interval) defect size detections data.

4.3.2.2 Likelihood Function for Non-Detections

For small defect sizes (above detection threshold) with low POD values, nondestructive evaluations can often result in "no-detections". The conditional probability of a true defect size given that the defect is not detected ($D = 0$) can then be expressed as:

$$Pr(a < A < a + da|D = 0) = \frac{Pr\,[a < A < a + da \cap D = 0]}{Pr\,(D = 0)}$$

$$= \frac{Pr(a < A < a + da)\,.\,Pr\,(D = 0|a < A < a + da)}{Pr\,(D = 0)} \quad (67)$$

Limit $da \to 0$ was applied to both sides of Eq. (67) to derive the conditional probability of not detecting a defect of true size, a, as shown in Eq. (68):

[33] For left censored data the lower defect size integral limit in likelihood function assumes a value equal to that of the detection threshold. This is because POD assumes a value of zero for defect sizes less than the detection threshold.

$$\lim_{da\to 0}\frac{Pr(a<A<a+da|D=0)}{da}=\frac{f(a|\psi)\times(1-POD(a))}{(1-M_{POD}(\psi))} \tag{68}$$

The likelihood function of ψ given non-detections data can be expressed as shown in Eq. (69), where, $Data_{nondet}$ represents non-detections data, a_{th} is detection threshold below which POD = 0, and a_d is true defect size (after correcting measured size a_d^* for measurement error using Eq. 63) below which "no-detections" decisions have been made.

$$\begin{aligned} L(\psi|Data_{nondet}) &= P(Data_{nondet}|\psi) \\ &= \frac{1}{(1-M_{POD}(\psi))}\int_{a_{th}}^{a_d}(1-POD(a))f(a|\psi)\,da \end{aligned} \tag{69}$$

4.3.2.3 Combined Likelihood Function (Detections and Non-Detections)

The likelihood function of true defect size PDF parameters, ψ, given nondestructive evaluation data consisting of both detections as well as non-detections can then be expressed as shown in Eq. (70), where, interval data consists of z defect size intervals each with certain number of defects ($e.g.,\ n^*_{interval,j}$ in j_{th} interval):

$$\begin{aligned} L(\psi|Data) &= P(Data|\psi) \\ &= P(Data_{exactdet}|\psi)\times\prod_{j=1}^{z}\left(P_j(Data_{intdet}|\psi)\right) \\ &\times P(Data_{nondet}|\psi) \end{aligned} \tag{70}$$

$$L(\psi|Data) = P(Data|\psi) =$$

$$\frac{1}{[M_{POD}(\psi)]^{n_e^*}} \prod_{i=1}^{n_e^*} \int_{E_{me}} POD(a_i^* - E_{me}) f\big((a_i^* - E_{me})|\psi\big) g_{a^*}(E_{me}) dE_{me} \times$$

$$\prod_{j=1}^{z} \left[\frac{1}{M_{POD}(\psi)} \int_{a_{j-1}^*}^{a_j^*} \int_{E_{me}} POD(a^* - E_{me}) f\big((a^* - E_{me})|\psi\big) g_{a^*}(E_{me}) dE_{me}\, da^* \right]^{n_{interval,j}^*} \times$$

$$\frac{1}{(1 - M_{POD}(\psi))} \int_{a_{th}}^{a_d} (1 - POD(a)) f(a|\psi)\, da \qquad (71)$$

Eq. (71) can also be expressed in terms of true defect size by correcting measured defect sizes for measurement errors first, as shown in Eq. (72):

$$\begin{aligned} L(\psi|Data) &= P(Data|\psi) \\ &= \frac{1}{[M_{POD}(\psi)]^{n_e^*}} \prod_{i=1}^{n_e^*} POD(a_i) f(a_i|\psi) \\ &\times \prod_{j=1}^{z} \left[\frac{1}{M_{POD}(\psi)} \int_{a_{j-1}}^{a_j} POD(a) f(a|\psi)\, da \right]^{n_{interval,j}^*} \\ &\times \frac{1}{(1 - M_{POD}(\psi))} \int_{a_{th}}^{a_d} (1 - POD(a)) f(a|\psi)\, da \end{aligned} \qquad (72)$$

The posterior distribution of true defect size PDF parameters, ψ, can then be estimated using Bayesian inference as:

$$\pi_1(\psi|Data) = \frac{P(Data|\psi)\pi_0(\psi)}{\int_\psi P(Data|\psi)\pi_0(\psi) d\psi} \qquad (73)$$

where, $\pi_1(\psi|Data)$ is posterior distribution of ψ given nondestructive evaluation data, and $\pi_0(\psi)$ is prior distribution of ψ. In order to consider and propagate the epistemic and

aleatory uncertainties associated with measurement errors, different realization of measurement error PDF can be obtained using Eq. (57) for each random value of bias and random error parameters. Corresponding to each realization of measurement error PDF, posterior distribution of true defect size PDF parameters is obtained using Eq. (73). Finally, all realizations of the posterior distribution are combined to determine the weighted average distribution for the true defect size PDF parameters. The posterior values of true defect size PDF parameters can then be used to estimate the corresponding marginal POD values (Eq. 61). The marginal POD values would then be used in deriving defect density model as presented in next section.

4.3.3 Bayesian Model for Estimating True Defect Density

The likelihood function of true number of defects, n, given observed number of defects, n^* $(= n_e^* + \sum_{j=1}^{z} n_{interval,j}^*)$ can be expressed by a binomial function (detection process is binary, i.e., either detection or no detection), as shown by Eq. (74):

$$L(n|n^*) = P(n^*|n) = \binom{n}{n^*} [M_{POD}(\psi)]^{n^*} [1 - M_{POD}(\psi)]^{n-n^*} \tag{74}$$

where, $M_{POD}(\psi)$ is the marginal POD value corresponding to posterior defect size PDF parameters, ψ, and $\binom{n}{n^*} = n!/\{n^*!\,(n-n^*)!\}$, where $n!$ represents factorial of n. In Eq. (74), the true number of defects, n, is unknown whereas n^* and $M_{POD}(\psi)$ are known. The true number of defects can then be estimated using Bayesian inference as shown in Eq. (75):

$$\pi_1(n|n^*) = \frac{P(n^*|n)\pi_0(n)}{\sum_n P(n^*|n)\pi_0(n)} \tag{75}$$

where, $\pi_1(n|n^*)$ is posterior distribution of true number of defects given the observation, n^*, and $\pi_0(n)$ is the prior distribution of number of defects. The prior distribution of number of defects can be estimated from a Poisson function, which gives the probability of observing n total number of defects in a volume V, given prior defect density ρ as shown in Eq. (76). Here Poisson distribution is used because defects are assumed to occur with the same average intensity and independent of each other.

$$\pi_0(n) = e^{-\rho V}\frac{(\rho V)^n}{n!} \tag{76}$$

The posterior distribution of true number of defects (Eq. 75) can then be used to obtain the posterior defect density. The standard conjugate prior employed for Poisson distribution likelihood (Eq. 76) is a two-parameter gamma distribution (*Simonen, Doctor, Schuster, & Heasler, 2003*), in which case the posterior has the same functional form as the gamma distribution. Assume that prior distribution of defect density is:

$$\pi_0(\rho) = gamma(\rho|\alpha_1, \alpha_2) \tag{77}$$

where, α_1 and α_2 are parameters of gamma distribution. Then the posterior distribution of defect density can be expressed as shown in Eq. (78).

$$\pi_1(\rho) = gamma(\rho|V + \alpha_1, n + \alpha_2) \quad (78)$$

4.3.4 Summary of Proposed Bayesian Approach

The proposed Bayesian approach (as summarized by Figure 39) improve upon existing techniques because it considers the detection uncertainties and measurement errors associated with nondestructive evaluation methods in a comprehensive manner. Further, the Bayesian approach incorporates prior knowledge of defect size and density, which is critical given the limited evidence or data available from nondestructive evaluations. For example, if instead maximum likelihood method is used to obtain point estimates of defect model parameters based only on the limited evidence, the results would not be reliable. To summarize, the proposed Bayesian approach considers both components of measurement errors (i.e., systematic and random) and associated uncertainties; considers probability of detection and associated uncertainties; incorporates prior knowledge of defect size and density; provides a framework for updating probability distributions of defect model parameters when new data become available; and is applicable to exact, interval, and censored measurements.

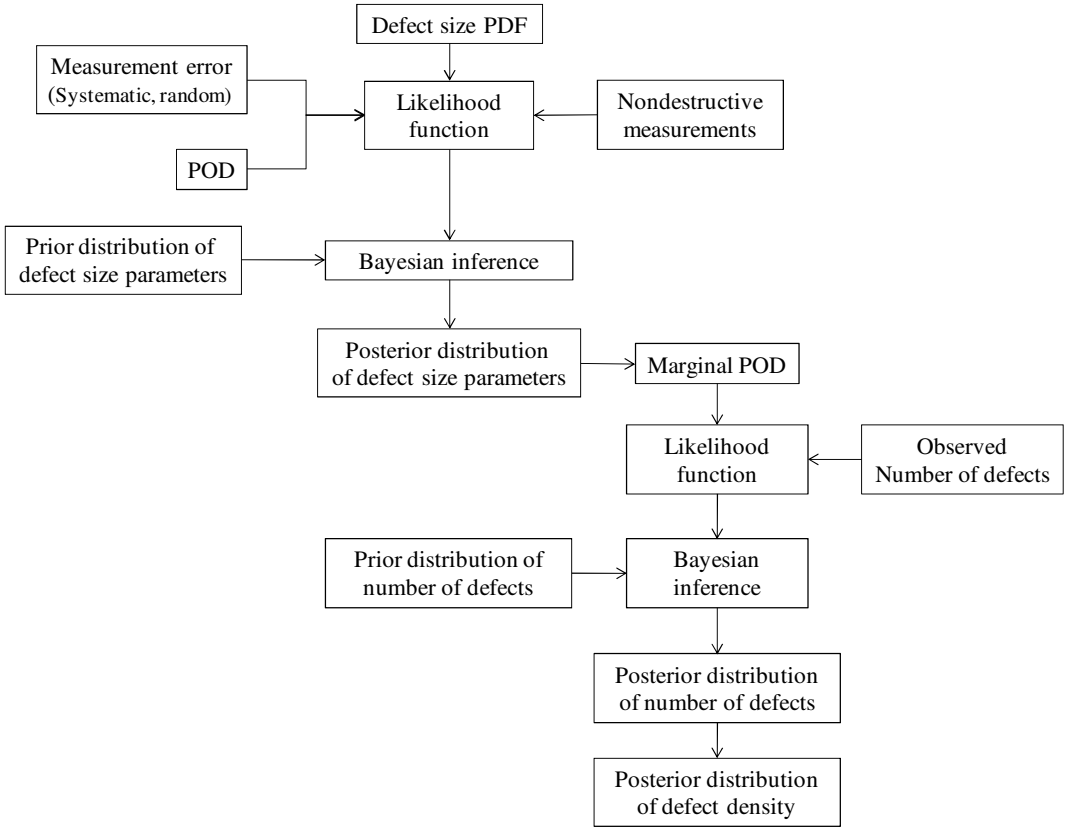

Figure 39: Bayesian approach for estimating true defect size and density

Further, there is a need for a tool to compute the Bayesian inference, so that the proposed Bayesian approach can be implemented for practical applications. WinBUGS is software that uses Markov Chain Monte Carlo (MCMC) methods for Bayesian analysis. However, two characteristics of the proposed Bayesian approach make WinBUGS not applicable. Firstly, the likelihood function (Eq. 72) consists of integration (WinBUGS does not provide integral function) and secondly, the likelihood function is not a standard PDF (e.g., normal). However, both these limitations can be overcome using OpenBUGS[34], which is an open source variant of WinBUGS. OpenBUGS is software for the Bayesian analysis of complex models using MCMC. An OpenBUGS routine was

[34] http://www.openbugs.info/w/

developed for solving the complex Bayesian inference of the proposed approach, which estimates the posterior distribution of true defect size PDF parameters. Simultaneously a MATLAB routine was also developed to implement the entire proposed Bayesian approach for estimating true defect size and density in structural components. An application of the proposed Bayesian approach is provided in Chapter 5 to estimate real defect size and density distributions based on uncertain in-service eddy current evaluation data.

4.4 An Integrated Approach Incorporating Bayesian Results for Assessing In-Service Steam Generator Tube Rupture Frequency

The defect size and density distributions estimated using the proposed Bayesian approach represent the health condition of the tubes at the inspection time. This can be used in the PPoF-based approach presented in Chapter 2 to estimate the SGTR frequency distributions. Using the PPoF-based approach, the degradation mechanisms can be simulated starting from the real health condition (defect size and density distributions determined through proposed Bayesian approach) at in-service inspections, to estimate the final defect size distributions at the mean life of the SG as shown in Figure 40.

The SGTR frequency for the remaining life of the SG can then be estimated by the probabilistic approach described in Chapter 2 of this dissertation. Since, in-service inspections are generally performed every 3 years (approximately), the SGTR frequency distributions can be estimated for every inspections to support in-service PSA of SMRs and risk informed maintenance, as shown in Figure 41.

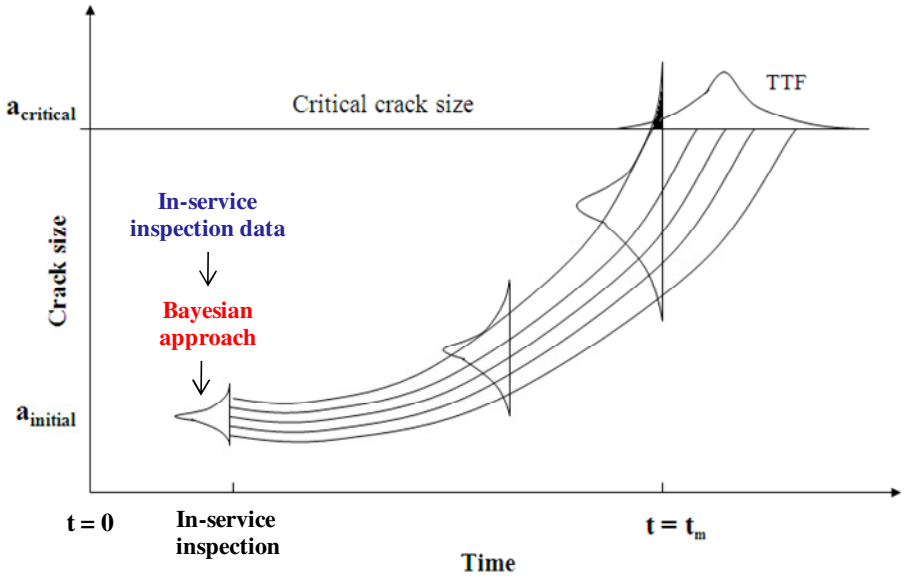

Figure 40: Flaw growth simulation using PPoF models starting from health condition at in-service inspection

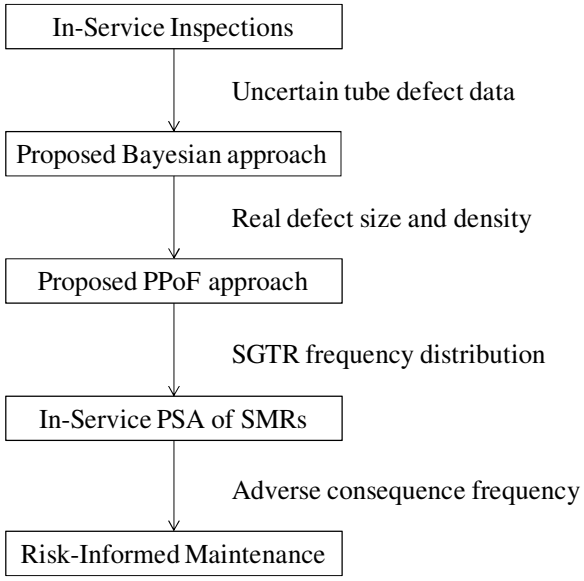

Figure 41: Estimating SGTR frequency using In-service inspection data

CHAPTER 5: ESTIMATING TRUE FLAW SIZE AND DENSITY DISTRIBUTIONS BASED ON IN-SERVICE EDDY CURRENT EVALUATION DATA

SG tubes are critical component of a PWR, and their failure can lead to catastrophic consequences. Several degradation mechanisms can affect the integrity of SG tubes during its operating lifetime. The accumulated damage due to these degradations may be in the form of cracks, pits, or flaws. Proactive maintenance activities are needed to detect defective or damaged SG tubes so that the health of those SG tubes can be restored. Therefore it is necessary to timely detect and characterize unknown existing tube defects considering the nondestructive evaluation uncertainties, and estimate the SGTR frequency.

The proposed Bayesian approach is used for estimating real/true defect size and density in SG tubes using eddy current nondestructive evaluation measurements, which included flaw sizes (through-wall depth). The eddy current evaluation technique, which is currently the main method for SG tube inspection during periodic safety maintenance, uses probes to detect the existence of tube damage by measuring distortions in the eddy current signals induced in the tubes. In power plant technical specifications, the SG tube plugging limit is generally set with respect to the flaw through-wall depth regardless of the flaw surface length. Hence, the flaw length data are generally not reported in the in-service inspection reports (*Liao & Guentay*, 2009). Since there is no operational data

available for the SMR design in consideration (still in pre-licensing stage), in-service eddy current inspection data for SG tubes from literature were considered to demonstrate the applicability of the Bayesian approach in estimating actual defect size and density considering all the detection uncertainties and measurement errors. In the following sections, POD and measurement errors are first modeled for eddy current testing using available data from literature, and then the proposed Bayesian approach is used to estimate the posterior distributions of true flaw size and density.

5.1 Modeling Eddy Current Evaluation Uncertainties

The eddy current measurement error is assessed in this research by a Bayesian regression analysis (*Azarkhail & Modarres, 2007*) between measured and true flaw depth (Figure 42) in light of available data from literature (*Kurtz et al., 1990*), to estimate the bias and random error parameters m, c and σ (Figure 43; Table 12). The parameters m, c and σ obtained through Bayesian regression were then used in Eq. (57) to estimate the PDF of measurement error as a function of measured flaw depths.

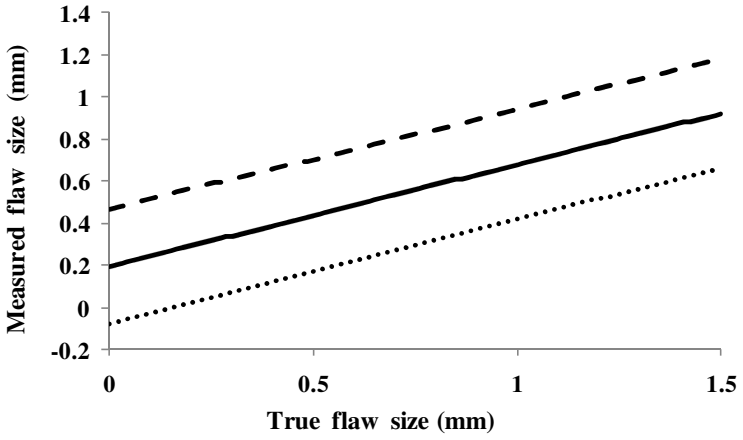

Figure 42: Measurement error regression analysis

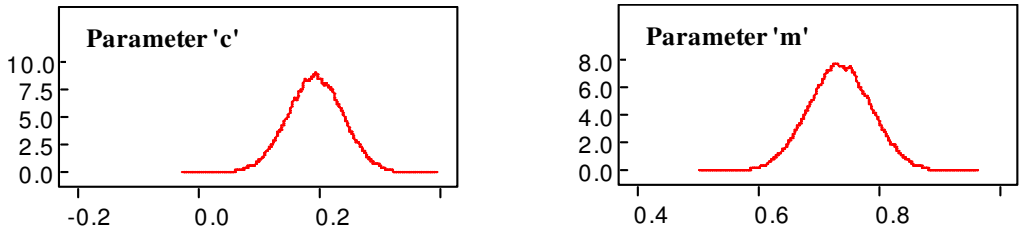

Figure 43: Distribution of parameters

Table 12: Measurement error parameter values from Bayesian regression

Parameters	Values
μ_m, σ_m	0.7352, 0.052
μ_C, σ_C	0.1933, 0.046
σ	0.13

In order to derive the POD model, it was assumed in this paper that eddy current signal response data were converted into equivalent hit/miss. A logistic function is found to best-fit hit/miss data for modeling POD (*Georgiou, 2006; Jenson et al., 2010*). The logistic function used to model POD in this paper is as shown in Eq. (79) (*Yuan et al., 2009*):

$$POD(a|\beta_1,\beta_2) = \begin{cases} 1 - \dfrac{1+e^{-\beta_1\beta_2}}{1+e^{\beta_1(a-\beta_2)}} & for\ a > a_{th} \\ 0 & otherwise \end{cases} \quad (79)$$

where, a is flaw size, a_{th} is threshold size for detection, and β_1 and β_2 are logistic function parameters. A flaw of size less than detection threshold will not be detected. The POD model parameters β_1 and β_2 were estimated by fitting Eq. (79) to averaged POD data available from literature (*Kurtz et al.,* 1992) using maximum likelihood estimation

(MLE) method, as shown in Table 13. Figure 44 illustrates the logistic function curve fitted on POD data, with detection threshold (a_{th}) assumed to be 0.05 mm.

Table 13: POD parameters

Parameters	Values
β_1	5.7
β_2	-0.067
a_{th}	0.05

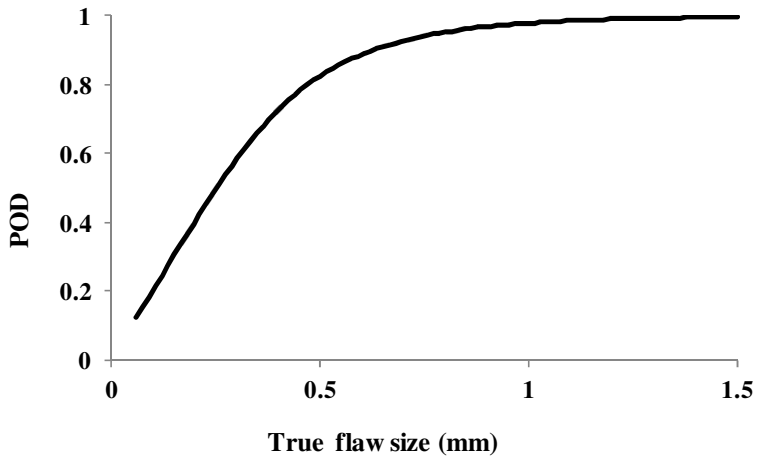

Figure 44: POD curve

5.2 Estimating True Flaw Size and Density Distributions Using Proposed Bayesian Approach

Flaws in nuclear reactor components are in most cases best fitted with an exponential distribution (*Simonen, Doctor, Schuster, & Heasler, 2003; Schuster, Simonen, & Doctor, 2008*) with smaller size flaws having higher probability density. Here the PDF of random variable, a, i.e., true flaw size in SG tubes, is defined assuming exponential distribution as shown in Eq. (80), where, λ is the flaw size intensity.

$$f(a|\lambda) = \lambda e^{-\lambda a} \tag{80}$$

The marginal POD, $M_{POD}(\lambda)$, which is a function of flaw size intensity only, was estimated using Eq. (61), as illustrated by Figure 45.

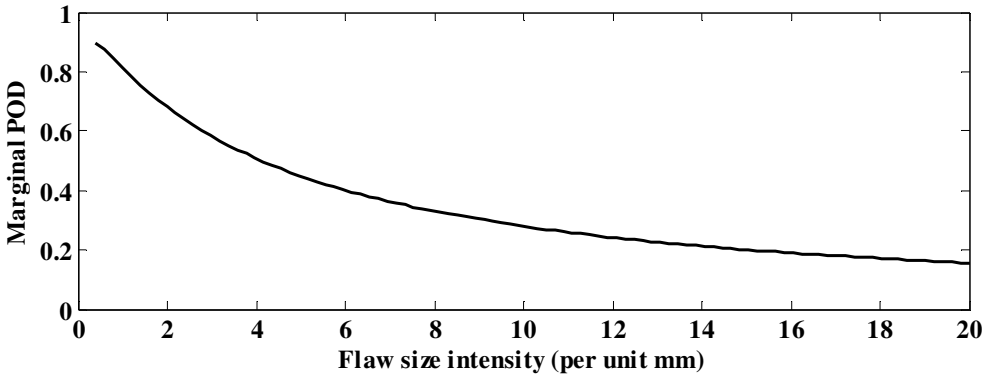

Figure 45: Marginal POD

Since the SMRs are not under operation yet, in-service inspection data available from literature for a PWR with Alloy 600 tubes (*Dvorsek & Cizelj, 1993*) were used to estimate the flaw severity distributions. The data will provide a conservative estimate of SGTR frequency, since degradations in Alloy 690 tubes would be less than Alloy 600. The eddy current evaluation data consisted of through-wall degradation measurements for flaws in tubes at all the tube support plate locations in the PWR. This data corresponds to in-service inspection at 10 years of PWR operation.

In most of the PWRs around the world the plugging criterion of 40% through-wall depth is still used (*Clark & Kurtz, 1988*). In this research, all flaw sizes above 40% through-wall for all support plates in the PWR were considered as plugged. Further, the expected POD is very close to 1 for these flaw sizes. The inspection data corresponding to flaw size intervals less than 40% through-wall were prorated for total number of tubes

in SMRs (≈ 1000 as compared to 5000 in PWR). Table 14 shows prorated in-service inspection data for all support plates for all flaws size intervals less than 40% through-wall (through-wall thickness = 1.5mm).

Table 14: Flaw size measurements (prorated) from eddy current evaluation

Measured flaw size intervals (mm)	Observed # of flaws from eddy current inspection
$a < 0.3$	62
$0.3 < a < 0.6$	6

As is evident from Table 14, the data consisted of both left censored and interval measurements. The flaw sizes were corrected for measurement errors using Eq. (63) considering various random sampling of measurement error parameters. Table 15 illustrates observed number of flaws for true flaw size intervals (corresponding to mean values of measurement error parameters). A lower bound true flaw size of 0.05 mm was assumed for reliable detection of flaws for first interval of Table 14 based on the detection threshold.

Table 15: True size corresponding to Table 14 (corrected for measurement errors)

True flaw size intervals (mm)	Observed # of flaws from eddy current evaluation
$a < 0.05$	-
$0.05 < a < 0.1451$	62
$0.1451 < a < 0.5532$	6

The likelihood function of true flaw size given the eddy current measurements was defined using Eq. (72). The Bayesian posterior inference of the flaw size intensity was carried out using the developed MATLAB routine. Uniform prior distribution was assumed for flaw size intensity. Several posterior distributions of flaw size intensity were obtained corresponding to different expected values of true size (obtained using Eq. 63 for random sampling of bias and random error parameters), which were used to obtain the weighted average posterior distribution of flaw size intensity, as shown in Figure 46. The results were also verified using OpenBUGS.

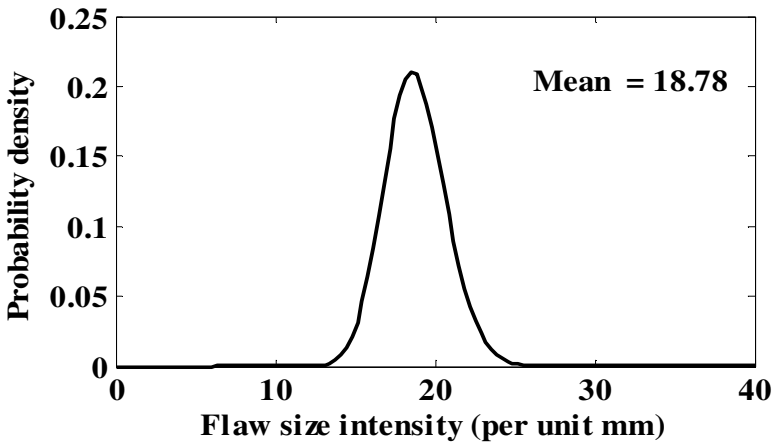

Figure 46: Posterior flaw size intensity distribution

The posterior flaw size distributions were then estimated using Eq. (80) corresponding to the mean, 2.5%, and 97.5% values of posterior flaw size intensity as shown in Figure 47. Posterior flaw size intensity values were then used to estimate the corresponding marginal POD values, $M_{POD}(\lambda)$. The likelihood function of true number of flaws given observed number of flaws was then defined using Eq. (74), and the Bayesian posterior inference of the true number of flaws (Eq. 75) computed.

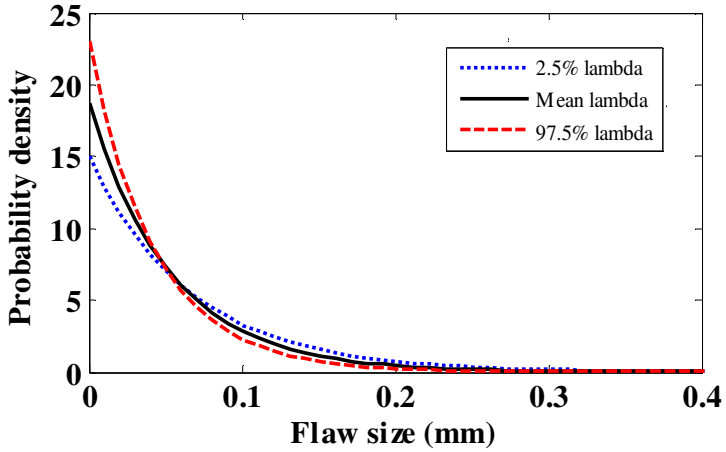

Figure 47: Posterior flaw size distributions

Uniform prior distribution was assumed for number of flaws to estimate the posterior distributions of true number of flaws. The true number of flaws was then used to estimate posterior distribution of flaw density for total tube volume in SMR. Figure 48 presents a box and whisker plot of true number of flaws by flaw size intervals. Table 16 presents the mean of estimated true number of flaws for different flaw depth intervals.

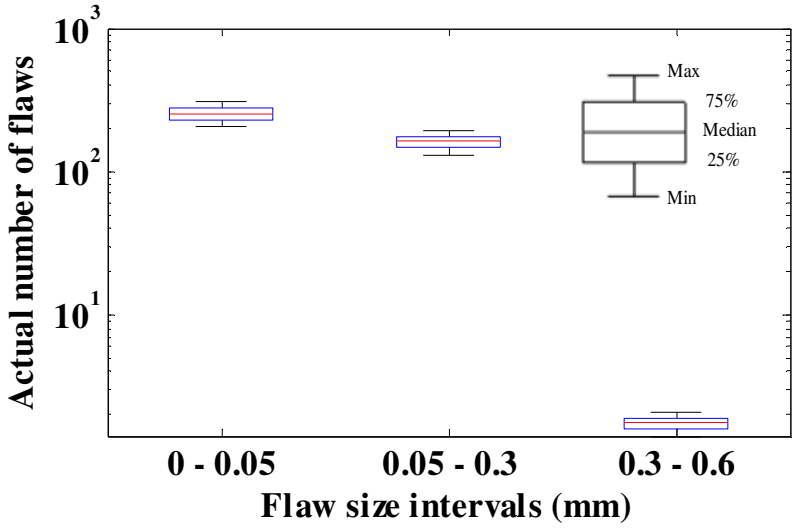

Figure 48: Box and whisker plot of actual/true number of flaws (log scale)

Table 16: Actual/True number of flaws

True flaw size (mm)	Mean number of flaws using 2.5% lambda (posterior)	Mean number of flaws using 50% lambda (posterior)	Mean number of flaws using 97.5% lambda (posterior)
$a \leq 0.05$	178.95	251.1	338.2
$0.05 < a \leq 0.3$	156.44	159.8	156.2
$0.3 < a \leq 0.6$	3.73	1.47	0.498

In Table 16, the mean number of flaws estimated using the proposed Bayesian approach after considering all uncertainties and prior information, is substantially higher than eddy current measurements (Tables 14 & 15), especially for very small sizes. For true flaw sizes less than 0.3 mm, the POD has very small values, which is evident in the number of actual/true flaws in those ranges. Therefore, it is critical to consider the detection uncertainties and measurement errors associated with nondestructive evaluation methods, in order to estimate the real defect size and density distributions in SG tubes. The defect size and density distributions estimated during in-service inspections can help in making appropriate and timely replacement/repair decisions, thereby preventing unanticipated failures. For the proposed Bayesian approach to be effective, it is critical to characterize the detection and measurement capability of a nondestructive evaluation method appropriately, with focus on the end application, e.g., material properties, geometry of structural component and defect attributes. This is because the actual/true number of flaws is sensitive to the POD and measurement errors for given nondestructive equipment.

The proposed Bayesian approach was also applied to ultrasonic inspection data for Pressure Vessel Research User Facility (PVRUF) flaws. The POD and measurement errors for ultrasonic inspection were first modeled, and then the posterior distribution of flaw size intensity parameters was obtained using the proposed MATLAB code. The posterior parameters were then used to determine the actual number of flaws in the vessel. The total actual number of vessel flaws determined using the Bayesian approach was found to be consistent with data used by Fracture Analysis of Vessels-Oak Ridge (FAVOR) code for PVRUF vessel.

CHAPTER 6: CONCLUSIONS AND SUGGESTED FUTURE WORK

Frequency of SGTR is required in PSA of PWRs to determine the potential of radionuclide release. The SGTR frequencies estimated from historical failure data are not applicable to new designs of SMR SGs that are substantially different from the operating fleet of PWRs. Further, normal operating conditions-induced SGTRs (low leak rate) need to be carefully investigated, as they are more vital to the overall safety and operability of SMRs than accident-induced SGTRs. This dissertation described the development of a probabilistic mechanistic-based approach for determining the frequency of SGTR failures. As opposed to using the historical data (which does not exist for the SMRs), the approach uses physics-of-failure that models the probable underlying failure mechanisms probabilistically (called PPoF).

Primary failure mechanisms occurring in the SMR SG tubes under the prevailing degradation conditions during normal operating conditions were identified, and their PPoF models developed. The PPoF models were formulated considering critical variables (e.g., among material properties, environmental conditions, stress agents, and geometry) that can lead to initiation and propagation of degradations in the tubes. Uncertainties associated with unknown or partially known factors such as manufacturing methods, material properties, model uncertainties, and measurement errors have been characterized. A finite element-based probabilistic approach has been developed to

estimate the operational stresses acting on the helical tubes in the SMR SG design under normal operating conditions. A probabilistic approach was formulated and a corresponding MATLAB routine developed to simulate damage propagation in the tubes using proposed PPoF models under the acting stress agents, propagating all the uncertainties to predict the distribution of the SGTR frequency.

An application of the PPoF-based SGTR frequency prediction approach has been successfully demonstrated for a typical new design of SMR SGs consisting of helical Alloy 690 tubes. Based on the results, it was concluded that fatigue-induced SGTR is 1.5 times less likely than fretting wear-induced SGTR. The PPoF-based SGTR frequency is plant-specific and more representative for use in risk-informed safety assessment of SMRs as well as existing PWRs. The PPoF approach can provide an effective tool for the evaluation of safety and reliability of SGs as well as other passive systems in SMRs.

Since the SG tubes are subjected to variety of operating conditions during their life-cycle, the degradations in tubes may not propagate exactly as anticipated during the licensing or pre-service phase. Hence, it is critical to characterize the health condition of the SG tubes during in-service inspections, and update the pre-service estimates of the SGTR frequency. Tube degradations/defects are usually characterized through nondestructive evaluation methods during in-service inspection of tubes. These inspection data are highly uncertain in nature due to detection uncertainties and measurement errors associated with nondestructive evaluation methods (e.g., eddy current). These uncertainties and errors if not considered properly can lead to under- or over-estimation of SGTR frequency. This dissertation presented a Bayesian approach that

combines prior knowledge of defect size and density with uncertain data from nondestructive evaluations, considering the POD, measurement errors, and associated uncertainties, to give a probabilistic description of defect size and density.

The Bayesian approach developed in this research considers both systematic (bias) and random error in nondestructive measurements, considers uncertainties in POD values and captures the combined effect of POD and measurement errors (including associated uncertainties) on measured defect sizes by a likelihood function. The approach is applicable to exact, interval, censored, and truncated measurements; and also provides a framework for updating parameter distribution as and when new information becomes available. For the proposed Bayesian approach to be effective, it is critical to characterize the detection and measurement capability of a nondestructive evaluation method appropriately, with focus on the end application, e.g., material properties, geometry of structural component and defect attributes. An application of the proposed Bayesian approach has been provided to estimate real/true flaw size and density distributions in SG tubes based on in-service eddy current evaluation data. The flaw size and density distributions estimated through the proposed Bayesian approach can be used to update the pre-service estimates of the SGTR frequency, which can support risk-informed maintenance of SG tubes and regulatory decision-making.

Future research efforts should focus on a number of more detailed researches as highlighted below:

1. More detailed 3-D thermal hydraulic analysis of the primary-side fluid-flow characteristics (e.g., gap turbulent flow velocities, fluid density) and secondary

side in SG tube bundles during normal operating conditions in the SMRs. This would help in making more realistic assessment of stresses acting on the tubes during normal conditions.

2. Because of their integral SGs and proximity to core, the effects of neutron embrittlement on the SG tube must also be studied and factored into the SGTR frequency assessment and health management.
3. There is need for better characterization of the manufacturing flaw characteristics for Alloy 690 tube materials that are used as input in the assessment of the SGTR frequency at the pre-service stage.
4. It is important to expand the scope of nondestructive evaluations to include the identification of degradation mechanisms from the detected flaw characteristics.
5. A more detailed analysis is required to investigate temperature transients-induced thermal stresses in the tubes during normal operating conditions, and potential for thermal fatigue.
6. Multi-tube rupture during accident condition should also be studied. This includes SGTR-induced pipe-whip, as well as high temperature degraded core-induced stresses on in-vessel SG tubes, and possible steam explosion and hydrogen detonation during a severe accident condition inside the reactor vessel unrelated to the SGTR.
7. The applicability of current nondestructive inspection techniques (e.g., eddy current) to helically-shaped tube bundles proposed for most of the SMRs also need to be assessed. This is because the helically-shaped tube bundles may

produce new inspection challenges as opposed to U-tube or straight-through tubes that are used in most of the existing large scale PWRs.

REFERENCES

Agarwala, B.N., "Electromigration failures in Au thin-film conductors", *Proceedings of 13th Annual Reliability Physics Symposium,* pp: 107-112, 1975.

Akaike, H., "A new look at the statistical model identification", *IEEE Transactions on Automatic Control*, Vol. 19, Issue 6, 1974.

ANSYS, "*ANSYS Structural Analysis Guide*", ANSYS Inc., Houston, 2005.

Archard, J.F., and Hirst, W., "The wear of metals under unlubricated conditions," *Proceedings of the Royal Society of London*, Vol. 236, Issue 1206, pp: 397-410, August 1956.

ASTM Standard E-1150, "*Standard Terminology Relating to Fatigue and Fracture Testing*", ASTM International, West Conshohocken, PA, 2010.

Au-Yang, M.K., "*Flow-induced vibration of power and process plant components*," ASME Press, New York, 2001.

Axisa, F., Desseaus, A., and Gilbert, R.J., "Experimental study of tube/support impact forces in multi-span PWR steam generator tubes," *Proceedings of the Symposium on Flow-induced Vibration*, Vol. 3, ASME Press, New York, pp. 139–148, 1984.

Axisa, F., Antunes, J., and Villard, B., "Random excitation of heat exchanger tubes by cross flow," *Journal of Fluids and Structures*, Vol. 4, Issue 3, pp: 321-341, 1990.

Azarkhail, M., and Modarres, M., "A Novel Bayesian Framework for Uncertainty Management in Physics-Based Reliability Models", *Proceedings of the ASME*

International Mechanical Engineering Congress and Exposition, November 11-15, 2007, Seattle, WA.

Bamford, W. H., Liaw, P. K., and Eason, E. D., "A Review of Corrosion Fatigue Crack Growth Behavior for Pressure Vessel Steels in Light Water Environments", in *Fatigue, Degradation, and Fracture*, W. H. Bamford, et al., Eds., PVP Vol. 195, The American Society of Mechanical Engineers, pp. 1–12, 1990.

Barsom, J. M., "Fatigue crack growth under variable amplitude loading in various bridge steels," In *Fatigue Crack Growth under Spectrum Loads*, ASTM STP 595, American Society for Testing and Materials, Philadelphia, PA, pp. 217-235, 1976.

Basquin, O. H. "The Exponential Law of Endurance Tests," *Proceedings of American Society of Testing Materials*, Vol. 10, pp: 625-630, 1910.

Beau, J.F., "Management of the human element in the physics of failure", *Proceedings of Third Annual Symposium on the Physics of Failure in Electronics,* pp: 264-279, 1964.

Beden, S. M., Abdullah, S. and Ariffin, A. K., "Review of Fatigue Crack Propagation Models for Metallic Components", *European Journal of Scientific Research*, Vol.28, Issue 3, pp.364-397, 2009.

Berge, P., and Donati, J.R., "Materials requirements for pressurized water reactor steam generator tubing," *Nuclear Technology*, Vol. 55, October 1981.

Bernard, J. L., and Salama, G. S., "Fatigue Crack Growth in Air Environment at 300°C for Stainless Steels", *Nuclear Technology*, Vol. 59, Issue 1, pp: 136–147, 1982.

Bishop, N., and Caserio, A., "Vibration fatigue analysis in the finite element environment", *Proceedings of the Americas Users' Conference*, Universal City, California, 1998.

Blevins, R.D., "Fretting Wear of Heat Exchanger Tubes, Part I Experiments, and Part II: Model", *ASME Journal of Pressure Vessel Technology*, Vol. 101, pp: 625-633, 1979.

Blevins, R.D., "*Flow-induced Vibration*," Van Nostrand Reinhold, New York, 1990.

Blevins, R.D., "Turbulence-Induced Vibration of Heat Exchanger Tubes in Cross Flow", *Proceedings of ASME Pressure Vessel and Piping Conference*, Vol. 273, pp: 199-210, 1994.

Bowles, J.B., "A Survey of Reliability-Prediction Procedures for Microelectronic Devices", *IEEE Transactions on Reliability*, Vol. 41, Issue 1, 1992.

Bretts, G., Kozol, J., and Lampert, H., "Failure physics and accelerated testing", *Proceedings of Second Annual Symposium on the Physics of Failure in Electronics*, pp: 189-207, September, 1963.

Brodeur, J.E., "Process control by means of accelerated testing", *Proceedings of 13th Annual Reliability Physics Symposium,* pp: 255-256, 1975.

Celeux, G., Persoz, M., Wandji, J.N., and Perrot, F., "Using Markov Chain Monte Carlo Methods to Solve Full Bayesian Modeling of PWR Vessel Crack Distributions", *Reliability Engineering and System Safety*, Vol. 66, Issue 3, pp: 243–252, 1999.

Chamberlain, S., Chookah, M., and Modarres, M., "Development of a probabilistic mechanistic model for reliability assessment of gas cylinders in compressed natural gas vehicles," *Journal of Risk and Reliability*, Vol. 223, Issue 4, pp: 289-299, 2009.

Chatterjee, K., and Modarres, M., "A probabilistic physics-of-failure approach to prediction of steam generator tube rupture frequency," *Proceedings of the International Topical Meeting on Probabilistic Safety Assessment and Analysis*, March 13-17, 2011, Wilmington, NC.

Chatterjee, K., and Modarres, M., "A Bayesian Probabilistic Approach to Improved Health Management of Steam Generator Tubes", *Proceedings of the Annual Conference of Prognostics and Health Management (PHM) Society*, September 25-29, 2011, Montreal, Canada.

Chatterjee, K., and Modarres, M., "A Probabilistic Physics-of-Failure Approach for Assessing the Frequency of Steam Generator Tube Ruptures", *Transactions of the American Nuclear Society: 1st Annual ANS SMR Conference*, October 30 – November 3, 2011, Washington, DC.

Chatterjee, K., Modarres, M., and Bernstein, J., "Fifty years of physics of failure", *Journal of the Reliability Information Analysis Center*, Vol. 20, Issue 1, January 2012.

Chatterjee, K., and Modarres, M., "A probabilistic physics-of-failure approach to prediction of steam generator tube rupture frequency," *Nuclear Science and Engineering*, Vol. 170, Issue 2, February 2012.

Chopra, O. K., Soppet, W. K., and Shack, W. J., "Effects of alloy chemistry, cold work, and water chemistry on corrosion fatigue and stress corrosion cracking of nickel alloys and welds," *NUREG/CR-6721*, Argonne National Laboratory, April 2001.

Church, H.F., and Roberts, B.C., "Failure mechanisms of electronic components", *Proceedings of Fourth Annual Symposium on the Physics of Failure in Electronics,* pp: 156-178, 1965.

Cinotti, L., Bruzzone, M., Meda, N., Corsini, G., Lombardi, C.V., Ricotti, M., and Conway, L.E., "Steam Generator of the International Reactor Innovative and Secure", *Proceedings of 10th International Conference on Nuclear Engineering,* Arlington, VA, April 14-18, 2002.

Cizelj, L., and Roussel, G., "Reliability of Degraded Steam Generator Tubes", In *Steam Generator Systems: Operational Reliability and Efficiency*, Valentin Uchanin (Ed.), March 2011, ISBN: 978-953-307-303-3, InTech, Available from: http://www.intechopen.com/articles/show/title/reliability-of-degraded-steam-generator-tubes

Cizelj, L., and Dvorsek, T., "The Relative impact of sizing errors on steam generator tube failure probability", *Proceedings of 3rd International Steam Generator and Heat Exchanger Conference*, Toronto, Canada, June 1998.

Clark, R.A., and Kurtz, R.J., "Compendium and comparison of international practice for plugging, repair and inspection of steam generator tubing", *NUREG/CR-5016,* April, 1988.

Conrad, T.R., Mielnik, R.J., and Musolino, L.S., "A test methodology to monitor and predict early life reliability failure mechanisms", *Proceedings of 26th Annual Reliability Physics Symposium,* pp: 126-130, 1988.

Connors, H.J., "Flow-induced vibration and wear of steam generator tubes," *Nuclear Technology*, Vol. 55, pp: 311–331, November 1981.

Cowles, M.K., "Review of WinBUGS 1.4", *The American Statistician*, Vol. 58, Issue 4, pp: 330-336, 2004.

Crook, D.L., "Method of determining reliability screens for time dependent dielectric breakdown", *Proceedings of 17th Annual Reliability Physics Symposium,* pp: 1-7, 1979.

Dasgupta, A., and Pecht, M., "Material failure mechanisms and damage models", *IEEE Transactions on Reliability*, Vol. 40, Issue 5, pp: 531-536, December 1991.

Datla, S.V., Jyrkama, M.I., and Pandey, M.D., "Probabilistic Modeling of Steam Generator Tube Pitting Corrosion", *Nuclear Engineering and Design*, Vol. 238, Issue 7, pp: 1771-1778, 2008.

Davis, H., "Introduction", *Proceedings of the First Annual Symposium on Physics of Failure in Electronics*, September 26-27, pp: 1-3, 1962.

Department of Defense, "Reliability Prediction of Electronic Equipment", Military Handbook, *MIL-HDBK-217F*, 1991.

Department of Defense, "Nondestructive Evaluation System Reliability Assessment", Military Handbook, *MIL-HDBK-1823*, 1999.

Diercks, D.R., Shack, W.J., and Muscara, J., "Overview of steam generator tube degradation and integrity issues," *Proceeding of 24th Water Reactor Safety Meeting*, October 21-23, 1996, Bethesda, MD.

Dodson, G.A., and Howard, B.T., "High stress aging to failure of semiconductor devices," *Proceedings of Seventh National Symposium on Reliability and Quality Control*, Philadelphia, PA, January 1961.

Dvorsek, T., and Cizelj, L., "An analysis of in-service inspection data at tube support plates of KRSKO steam generators", *Proceedings of Regional Meeting: Nuclear Energy in Central Europ*e, June 13-16, 1993, Portoroz, Slovenia.

Earles, D.R., and Eddins, M.F., "Reliability physics (the physics of failure)", *Proceedings of First Annual Symposium on the Physics of Failure in Electronics*, pp: 179-193, September 26-27, 1962.

Ebel, G.H., "Reliability physics in electronics: a historical view", *IEEE Transactions on Reliability*, Vol. 47, Issue 3, September 1998.

Engel, P.A., "Failure models for mechanical wear modes and mechanisms", *IEEE Transactions on Reliability*, Vol. 42, Issue 2, June 1993.

Fitch, E.C., "Fretting Wear in Lubricated Systems", in *Proactive maintenance for mechanical systems: an activity conducted to detect and correct root cause aberrations of failure*, Editor: Fitch, E.C., Elsevier Advanced Technology, 1992.

Forman, R. G., "Study of fatigue crack initiation from flaws using fracture mechanics theory", *Engineering Fracture Mechanics*, Vol. 4, Issue 2, pp. 333–345, 1972.

Frankel, H., and Kinsolving, W., "Reliability testing for hostile environments", *Proceedings of Eighth Annual Reliability Physics Symposium,* pp: 219, 1970.

Frick, T.M., Sobek, T.E., and Reavis, J.R., "Overview on the development and implementation of methodologies to compute vibration and wear of steam generator tubes", *Symposium on Flow-Induced Vibrations in Heat Exchangers*, New Orleans, Louisiana, pp: 149–160, December 1984.

Georgiou, G.A., "Probability of Detection (PoD) Curves: Derivation, Applications and Limitations", *Research Report 454*, 2006, Retrieved from http://www.hse.gov.uk/research/rrhtm/rr454.htm

Gill, W., and Workman, W., "Reliability screening procedures for integrated circuits", *Proceedings of Fifth Annual Symposium on the Physics of Failure in Electronics,* pp: 101-140, 1966.

Gosselin, S.R., Simonen, F.A., Pilli, S.P., Lydell, B.O.Y., "Probabilities of Failure and Uncertainty Estimate Information for Passive Components – A Literature Review", *NUREG/CR-6936*, May 2007.

Griffith, A. A. "The phenomena of rupture and flow in solids," *Philosophical Transactions of the Royal Society*, Vol. 221, pp: 163-198, 1921.

Haggag, McMahon, Hess, Cheng, Lee, and Lyding, "A Probabilistic-Physics-of-Failure/Short-Time-Test Approach to Reliability Assurance for High-Performance Chips: Models for Deep-Submicron Transistors and Optical Interconnects", *Proceedings of IEEE Integrated Reliability Workshop*, pp: 179-182, October 23-26, 2000.

Hall, P.L., and Strutt, J.E., "Probabilistic physics-of-failure models for component reliabilities using Monte Carlo simulation and Weibull analysis: a parametric study", *Reliability Engineering & System Safety*, Vol. 80, Issue 3, pp: 233-242, June 2003.

Hieber, H., and Pape, K., "Lifetime of bonded contacts on thin film metallization", *Proceedings of 22nd Annual Reliability Physics Symposium,* pp: 128-133, 1984.

Hollingshead, C.O., "A system oriented components selection optimization technique", *Proceedings of Eighth Annual Reliability Physics Symposium,* pp: 220-225, 1970.

Hong, S.M., and Kim, I.S., "Impact fretting wear of alloy 690 tubes at 25C and 290C", *Wear*, Vol. 259, pp: 356-360, 2005.

Hofmann, D., "Common Sources of Errors in Measurement Systems", In Sydenham, P. & Thorn, R. (Eds.), *Handbook of Measuring System Design*, pp: 289-294, 2005. doi:10.1002/0471497398

Hovey, P., Meeker, W.Q., and Li, M., "Joint Estimation of the Flaw Size Distribution and POD Function", *Proceedings of the Review of Progress in Quantitative Nondestructive Evaluation*, July 20-25, 2008, Chicago, Illinois.

Hu, J.M., Pecht, M., and Dasgupta, A., "A Probabilistic Approach for Predicting Thermal Fatigue Life of Wire Bonding in Microelectronics", *Journal of Electronic Packaging*, Vol. 113, Issue 3, pp: 275-285, 1991.

Hudson, C. M., "A Root-Mean-Square Approach for Predicting Fatigue Crack Growth under Random Loading", *In Methods and Models for Predicting Fatigue*

Crack Growth under Random Loading, J. B. Chang and C .M. Hudson, Eds., American Society for Testing and Materials, pp. 41-52, 1981.

Hyslop, D.R., and Imbens, G.W., "Bias from Classical and other Forms of Measurement Error", *Journal of Business and Economic Statistics*, Vol. 19, Issue 4, October 2001.

Ingram, G.E., "Prediction of Device Reliability by Mechanisms-of-Failure Principles", *Proceedings of Third Annual Symposium on the Physics of Failure in Electronics*, pp: 200-209, 1964.

International Atomic Energy Agency, "Applications of probabilistic safety assessment (PSA) for nuclear power plants", *Report No. IAEA-TECDOC-1200*, February 2001.

International Atomic Energy Agency, "Innovative small and medium sized reactors: Design features, safety approaches and R&D trends", *Report No. IAEA-TECDOC-1451*, May 2005.

International Atomic Energy Agency, "Strategy for Assessment of WWER Steam Generator Tube Integrity", *Report No. IAEA-TECDOC-1577*, December 2007, Retrieved from http://www-pub.iaea.org/MTCD/publications/PDF/te_1577_web.pdf

Jaech, J.L., "A Program to Estimate Measurement Error in Nondestructive Evaluation of Reactor Fuel Element Quality", *Technometrics*, Vol. 6, Issue 3, pp: 293 – 300, 1964.

James, L. A., and Jones, D.P., "Fatigue Crack Growth Rates for Austenitic Stainless Steel in Air", in *Predictive Capabilities in Environmentally Assisted Cracking,* PVP Vol. 99, The American Society of Mechanical Engineers, New York, pp. 363–414, 1985.

Jenson, F., Mahaut, S., Calmon P., and Poidevin, C., "Simulation Based POD Evaluation of NDI Techniques", *Proceedings of 10th European Conference on Non-Destructive Testing*, Moscow, June 7-11, 2010.

Jo, J.C., and Jhung, M.J., "Flow-induced vibration and fretting-wear predictions of steam generator helical tubes," *Nuclear Engineering and Design*, Vol. 238, Issue 4, pp: 890–903, 2008.

Keen, R.S., Loewenstern, L.R., and Schnable, G.L., "Mechanisms of Contact Failure in Semiconductor Devices", *Proceedings of IEEE Sixth Annual Reliability Physics Symposium,* pp: 216-233, 1967.

Kim, I.K., "Assessment of failure for fretting-wear of steam generator U-tubes", *Proceedings of the 14th International Conference on Structural Mechanics in Reactor Technology*, August 17-22, 1997, Lyon, France.

Kim, S.T., Tadjiev, D., and Yang, H.T., "Fatigue life prediction under random loading conditions in 7475-T7351 Aluminum alloy using the RMS model," *International Journal of Damage Mechanics*, Vol. 15, Issue 1, pp: 89-102, 2006.

Ko, P.L., "Heat Exchanger Tube Fretting Wear: Review and Application to Design", *Journal of Tribology*, Vol. 107, pp: 149-156, April 1985.

Kurtz, R.J., Clark, R.A., Bradley, E.R., Bowen, W.M., Doctor, P.G., Ferris, R.H., and Simonen, F.A., "Steam Generator Tube Integrity Program/Steam Generator Group Project", *NRC Publication No. NUREG/CR-5117*, 1990.

Kurtz, R.J., Heasler, P.G., and Anderson, C.M., "Performance Demonstration Requirements for Eddy Current Steam Generator Tube Inspection", *Proceedings of the 20th Water Reactor Safety Information Meeting*, October 21-23, 1992, Bethesda, MD.

Lee, J.B., Park, J.H., Lee, S.H., Kim, H., and Chung, H., "Statistical Estimation of Crack Growth Behaviors in Steam Generator Tubes using Monte Carlo Method", *Proceedings of the 18th International Conference On Structural Mechanics In Reactor Technology*, Beijing, China, August 7-12, 2005.

Lee, Y. and Kim, I., "The effect of subsurface deformation on the wear behavior of steam generator tube materials", *Wear*, Vol. 253, Issues 3-4, pp: 438-447, August 2002.

Lee, Y., Kim, I., Kang, S., and Chung, H., "A study on wear coefficients and mechanisms of steam generator tube materials," *Wear*, Vol. 250, Issues 1-12, pp: 718–725, 2001.

Li, M., and Meeker, W.Q., "A Noise Interference Model for Estimating Probability of Detection for Nondestructive Evaluations", *Proceedings of the Review of Progress in Quantitative Nondestructive Evaluation*, July 20-25, 2008, Chicago, Illinois.

Liao, Y., and Guentay, S., "Potential steam generator tube rupture in the presence of severe accident thermal challenge and tube flaws due to foreign object wear," *Nuclear Engineering and Design*, Vol. 239, Issue 6, pp: 1128–1135, 2009.

Lim, M., Oh, S., and Lee, Y., "Friction and wear of Inconel 690 and Inconel 600 for steam generator tube in room temperature water," *Nuclear Engineering and Design*, Vol. 226, Issue 2, pp: 97-105, December 2003.

Matik, Z., and Sruk, V., "The Physics-of-Failure Approach in Reliability Engineering", *Proceedings of IEEE International Conference on Information Technology Interfaces*, pp: 745-750, June 23-26, 2008.

McLinn, J., "A short history of reliability," *The Journal of the Reliability Information Analysis Center*, January 2011.

Mendel, M., "The case for probabilistic physics of failure", Chapter in *Reliability and Maintenance of Complex Systems*, Edited by Ozekici, S., Springer, 1996.

Modarres, M., Kaminskiy, M., and Krivtsov, V., "*Reliability engineering and risk analysis: A practical guide*", Marcel Dekker, New York, 1999.

Modarres, M., "Probabilistic risk assessment", Chapter in *Handbook of Performability Engineering*, Ed. Mishra, K.B., Springer, 2008.

Moss, R.E.S., and Kiureghian, A.D., "Incorporating parameter uncertainty into attenuation relationships", *Proceedings of 8th U.S. National Conference on Earthquake Engineering*, San Francisco, 2006.

Olin, B.D., and Meeker, W.Q., "Applications of Statistical Methods to Nondestructive Evaluation", *Technometrics*, Vol. 38, Issue 2, pp: 95-112, 1996.

Paris, P.C., and Erdogan, F., "A Critical Analysis of Crack Propagation Laws", *Journal of Basic Engineering; Transaction*, American Society of Mechanical Engineers, Vol. 85, pp. 528-534, 1963.

Park, H., Kim, Y., Lee, B., and Rheem, K., "Effect of heat treatment on fatigue crack growth rate of Inconel 690 and Inconel 600," *Journal of Nuclear Materials*, Vol. 231, Issue 3, pp: 204-212, 1996.

Partridge, J., Hall, E.C., and Hanley, L.D., "The application of failure analysis in procuring and screening of integrated circuits", *Proceedings of Fourth Annual Symposium on the Physics of Failure in Electronics,* pp: 96-139, 1965.

Payne, D.A., "Concerning the physics of failure of Barium Titanate capacitors", *Proceedings of IEEE Sixth Annual Symposium on Reliability Physics,* pp: 257-264, 1967.

Pecht, M., Dasgupta, A., Barker, D., Leonard, C.T., "The reliability physics approach to failure prediction modeling", *Quality and Reliability Engineering International*, Vol. 6, Issue 4, pp: 267-273, September/October 1990.

Pecht, M., and Dasgupta, A., "Physics-of-failure: an approach to reliable product development", *Proceedings of IEEE International Integrated Reliability Workshop*, pp: 1-4, October 22-25, 1995.

Pettigrew, M.J., Carlucci, L.N., Taylor, C.E., Fisher, N.J., "Flow induced vibration and related technologies in nuclear components", *Nuclear Engineering and Design*, Vol. 131, pp: 81–100, 1991.

Poloski, J. P., Marksberry, D.G., Atwood, C.L., and Galyean, W.J, "Rates of initiating Event at U.S. nuclear power plants: 1987-1995," *NUREG/CR-5750*, February 1999.

Rodriguez, E.S. and Provan, J.W., "Part II: Development of a General Failure Control System for Estimating the Reliability of Deteriorating Structures", *Corrosion*, Vol. 45, Issue 3, pp: 193-206, 1989. doi:10.5006/1.3577841

Ryerson, C.M., "Project control to provide for the physics of failure in electronics", *Proceedings of First Annual Symposium on the Physics of Failure in Electronics*, pp: 68-72, September 26-27, 1962.

Ryerson, C.M., "Mathematical Modeling For Predicting Failure Rates Of Component Part", *Proceedings of IEEE Sixth Annual Reliability Physics Symposium*, pp: 10-15, 1967.

Schallor, R.F., Pratt, D.P., and Pellegrino, B.A., "Robotic inspection confirms steam generator modification plan", *Power Engineering*, pp: 41-43, September 1995.

Schenck, J.F., "Progressive failure mechanisms of a commercial silicon diode", *Proceedings of Fifth Annual Symposium on the Physics of Failure in Electronics,* pp: 18-35, 1966.

Schuster, G.J., Simonen, F.A., and Doctor, S.R., "Fabrication Crack Density and Distribution in Repairs to Reactor Pressure Vessel and Piping Welds", *NUREG/CR-6945*, U.S. Nuclear Regulatory Commission, 2008.

Schwarz, G., "Estimating the dimension of a model", *The Annals of Statistics*, Vol. 6, Issue 2, pp: 461-464, 1978.

Schwuttke, G.H., "Yield problems in LSI technology", *Proceedings of Eighth Annual Reliability Physics Symposium,* pp: 274-280, 1970.

Shiomi, H., "Cumulative degradation model and its application to component life estimation", *Proceedings of Fourth Annual Symposium on the Physics of Failure in Electronics*, pp: 74-94, 1965.

Simonen, F.A., Doctor, S.R., Schuster, G.J., and Heasler, P.G., "A Generalized Procedure for Generating Crack Related Inputs for the FAVOR Code", *NUREG/CR-6817*, U.S. Nuclear Regulatory Commission, 2003.

Tamburrino, A.L., "Analysis of requirements in reliability physics", *Proceedings of Second Annual Symposium on the Physics of Failure in Electronics*, pp: 1-24, September, 1963.

Taylor, C.E., and Pettigrew, M.J., "Random excitation forces in heat exchanger tube bundles," *Journal of Pressure Vessel Technology*, Vol. 122, Issue 4, pp: 509-514, November 2000.

Thomas, R.E., "Some unifying concepts in reliability physics, mathematical models, and statistics", *Proceedings of Fifth Annual Symposium on the Physics of Failure in Electronics,* pp: 1-17, 1966.

Tregoning, R., Abramson, L., and Scott, P., "Estimating loss-of-coolant accident (LOCA) frequencies through the elicitation process," *NUREG-1829*, June 2005.

US NRC, "Rapidly propagating fatigue cracks in steam generator tubes," *NRC Bulletin No. 88-02*, February 5, 1988.

US NRC, “Stress Corrosion Cracking in PWR Steam Generator Tubes”, *NRC Bulletin No. 90-49*, August 6, 1990.

US NRC, “NRC’s response to the February 15,2000 steam generator tube rupture at Indian Point Unit 2 power plant”, *Case No. 00-03S*, August 29, 2000.

US NRC, “Tube leakage due to a fabrication flaw in a replacement steam generator,” *NRC Information Notice 2004-16*, August 2004.

US NRC, “Resolution of generic safety issues: issue 188: Steam generator tube leaks or ruptures, concurrent with containment bypass from main steam line or feedwater line breaches,” *NUREG-0933*, August 2010.

US NRC, “Backgrounder on Steam Generator Tube Issues”, *NRC Fact Sheets*, February 4, 2011.

Vaccaro, J., “Reliability and Physics of Failure Program at RADC”, *Proceedings of First Annual Symposium on the Physics of Failure in Electronics*, pp: 4-10, September 26-27, 1962.

Wade, K.C., “Steam Generator Degradation and Its Impact on Continued Operation of Pressurized Water Reactors in the United States”, *Energy Information Administration/ Electric Power Monthly*, August 1995.

Walker, E.K., “The effect of stress ratio during crack propagation and fatigue for 2024-T3 and 7076-T6 aluminum”, In *Effect of environment and complex load history on fatigue life*, American Society for Testing and Materials, Philadelphia, pp.1–14, 1970.

Wang, Y., and Meeker, W.Q., "A Statistical Model to Adjust for Crack-Size Bias in the Computation of Probability of Detection", *Proceedings of the Review of Progress in Quantitative Nondestructive Evaluation*, July 31-August 5, 2005, Brunswick, Maine.

Weaver, D.S., Ziada, S., Au-Yang, M.K., and Chen, S.S., "Flow-induced vibrations in power and process plant components – Progress and prospects", *Journal of Pressure Vessel technology*, Volume 122, Issue 3, pp: 339-348, August 2000.

White, M., and Bernstein, J.B., "Microelectronics Reliability: Physics-of-Failure Based Modeling and Lifetime Evaluation", *JPL Publication 08-5 2/08*, Jet Propulsion Laboratory, Pasadena, California, 2008.

Workman, W., "Failure analysis techniques", *Proceedings of Third Annual Symposium on the Physics of Failure in Electronics*, pp: 238-263, September, 1964.

Young, B.A., and King, P.J., "Corrosion Fatigue Results for Alloy 690 Tubing in a PWR Secondary Environment", *ASME Pressure Vessels and Piping Conference*, July 17–21, 2005, Denver, Colorado.

Young, B.A., Gaoa, X., Srivatsan, T.S., and King, P.J., "An investigation of the fatigue crack growth behavior of INCONEL 690", *Materials Science and Engineering*, Vol. 416, Issues 1-2, 25, pp: 187-191, January 2006.

Young, B.A., Van Der Sluys, W.A., and King, P.J., "Development of a circumferentially through-wall cracked tube specimen for fatigue crack growth rate tests", *Journal of ASTM International*, Vol. 3, No. 6, May 2006.

Yuan, X.X., Mao, D., and Pandey, M.D., "A Bayesian Approach to Modeling and Predicting Pitting Flaws in Steam Generator Tubes", *Reliability Engineering and System Safety*, Vol. 94, Issue 11, pp: 1838-1847, 2009.

Zierdt, C.H., "Diagnostic techniques in semiconductor device stress response analysis", *Proceedings of First Annual Symposium on the Physics of Failure in Electronics*, pp: 91-97, September 26-27, 1962.